# ON THE DETERMINATION OF MICROSCOPIC REACTOR PARAMETERS USING AN EXPONENTIAL ASSEMBLY

# ON THE DETERMINATION OF MICROSCOPIC REACTOR PARAMETERS USING AN EXPONENTIAL ASSEMBLY

PROEFSCHRIFT

TER VERKRIJGING VAN DE GRAAD VAN DOCTOR IN DE TECHNISCHE WETENSCHAPPEN AAN DE TECHNISCHE HOGESCHOOL TE DELFT OP GEZAG VAN DE RECTOR MAGNIFICUS IR. H. J. DE WIJS, HOOGLERAAR IN DE AFDELING DER MIJNBOUWKUNDE, VOOR EEN COMMISSIE UIT DE SENAAT TE VERDEDIGEN OP WOENSDAG 12 JANUARI 1966 DES NAMIDDAGS TE 4 UUR

DOOR


HANS ROBERT KLEIJN

WERKTUIGKUNDIG INGENIEUR

GEBOREN TE AMSTERDAM





1965

DRUKKERIJ HOLLAND N.V., AMSTERDAM

*Dit proefschrift is goedgekeurd door de promotor*

PROF. DR J. J. WENT

"Pooh's found the North Pole," said Christopher Robin. "Isn't that lovely?"
Pooh looked modestly down.
"Is that it?" said Eeyore.
"Yes", said Christopher Robin.
"Is that what we were looking for?"
"Yes", said Pooh.
"Oh!" said Eeyore. "Well, anyhow — it didn't rain", he said.

*From A. A. Milne, Winnie—The Pooh*
*(Expotition to North Pole.)*

# CONTENTS

# INTRODUCTION

The neutron physics program associated with the design of a nuclear power reactor which differs from existing units (even of the same type) still consists of closely related theoretical and experimental work. In particular this is true when new physical concepts are planned to be incorporated. Separately neither calculations nor experiments offer as yet a sufficiently solid basis for determining system optimization and operational performance. For instance, initial criticality of the PATHFINDER-reactor, a boiling water-reactor (BWR) with integral nuclear superheat, was reached in 1963 on 15 boiler fuel elements, while only 12 had been calculated [1]. Although a tendency towards convergence seems to exist between theoretical and experimental results, there is still a strong need for more experimental data.

Generally, the integral characteristics of a reactor are determined from design calculations using semi-empirical data, incorporating the fundamental reactor physical behaviour frequently learned either from only a few experiments or from approximative neutron balance calculations. This includes that when a better understanding is obtained of the laws that govern the fundamental aspects, the engineering design methods may be adjusted accordingly, so that they will yield more accurate information.

In 1960 the experimental facilities of the Physics Division of the Reactor Instituut, an interacademic university laboratory at Delft, were extended with a light water moderated exponential assembly, fueled with annularly shaped natural uranium metal rods. This facility was designated LEAD (Light water Exponential Assembly Delft). Since the enrichment of the fuel is not essential as far as the fundamental reactor physical behaviour of a neutron multiplying system is concerned – reactivity and burn-up are in this respect considered as integral characteristics – even a natural uranium fueled facility such as LEAD can be used advantageously for basic research.

After sufficient knowledge was obtained concerning the integral neutron physics characteristics of this facility (such as the material buckling $B_m^2$ and related parameters), a research program of a more advanced nature was initiated.

Directly related to the reactivity of a reactor system – and thus to criticality and fuel cycle, and consequently to its economy – is the infinite multiplication factor $k_\infty$ which may, in case of a heterogeneous reactor lattice, be determined from a neutron analysis of a unit cell. The results for the unit cell, either obtained from experiments or by theoretical methods, can then be used in the homogenization of the reactor lattice

so that a multi-group, multi-region reactor program may be used to investigate the overall neutron behaviour of the reactor. Using Fermi's classic approach to the composition of the factor $k_\infty$ for a thermal reactor system, the formal but very practical 'four factor' formula may be written as:

$$k_\infty = \eta\, \varepsilon\, p\, f$$

where $\eta$ = number of fission neutrons obtained as a result of the absorption of one thermal neutron in the fuel,

$\varepsilon$ = fast fission factor indicating the fractional increase of the fission neutron yield due to absorption of fast neutrons only,

$p$ = resonance escape probability, indicating the fraction of neutrons with higher than thermal energies that escape capture in the fuel,

$f$ = thermal utilization factor, indicating the fraction of thermal neutrons in the system that is absorbed in the fuel.

The factor $\eta$ is a nuclear physics constant of the fissile material applied, depending only on the neutron spectrum near and in the fuel, while $\varepsilon$ depends on the lattice composition in general. Assuming burn-up to be low, so that the plutonium content of the fuel may be neglected, neither factor changes remarkably under the various operational conditions of a water-reactor.

Most sensitive to the operational conditions of such a system – in particular to changes in the moderator-to-fuel volume ratio – are the factors of $p$ and $f$. Since the agreement between the results of theory and experiment with regard to these factors, for lattices showing large spectral shifts across the unit cell, was far from acceptable [2], it was decided that the object of study should be an experimental determination of $p$ and $f$ from microscopic flux distributions measured by neutron activation.

This program was not to be performed with a particular reactor in mind but mainly to obtain experience with experimental techniques utilized to determine fine structure parameters and to make a comparison with present day calculational models. At the same time the usefulness, as far as physics is concerned, could be demonstrated of an exponential assembly in reactor design, instead of a more costly critical or near critical facility. In order to obtain sufficiently high neutron levels in the exponential facility for these measurements it was necessary to use the 200 kW swimming pool reactor HOR of the Reactor Instituut as a neutron source.

The available annularly shaped fuel slugs allowed to add an advanced feature to the exponential assembly. In regard to the future development of water reactors, indicating the practical applicability of nuclear superheat as is demonstrated, for example, by the BONUS and PATHFINDER plants, LEAD was re-designed to simulate a section of an integral nuclear superheat

lattice where steam would be generated due to boiling of water on the outside of the elements and raised above its saturation temperature inside the elements. An example of a possible coolant circulation of such a reactor system where boiling of water and superheating of steam occurs *throughout* the entire core is given in Fig. I. The program was consequently directed towards the determination of the factors $p$ and $f$ under various conditions of boiling of the moderator, which was simulated by injection of air. Moderation due to superheated steam was accounted for by applying expanded polystyrene in the 'steam' region.

This thesis is a compilation of the work which has been performed in the course of this research program. First an analysis has been made of an exponential assembly in general when used in combination with a reactor as a neutron source. This analysis is given in Chapter 1, together with some remarks about the practical use of exponential assemblies and a description of the LEAD facility. The method of simulating boiling of water

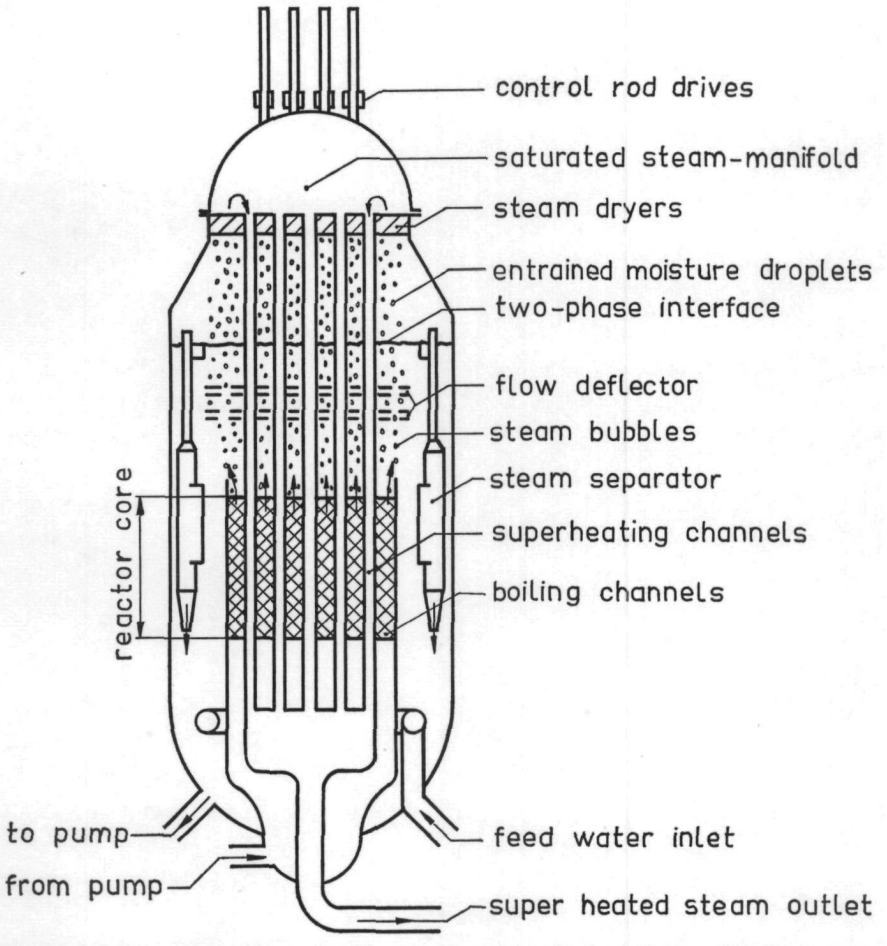


Fig. I. Possible coolant circulation in proposed integral nuclear superheat reactor. Superheating occurs throughout the entire core.

and the determination of the associated moderator void fractions are outlined in detail in Chapter 2. Chapter 3 is devoted to some reactor physics problems that arise with the use of integral nuclear superheat reactors. In Chapters 4 and Chapter 5 the measurements are described in relation to the resonance escape probability and the thermal utilization factor respectively. The results of these measurements have been compared with those of calculation models.

## REFERENCES

1. Nucleonics, Vol. 22, No. 5 (1964).
2. H. KOUTS, General summary, Light Water Lattices, Report of a Panel, Technical Reports Series No. 12, IAEA, Vienna (1962).

CHAPTER 1

# THE EXPONENTIAL ASSEMBLY

## 1.1 *Introduction*

Frequently the first experimental data concerning the neutron physics properties of a particular thermal reactor are obtained either from substitution experiments or from exponential, subcritical or even critical assemblies. Which of these systems is to be preferred depends not only on the type of reactor envisaged and the parameters required, but also on the eventual availability of facilities and the financial support of the experimental program.

Substitution techniques consist of the replacement of a fraction of a reference core by the lattice section that one wants to examine. In general this technique is applied to determine integral reactivity effects (material buckling and critical size) for which it is essential that the reference core can be made critical. From the difference in neutron balance these quantities are evaluated for the test lattice. Problems related to these experiments have, for instance, been discussed by NAUDET [1], GRAVES [2], CASINI, *et al.* [3] and BLAESSER [4]. However more conveniently substitution experiments may be performed to obtain microscopic reactor parameters. It is even possible to determine these parameters under operational conditions such as elevated temperatures, etc. In that case the operational conditions have to be realized or simulated only in the test lattice which is from a technological point of view considerably simpler than in a full scale core. For fine structure measurements the size of the test lattice must be large with respect to the mean free path of the neutrons in the energy range to which the parameter that one determines relate. More generally, the neutron energy spectrum at points where measurements in the test lattice are made, should resemble that of corresponding locations in the actual core. For purposes of comparison an infinite lattice spectrum or equilibrium spectrum would be preferable. The low-power PHYSICAL CONSTANTS TESTING REACTOR in the USA and the reactor HECTOR at Winfrith, England were constructed especially for this type of experiment. Although the test samples can be relatively small substitution experiments require a 'driver' reactor, the depreciation and costs of operation of which add to the total expenses.

A critical assembly may be regarded as a zero-power mock-up of the proposed core. The neutron fluxes in these systems are usually limited to a value which permits neutron activation experiments for flux mapping. For this reason the shielding of these reactors is generally designed for low power

operation (up to approximately 1 kW). The KRITO-reactor of the Reactor Centrum Nederland (RCN) is such a facility. The advantages of low power operation are obvious; no special cooling facilities are necessary and, in general, containment requirements are very simple except in those cases where plutonium is used as a fuel. The usefulness of experiments with zero-power reactors is a consequence of the fact that the neutron behaviour does not depend upon the reactor power level, because even at high power levels the neutron density is small with respect to the typical atomic densities. As a result the effects of neutron-neutron interactions are negligible. Hence the neutrons diffuse independently of each other; that is the probability that a neutron will travel a certain distance in a reactor system is not influenced by the presence of others. Therefore equations describing the transport of neutrons, for example the Boltzmann-equation, turn out to be linear in the neutron density. Their solution is much simpler than the solution of the equations describing the transport of gases, see for example WEINBERG and WIGNER [5]. However it should be noted that the equations usually apply to systems in which the neutron population is such that statistical fluctuations in the neutron density may be ignored.

In this thesis a subcritical facility with a relatively low multiplication will be referred to as an exponential assembly. Since leakage and/or absorption of neutrons are in excess of their production a self-sustaining neutron-induced chain reaction of fissions is not possible. In order to maintain a certain neutron level in such an assembly the neutrons must be supplied by an external source. This may be any type of artificial neutron source, such as mixtures of polonium or plutonium with beryllium based on an $(\alpha, n)$-reaction, or a combination of antimony and beryllium based on a $(\gamma, n)$-reaction, neutrons obtained via an accelerator, or neutrons leaking from a nuclear reactor. The last type of source has been used in most of the experiments described in this thesis.

### 1.2 *Use of exponential assemblies*

Exponential assemblies have proved to be useful for the experimental study of multiplying characteristics of reactor systems operating on thermal neutrons. In addition they are excellent devices for training students majoring in nuclear engineering. More than one hundred exponential assemblies are in use at universities in the USA.

An exponential facility is smaller than a critical assembly having the same lattice composition and geometry. Consequently the exponential facility requires less fissile material. Furthermore no complicated and expensive control mechanisms and instrumentation systems are required. Exponential assemblies are easily accessible and in general, moderator-to-fuel ratios can be varied conveniently. In addition the activation level of fuel elements is such that fuel manipulation presents no special problems. These merits lead to easy operation with low operating costs. The speed

with which data can be collected from exponential facilities makes them particularly well-suited for extensive series of measurements.

Originally, exponential assemblies were used only to determine integral reactivity effects such as neutron leakage, material buckling and reflector savings. For these types of experiments neutron fluxes of the order of $10^4$ $n/cm^2 \cdot s$ are sufficient and can be readily obtained using, for example, polonium-beryllium neutron sources. Later, differences were found between the values of the material bucklings measured in exponential assemblies and those measured in critical cores. These differences are due to a greater leakage of fast neutrons from exponential assemblies than from critical cores resulting in spectral differences throughout the assemblies. To what extent the spectra are influenced depends upon the geometry and the type of lattice. Therefore the locations in the exponential assembly where measurements are made, have to be carefully chosen (see also section 1.4).

In view of the current interest in the optimization of the average power densities in and the fuel cycles of water moderated reactors, where the critical size no longer presents a problem since the enrichment of the fuel may always be adjusted, attention has been shifted towards fine structure parameters. In water-moderated reactors first-flight neutrons are important due to the low hydrogen scattering cross-sections at higher neutron energies. In addition the contribution of thermal neutrons to the migration length is low even in spite of the relatively low Fermi-age. This means that fast neutron leakage from water-moderated systems is predominant. Furthermore the transport mean free path is small (on the order of 0.5 cm), as a result of which thermal flux peaking occurs in between the fuel rods. The nuclear properties of these reactors led to the development of refined calculation methods and experimental techniques.

In order to verify current calculation models, increased efforts have been devoted to the development of methods to experimentally determine the thermal utilization factor, resonance capture, fast fission effect, neutron temperature and local power which can be related to effects such as burn-out. Furthermore, emphasis has been placed on measurements concerning the energy distribution of the neutrons (spectral indices) in regard to burn-up predictions. Exponential assemblies may be very useful tools in this respect, if the data are properly interpreted; especially as far as the neutron energy spectrum is concerned.

The experimental determination of fine structure parameters requires frequent activation of small foils or wires of various materials. To obtain sufficient precision in the reaction rates a neutron flux in the region of $10^7$ $n/cm^2 \cdot s$ to $10^8$ $n/cm^2 \cdot s$ is desirable in the lattice cell where the detectors are to be activated. On the order of $10^6$ Ci of antimony or $10^5$ Ci of radium are required to produce these neutron levels from reactions with beryllium. At the Swiss reactor centre in Würenlingen five remotely operated antimony sources with a total strength of $10^5$ Ci($10^{11}$ $n/s$) are in use with the sub-critical facility MINOR [6]. In general it is not practical to obtain such a

flux level with artificial neutron sources. Preference should be given to the use of a reactor as a source when microscopic parameters are to be determined.

Originally subcritical experiments were used only as static devices in which an equilibrium condition was maintained between the neutrons supplied by the external source and those produced and absorbed in the assembly. However varying the source strength either in a pulsed manner or in a sinusoidal way influences the balance, and thus permits to obtain reactivity effects, neutron lifetime and related parameters. MEISTER [7] and KÜCHLE [8] used a pulsed 150 keV Cockcroft-Walton D-T accelerator to investigate prompt neutron decay and reactivity effects in $D_2O$-moderated natural uranium lattices. OGURA, *et al.* [9], used a 300 keV accelerator of this type for determining $k_{\text{eff}}$. KERSTEN [10] applied an accelerator to study the relative effective fraction of delayed neutrons ($\beta_{\text{eff}}/l$) in a subcritical aqueous suspension reactor, in which the fuel is circulating. The theory of pulsed neutron source experiments has been described by BECKURTS [11] and GARELIS, *et al.* [12]. The impulse response of an exponential assembly in particular has been treated by UHRIG [13, 14].

So far, only the advantages of exponential experiments have been outlined. However it should also be noted that their inherent disadvantages limit to a certain extent their application.

In addition to higher leakage rates in comparison with critical assemblies, source effects which are totally absent in a critical facility may cause difficulties in exponential experiments. Furthermore many measurements have been performed in exponential assemblies where the external circumstances are different from those in the actual reactor. Most of the experimental work, for instance, has been done at room-temperature rather than at the desired operating temperature. However in some cases it is possible to simulate some of the high temperature effects such as boiling, see for example Chapter 2. The lack of poisonous fission products and the use of a fuel, the composition of which generally differs from the true composition during the core lifetime can make the distribution of the neutron flux in space and energy in the experiments quite different from that in the actual reactor. Where possible one tries presently to compensate for these effects. In some experiments, carried out at the British reactor establishment in Winfrith, fuel compositions have been adjusted to operational conditions by adding plutonium walls to uranium pellets. Thus the effect of neutron resonance absorption after prolonged irradiation was simulated. In Canadian experiments fission products were added to the fuel to make the experimental conditions more realistic.

Moreover the study of non-uniform lattices and the measurement of small reactivity effects cannot be performed with subcritical facilities when accuracy is required. As a result exponential assemblies usually supply second order information about the nuclear parameters of a cold-clean core. However the experimental results can be compared with theoretical

predictions. As the results of experiments and theory agree more closely, they can be extrapolated with more confidence to the true situation. Therefore exponential experiments provide a relatively inexpensive method to obtain reactor parameters and in addition the possibility to verify not only experimental techniques but also theoretical models.

### 1.3 *Neutron distribution in exponential assemblies.*

As mentioned in the preceding section both the energy and spatial distribution of the neutrons in an exponential assembly generally differ from those in a critical facility. (It should be noted here that local irregularities which occur in a critical facility as a result of the presence of control elements have not been considered). The order of magnitude of these differences depends on a number of factors but primarily on the effective multiplication factor of the assembly. Furthermore – in view of streaming effects – the position of the external source in relation to the geometry and composition of the assembly may be important. Moreover the geometry and the energy spectrum of the source neutrons affect the distribution within the assembly to a certain extent. In some exponential experiments the source has been located in a pedestal which is used as a thermalizer for the source neutrons as well as for source geometry transformation. For small assemblies this may introduce additional problems, as described by KLEIJN, *et al.* [15]. It is obvious that the spatial and energy distribution of the neutrons in an exponential assembly are also influenced by the presence of a reflector.

Because the initial interest in exponential assemblies was related to the study of multiplication rates, one cared only about the asymptotic macroscopic neutron distribution which occurs in relatively large assemblies far from sources and boundaries. To obtain the asymptotic spatial distribution in large natural uranium fueled assemblies FERMI simplified the problem by assuming that the macroscopic thermal neutron flux $\phi_{th}$, at a distance from boundaries and from the extraneous source may be given as a solution of the wave equation:

$$\nabla^2\phi_{th} + B_m^2\phi_{th} = 0 \tag{1.3.1}$$

where $B_m^2$ is the material buckling of the given fuel-moderator system, see GLASSTONE and EDLUND [16]. For a homogeneous bare cylindrically shaped assembly, where the neutrons are supplied by a thermal point source located on the axis at one of the ends, and with the usual boundary conditions, the general solution of Eq. (1.3.1) can easily be found to be:

$$\phi_{th}(r, z) = \sum_{i=1}^{\infty} A_i J_0(\psi_i r) \sinh \beta_i(H-z) \tag{1.3.2}$$

where $H$ = extrapolated height of the assembly

and $\beta_i^2 = \psi_i^2 - B_m^2$.

The values of $\psi_i$ are determined from the relation $J_0(\psi_i R)=0$ in which $R$ is the extrapolated radius of the core. At distances far from the source the contribution of higher harmonics to the total flux may be neglected and Eq. (1.3.2.) can be simplified to:

$$\phi_{th}(r, z) = CJ_0(\psi r)\, e^{-\beta z}\,[1-e^{-2\beta(H-z)}] \tag{1.3.3}$$

in which $C$ is a constant, determined among other things by the source strength. In this case $\psi \equiv \psi_1$ which equals $2.405/R$. The term between the brackets, representing the 'end' effect is not very different from unity as long as $z \ll H$. The exponential behaviour of the neutron flux follows from the term $e^{-\beta z}$. This factor characterises an 'exponential assembly'. The spatial distribution of the epi-thermal neutrons in a bare system will be equivalent to that of the thermal neutrons over a large section of the core. Deviations occur near the boundaries as a result of the differences in cross-sections.

In principle the same approach to obtain the flux distribution has been recommended by KOUTS [17], who adds that in case the assembly is reflected the thermal flux is still given by Eq. (1.3.3) at distances far from the core-reflector interface. However in small highly enriched under-moderated assemblies there is hardly any place 'far' from the interface. A rule of thumb is that the influence of a reflector on the flux distribution in the core is not noticeable more than a migration length from the edge of the core. The influence of the source on the neutron distribution in relation to the multiplication factor has been treated more rigorously by WEINBERG and WIGNER [5].

A rather sophisticated analysis of the macroscopic thermal neutron distribution in a bare exponential assembly has been given by PEAK, *et al.* [18]. PEAK first calculates the distribution of neutrons emitted by the source and which then diffuse through the assembly. For a bare cylindrically shaped homogeneous assembly where a plane thermal source is adjacent to one end, the neutron flux due solely to source neutrons, $\phi_s$ is then found to be:

$$\phi_s(r, z) = \frac{2S}{DR} \sum_{i=1}^{\infty} \left[ \frac{J_0(\psi_i r)\, \sinh\,(\gamma_i [H-z])}{\psi_i J_1(\psi_i R)\, \gamma_i \cosh \gamma_i H} \right] \tag{1.3.4}$$

where $S = S(r) =$ a constant source strength

and $\gamma_i^2 = \dfrac{\Sigma_a}{D} + \psi_i^2 = \dfrac{1}{L^2} + \psi_i^2$.

The source neutrons cause fissions and give rise to fission energy neutrons. A fraction of these neutrons will leak from the assembly while the rest will be captured or slowed down to thermal energies. From PEAK's results which are based on FERMI-age theory, it was derived that the total distri-

bution of thermal neutrons, consisting of source neutrons and lattice born neutrons may be given by Eq. (1.3.5.).

$$(1.3.5)\quad \left\{ \phi_{th}(r,z) = \frac{2S}{DR} \sum_{i=1}^{\infty} \sum_{n=1}^{\infty} \left\{ \left[ \frac{J_0(\psi_i r)}{\psi_i J_1(\psi_i R)\, \gamma_i \cosh(\gamma_i H)} \right] \times \right. \right.$$
$$\left. \left. \left[ \sinh \gamma_i (H-z) + 2 \left( \frac{k_{i,n}}{1-k_{i,n}} \right) \left( \frac{n\pi}{n^2\pi^2 + \gamma_i^2 H^2} \right) \sinh \gamma_i H \sin \frac{n\pi z}{H} \right] \right\} \right.$$

where

$$k_{i,n} = \frac{k_\infty \exp(-B_{i,n}^2 \tau)}{1 + L^2 B_{i,n}^2}$$

and

$$B_{i,n}^2 = \frac{n^2\pi^2}{H^2} + \psi_i^2 \quad \text{(geometrical buckling).}$$

Implicitly the assumption has been made that the absorption cross-sections for the source neutrons equalize the cross-sections for thermalized neutrons.

For a critical facility with the same geometry the thermal flux distribution is given by Eq. (1.3.6).

$$(1.3.6)\quad \phi_{th}^{crit}(r,z) = C J_0(\psi_1 r) \sin \frac{(\pi z)}{H}$$

where $C$ is a power-dependent constant.

Analysing Eq. (1.3.5) and making a comparison with Eq. (1.3.6) one observes that:

*a*) The last term of the sum in the brackets of Eq. (1.3.5) obviously represents the contribution of the fuel-moderator system since it contains $k_{i,n}$.

*b*) When the $k_{i,n}$ are extremely small one measures the diffusion length of the source neutrons in the assembly rather than a material buckling.

*c*) The first mode radial distribution in an exponential assembly is equivalent to the radial distribution in a critical facility. Far from the source and boundaries the higher modes in the radial distribution have disappeared and consequently the neutron distribution is given by the first mode. It is this fact that was recognized by FERMI.

In practical cases, the first term in the brackets of Eq. (1.3.5) which represents the contribution of the external source disappears rather rapidly with increasing values of $z$. The exponential decay of the neutron flux results from the second term and is contained in the factor $\sin(n\pi z/H)$ [5].

Further it can be shown that when $k_{1,n}$ approaches unity the exponential nature of the flux disappears and the sinusoidal distribution in the axial direction becomes predominant. In that case the neutron multiplication in the assembly may be approximated by $1/(1-k_{1,1})$.

When the assembly is radially reflected, as is the case for LEAD (see section 1.4), the neutron distribution may be found by a method analogous to PEAK's. However the boundary conditions are more involved and consequently the mathematical treatment of the problem is more complicated. The final results obtained from a complete analysis of this problem would not yield easily interpretable information. To indicate the calculation method an initial analysis of the LEAD core according to the following simplified model will be given below, where:

*a*) The core consists of a homogeneous mixture of a hydrogeneous moderator with slightly enriched or natural uranium in a cylindrical geometry.

*b*) The core is radially surrounded by a finite reflector of the same material as the moderator. In axial directions the core is bare.

*c*) The size of the core and the reflector is such that diffusion theory is applicable.

*d*) The neutron source is a plane thermal source adjacent to one of the unreflected boundaries. The assumption of a thermal source is justified because 1) the spectrum of neutrons entering LEAD is soft in comparison to a fission spectrum and 2) most of the neutrons will be slowed down to thermal energies within the first 10 cm above the assembly bottom.

The geometry of this model and coordinate system used are shown in Fig. 1.1.

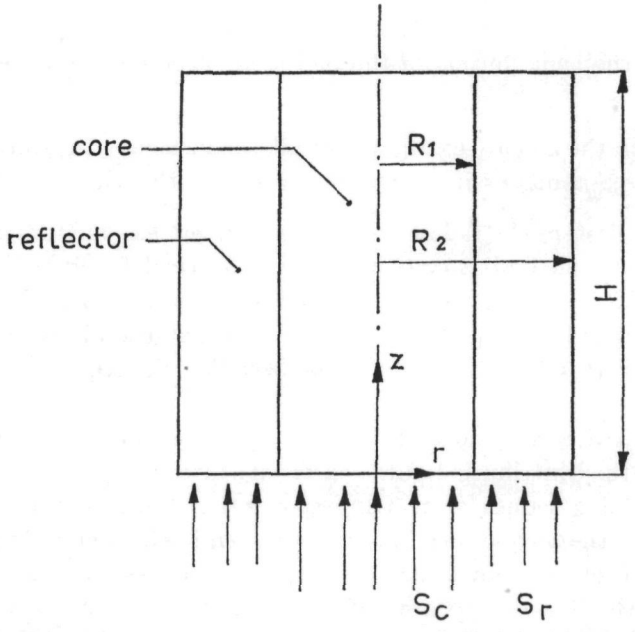


Fig. 1.1. Core-source geometry and coordinate system used in a diffusion calculation of the neutron flux distribution in an exponential assembly.

Superscripts $c$ and $r$ shall indicate whether the parameters in Eqs. (1.3.7–13) refer to neutrons in the core or in the reflector, while the subscript $s$ stands for source neutrons.

The diffusion equation for source neutrons can be written as:

$$\nabla^2 \phi_s(r, z) - \frac{\phi_s(r, z)}{L_s^2} = 0. \tag{1.3.7}$$

Applying a two-group diffusion method to calculate the spatial distribution of the lattice born neutrons, the following equations result:

1. Core region

For the fast energy group (subscript $f$):

$$D_f^c \nabla^2 \phi_f^c(r, z) - \Sigma_f^c \phi_f^c(r, z) + \frac{k_\infty}{p} [\Sigma_{th}^c \phi_{th}^c + \Sigma_s^c \phi_s^c(r, z)] = 0. \tag{1.3.8}$$

For the thermal energy group (subscript $th$):

$$D_{th}^c \nabla^2 \phi_{th}^c(r, z) - \Sigma_{th}^c \phi_{th}^c(r, z) + p\Sigma_f^c \phi_f^c(r, z) = 0 \tag{1.3.9}$$

2. Reflector region

For the fast energy group:

$$D_f^r \nabla^2 \phi_f^r(r, z) - \Sigma_f^r \phi_f^r(r, z) = 0. \tag{1.3.10}$$

For the thermal energy group:

$$D_{th}^r \nabla^2 \phi_{th}^r(r, z) - \Sigma_{th}^r \phi_{th}^r(r, z) + \Sigma_f^r \phi_f^r(r, z) = 0. \tag{1.3.11}$$

The $\Sigma_f^c$ and $\Sigma_f^r$ are the removal cross-sections while $\Sigma_{th}^c$, $\Sigma_{th}^r$ and $\Sigma_s$ are pure absorption cross-sections. $D$ is the diffusion constant for the energy group and region under consideration. The factor $p$ in Eq. (1.3.8) and Eq. (1.3.9) is the resonance escape probability and $k_\infty$ is the infinite multiplication factor. The nuclear constants for the thermal group and the source neutrons in each region are assumed to be equal.

The total thermal flux in the core is:

$$\phi_{\text{total}}^c = \phi_s^c + \phi_{th}^c. \tag{1.3.12}$$

The solution for $\phi_{\text{total}}^c$ may be obtained from Eqs. (1.3.7–12) using the following boundary conditions:

1. At the axis ($r = 0$; $0 \leqq z \leqq H$):

$$\frac{\partial \phi_s^c}{\partial r} = \frac{\partial \phi_{th}^c}{\partial r} = \frac{\partial \phi_f^c}{\partial r} = 0.$$

2. At the core-reflector interface ($r=R_1$; $0 \leqq z \leqq H$):

$$\phi_s{}^c = \phi_s{}^r$$

$$\phi_{th}{}^c = \phi_{th}{}^r$$

$$\phi_f{}^c = \phi_{th}{}^r$$

$$D_s{}^c \frac{\partial \phi_s{}^c}{\partial r} = D_s{}^r \frac{\partial \phi_s{}^r}{\partial r}$$

$$D_{th}{}^c \frac{\partial \phi_{th}{}^c}{\partial r} = D_{th}{}^r \frac{\partial \phi_{th}{}^r}{\partial r}$$

$$D_f{}^c \frac{\partial \phi_f{}^c}{\partial r} = D_f{}^r \frac{\partial \phi_f{}^r}{\partial r}.$$

3. At the horizontal plane $z=0$ $(0 \leqq r \leqq R_2)$:

$$-D_s{}^c \frac{\partial \phi_s{}^c}{\partial r} = S^c \quad \text{(constant source strength)}$$

$$-D_s{}^r \frac{\partial \phi_s{}^r}{\partial r} = S^r \quad \text{(constant source strength)}$$

$$\phi_{th}{}^c = \phi_{th}{}^r = \phi_f{}^c = \phi_f{}^r = 0.$$

4. At the horizontal plane $z=H$ $(0 \leqq r \leqq R_2)$:

$$\phi_s{}^c = \phi_{th}{}^c = \phi_f{}^c = \phi_s{}^r = \phi_{th}{}^r = \phi_f{}^r = 0$$

5. At the outer reflector boundary ($r=R_2$; $0 \leqq z \leqq H$):

$$\phi_s{}^r = \phi_{th}{}^r = \phi_f{}^r = 0$$

Furthermore the total neutron flux is nowhere negative. Prior to determining $\phi_{th}{}^c$ the source flux $\phi_s{}^c$ has to be calculated. Using a method developed by KAPER and HANGELBROEK [19] to obtain the flux distribution due to source neutrons only, the function $\phi_s{}^c(r, z)$ must then be separated into two functions. One of these functions describes only bare core conditions, while the other accounts for the additional effects introduced by the reflector. Both functions are subjected to different boundary conditions at the core-reflector interface and at the plane $z=0$ but in such a way, that their sum contains the initial boundary conditions.

When further simplifying the calculation model in such a way that the source neutrons are only incident upon the core region ($S(r)=S^c$ for $0 \leqq r \leqq R_1$ and $S(r)=0$ for $R_1 \leqq r \leqq R_2$) and normalizing $R_1$ to unity the following solution may be found for $\phi_s{}^c$:

$$\text{(1.3.13)} \quad \phi_s{}^c(r,z) = \left\{ \frac{2}{D_s{}^c} \sum_{i=1}^{\infty} \frac{J_0(\psi_i r)}{\psi_i J_1(\psi_i R_1)} \frac{\sin \gamma_i (H-z)}{\gamma_i \cosh \gamma_i H} + \frac{2}{H} \sum_{j=0}^{\infty} P_j I_0(\delta_j r) \cos \theta_j z \right\} S^c$$

where: $P_j$ is a constant depending on the nuclear properties and the dimensions of the core and the reflector,

$$\theta_j = (j+\tfrac{1}{2})\frac{\pi}{H} \quad \text{and} \quad \delta_j^2 = \theta_j^2 + \frac{1}{(L^c)^2}.$$

In this case the radial distribution of source neutrons is essentially a $z$-dependent combination of $J_0$ and $I_0$ functions. Comparing Eq. (1.3.13) with Eq. (1.3.4) the conclusion may be that the $I_0$ function in Eq. (1.3.13) represents the reflector influence. So far the analysis has not been too complicated and the expression for $\phi_{th}{}^c$ may now be obtained in a straightforward way. However the analytical complexity of the final result is such that practical rules of general validity in regard to the influence of the reflector on the neutron flux distribution in the core, more accurate than the rule of thumb mentioned earlier, can not be derived. Therefore it is not very meaningful to further continue this analysis.

It is obvious that even for this simple system a numerical treatment using a digital computer is preferable when one is interested in the actual flux distribution. The disadvantage of a numerical analysis is also that of drawing conclusions from the results which are of general validity unless many cases have been calculated.

Whereas the prime interest in this project was devoted to microscopic reactor parameters, the macroscopic flux distribution in LEAD has not been calculated but was only obtained experimentally, see Fig. 1.7 and Fig. 1.8. Knowledge of this distribution is required for proper selection of positions in the assembly suitable for fine structure measurements and for corrections to be applied to the results of these measurements (see Chapters 4 and 5).

## 1.4 *The Light water Exponential Assembly in Delft* (LEAD).

### 1.4.1 Construction of the assembly.

The exponential assembly LEAD consists of a tank, 140 cm square, 125 cm in height, made of 10 mm thick aluminium. In this tank the fuel elements are positioned vertically, in an array determined by guide holes drilled in two removable grid plates (Fig. 1.2). These plates are made of 20 mm thick Perspex. One grid plate is located near the bottom of the tank, while the second is fixed at about 20 cm above the bottom. This construction ensures a stable position of the elements in combination with easy access to the space between the elements so as to facilitate flux mapping, etc. Different lattice configurations can be studied in the facility by using appropriate grid plates.

Each fuel element is composed of five annularly shaped natural uranium metal slugs with an outer diameter of 28.5 mm and an inner diameter of 15.0 mm. The length of one slug is 205 mm, consequently an element is 1025 mm long. The slugs are canned in a 0.75 mm thick aluminium tube

(purity 99.5 %) to which an aluminium bottom plug is welded. The elements are provided with aluminium and rubber top plugs, which can be removed easily to permit insertion of different cladding materials or neutron detectors inside the fuel annulus. About 330 elements (corresponding to 2.9 tons of natural uranium) are placed inside the tank.

The tank is filled with light water up to a level just beneath the top of the fuel elements because the top plugs are not completely water-tight. In order to prevent a direct water-fuel contact, as a result of which contaminations may occur, the tank is equiped with an overflow device.

Since the assembly has neither a top nor a bottom reflector, simple end-corrections can be made in the axial neutron distribution to obtain the

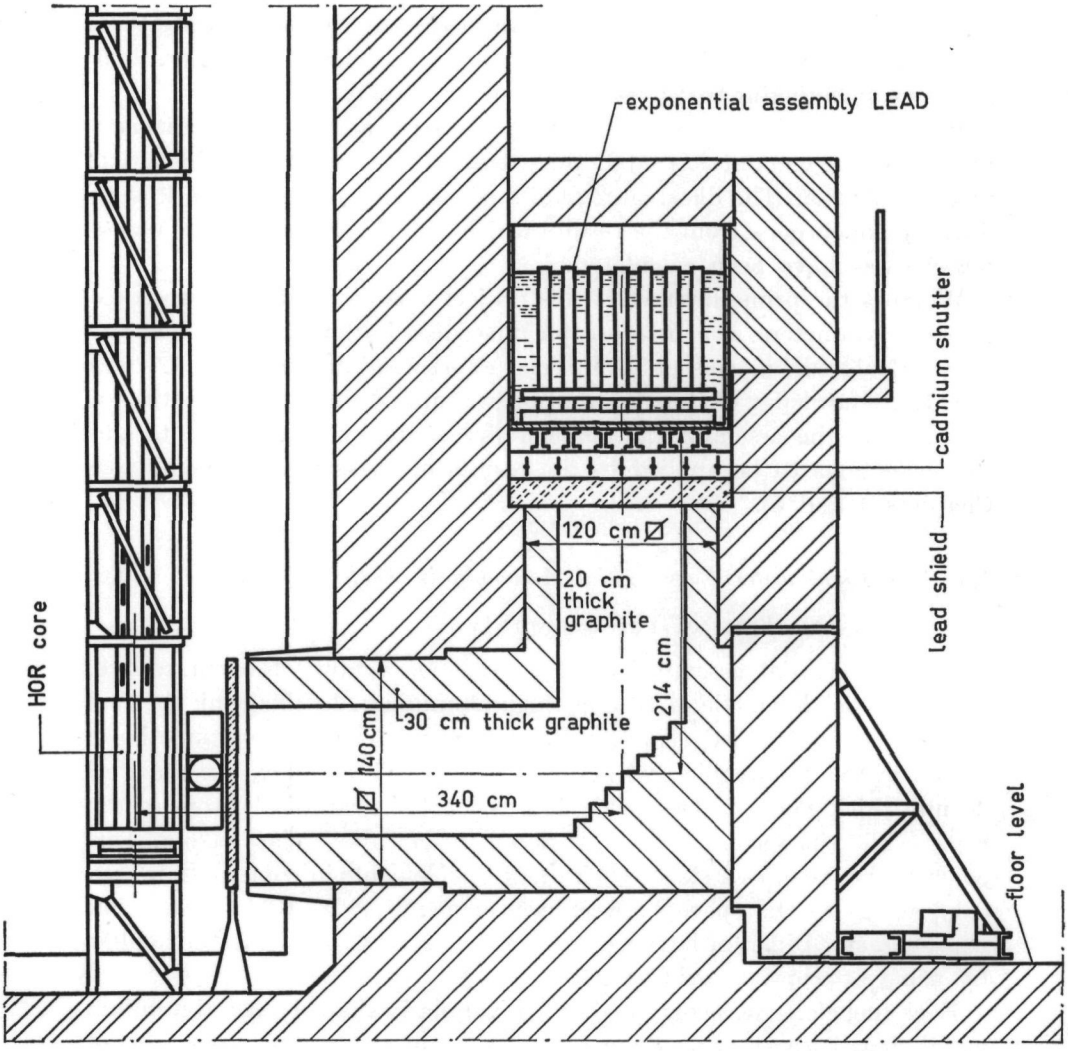


Fig. 1.3. Cross-section of the exponential assembly LEAD placed in the vertical access of the thermal column of the HOR.

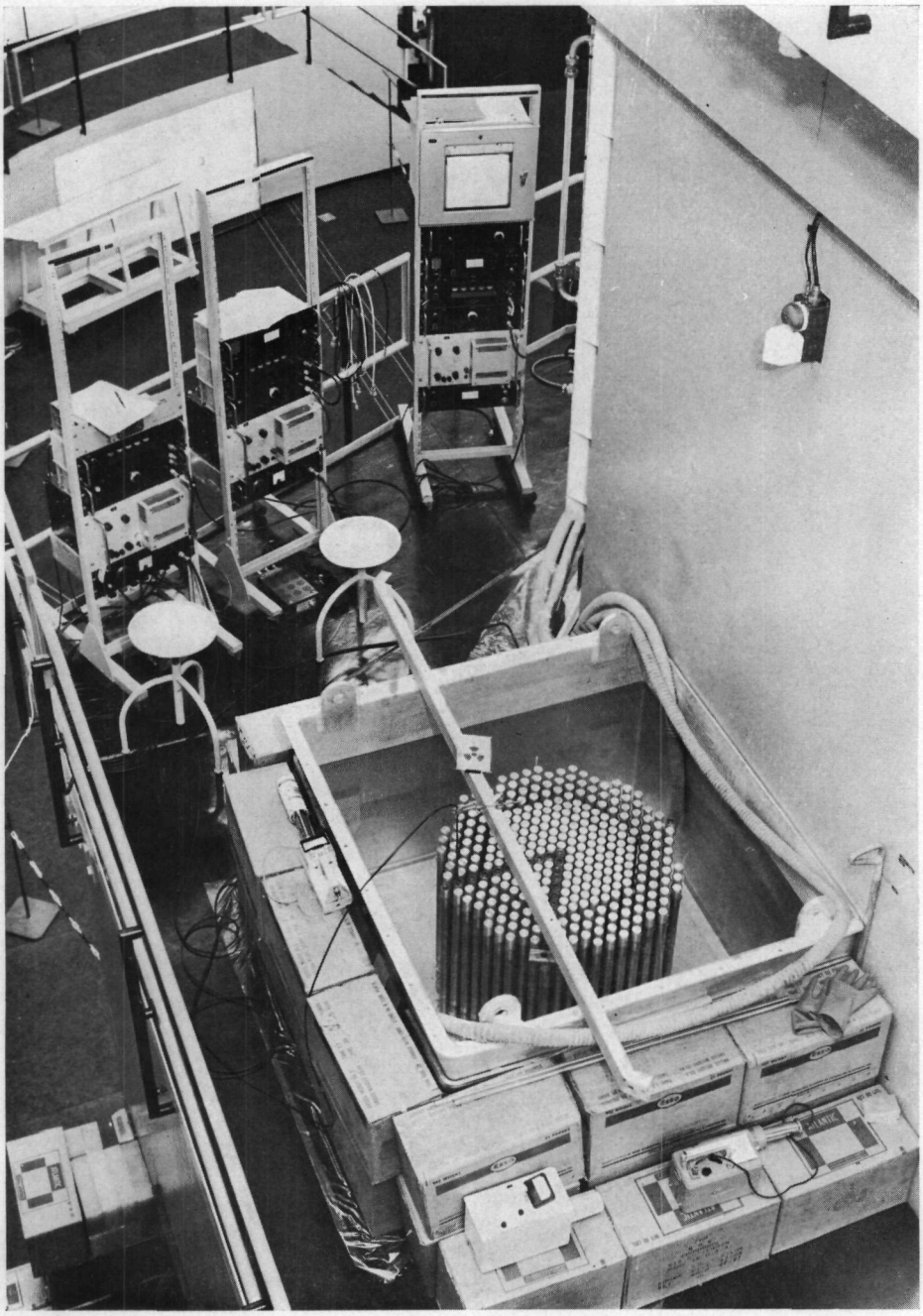

Fig. 1.2. The exponential assembly LEAD. The top shield has been removed.

exponential decay of the neutron flux. Radially the core is surrounded by a water reflector which is thick enough to be considered infinite from a reactor physics point of view. Precautions have been taken in regard to the conductivity and pH of the water, in order to reduce corrosion of the aluminium cladding.

The tank was placed in the vertical access to the thermal column of the swimming pool reactor HOR of the REACTOR INSTITUUT at Delft, which reactor served as the neutron source (Fig. 1.3). During the measurements the reactor power was limited to 200 kW. At this power level a neutron flux on the order of $3.10^7$ $n/cm^2 \cdot s$ was measured near the bottom of the aluminium tank.

The assembly is surrounded by gamma- and neutron shields when the reactor is operating; specifically, a 60 cm thick normal concrete block covers the top, which reduces radiation below the maximum permissible level. A cadmium shutter was placed underneath the tank permitting the thermal neutron level in the assembly to be lowered when no measurements are being made. However, since the spectrum of the neutrons entering the assembly is rather hard – with copper foils a cadmium-ratio of about 20 has been measured underneath the shutter – the thermal neutron level is reduced only by a factor of 4 when the shutter is closed. At the time that the shutter was designed it could, because of other experiments to be carried out in the thermal column, not be foreseen that, in order to reach sufficiently high neutron levels in the assembly, it would be necessary to remove most of the graphite from the column. This fact accounts for the hardness of the spectrum. Using boron as effective shutter material would have been more appropriate.

### 1.4.2. Core arrangement

As already briefly outlined in the introductory Chapter techniques for the experimental determination of fine structure parameters such as the *thermal utilization factor*, the *resonance escape probability* and the *fast fission factor*, can be conveniently tested when applied to lattices with strong heterogeneities. It was possible to realize an exponential assembly with a lattice composition showing these heterogeneities using the annularly shaped fuel slugs.

Rather than constructing a simple assembly it was believed instructive to add some special features to assist in relating the experiments to power reactor conditions. The LEAD facility should then represent a section of a boiling water reactor lattice with integral nuclear superheat throughout the entire core. This reactor concept may be advantageous for intermediate power levels, see Chapter 3. Steam is supposed to be generated as a result of boiling of water on the outside of the fuel elements while the steam is thought to obtain a superheated condition inside the elements. Boiling of water is simulated by air injection in the water region while the influence of the presence of superheated steam on the neutron moderation

has been taken into account by inserting expanded polystyrene in the 'steam' region. Thus, as far as neutron diffusion is concerned, operational conditions with respect to temperature were obtained. It should be recognized that no Doppler-effects can be demonstrated this way. In Chapter 2 the simulation of operational conditions is treated in more detail.

In order to simulate additional power reactor requirements the condition was set that the horizontal flux distribution should be as flat as possible throughout the assembly, when the moderator void fraction was about 35 %. This value was chosen on the basis that it represents approximately the average value in existing boiling water-reactors. In general the void fraction near the outlet of the fuel channels in a boiling water-reactor is limited to about 70 % because of instability phenomena which may arise when this value is exceeded in the temperature range where these reactors are normally operated. Whereas only natural uranium was available the one method of influencing the horizontal flux distribution was to change the moderator-to-fuel volume ratio of the unit cell over the radius of the core. Consequently the value of $k_\infty$ is primarily affected due to a change in the product of $p$ and $f$ rather than a change in $\eta$ which is common practice for power reactor cores.

Instead of applying a continuous radial increase of the water-to-uranium

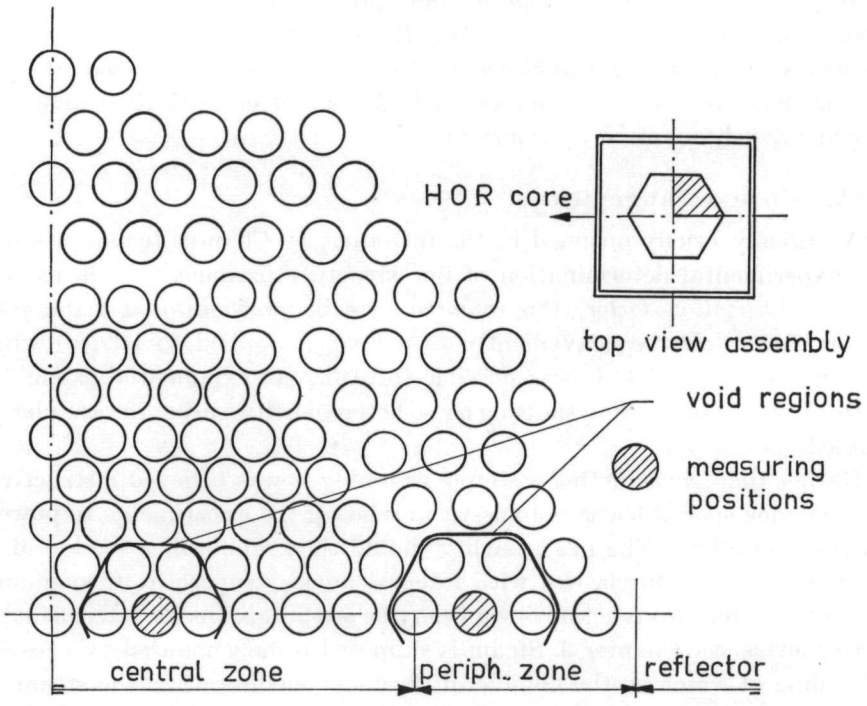


Fig. 1.4. Configuration of fuel elements in the two-zone LEAD core. Only one quarter-section has been drawn. The regions, which could be voided and in which the microscopic parameters have been measured are indicated.

ratio it was decided to make two concentrical core regions of about equal volumes with uniform but different values of the water-to-fuel volume ratio, as is illustrated in Fig. 1.4.

In order to determine the appropriate water-to-fuel volume ratio in each of the two zones, the product of the thermal utilization factor $f$ and the resonance escape probability $p$ was calculated for different values of the water-uranium ratio and different void fractions in the unit cell. Actually the value of $k_\infty$ should have been determined. However it can be shown that variations which occur in $\eta$ and $\varepsilon$ do not seriously affect the value of water-to-fuel ratio that corresponds to maximum neutron multiplication. For elements clad on the outside with 1.5 mm and on the inside with 1 mm thick aluminium the factors $f$ and $p$ have been calculated for water-to-fuel ratios varying between 0.65 and 4.00; and for void fractions of 0 %; 20 %; 35 % and 50 %. As mentioned earlier, in the assembly itself the outside cladding could be reduced to 0.75 mm. An inside cladding was not used except for rods surrounding the unit cells where the fine structure measurements were made. In these cases 0.3 mm thick pure nickel was used as a material neutron physically equivalent to claddings applied in superheated steam environments. The thermal and epi-thermal neutron flux distributions through the unit cell from which $f$ and $p$ have been calculated, were obtained using two group diffusion theory. The nuclear constants used in the calculations are given in Table I.1.

TABLE I. 1

Nuclear constants used in the diffusion calculations of $p$ and $f$ (taken from ref. [20]).

| Energy group | Constant | | Material | | |
|---|---|---|---|---|---|
| | | | Nat. U | $H_2O$ | Al |
| Thermal | $\Sigma_a(2200)$ | [cm$^{-1}$] | 0.364 | 0.022 | 0.014 |
| | $\Sigma_s$ | [cm$^{-1}$] | 0.397 | 3.45 | 0.084 |
| | $D$ | [cm] | 0.725 | 0.142 | 3.96 |
| | $L^2$ | [cm$^2$] | 2.26 | 7.28 | 400 |
| Fast | $\Sigma_{rem}$ | [cm$^{-1}$] | | 0.585 | |
| | $\Sigma_a$ | [cm$^{-1}$] | 0.0825 | | |
| | $D$ | [cm] | 0.806 | 0.0977 | |

Neutron leakage from the unit cell was ignored (infinite lattice approximation). The effect of the cladding material on the value of $f$ has been taken into account. In the calculation of $p$ absorption of epi-thermal and fast neutrons in the cladding material was neglected. Since the space inside the fuel annulus was not to be filled with water, the fuel distribution was thought to be homogeneously distributed inside the outer radius of the fuel element (see also Chapter 4). The voids were assumed to be homogeneously spread throughout the water, and their influence on the parameters was incorporated by using the reduced water densities in the

cross-section determinations. The results are plotted in Fig. 1.5 showing $p \cdot f$ as a function of the unit cell radius for various void fractions, and as a function of the water-to-fuel volume ratio in the zero-void condition.

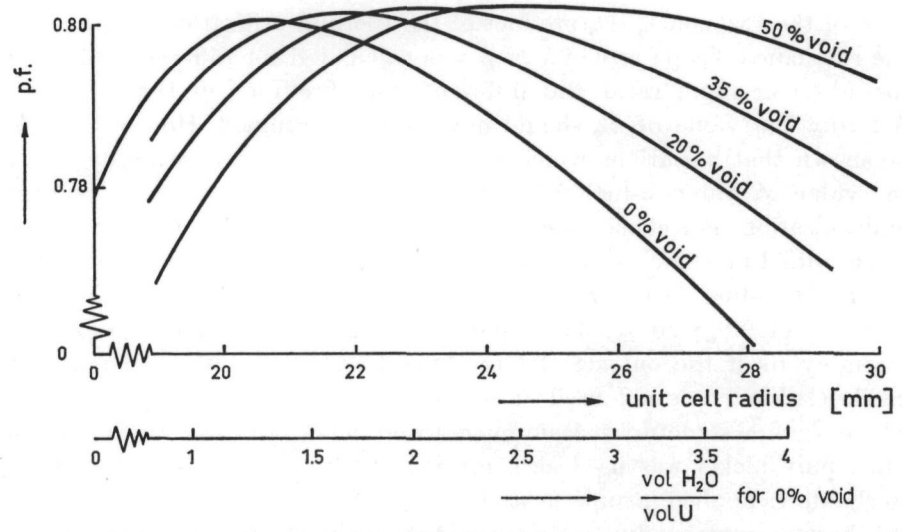


Fig. 1.5. The product $p.f$ calculated by diffusion theory as a function of the unit cell radius for various void fractions in the water and as a function of the water-to-fuel volume ratio in the zero void condition.

A few checks on the $f$-value were made using Carlson's $S_4$ approximation [5] to the transport equation. This method was selected in view of an available computer program. The results of these calculations showed that the $f$-values obtained by diffusion theory were on the order of 3.5 % higher. The differences increase when the water-to-uranium ratio increases. Because the interest was devoted to the position of the maxima of $p \cdot f$ and their shifts as a function of the water-to-fuel ratio rather than to the absolute values the use of diffusion theory was justified [21].

The values of the water-to-fuel ratios for the two regions were selected from Fig. 1.5 on the basis of the following arguments: The effective multiplication factor $k_{\text{eff}}$ of the assembly as a whole should be as high as possible under all circumstances (zero-void and voided conditions) while further flux flattening should occur with increasing void fractions reaching an optimum at about 35 % void. The latter condition requires the peripheral zone to be critically moderated in this situation, resulting in over-moderation when no voids occur. To obtain the flattening effect the central zone has to be undermoderated in the voided condition. In combination with the required high multiplication the choice of an optimum moderated central zone in the zero-void condition is obvious.

For the central zone a water-to-fuel volume ratio of 1.14 was selected which corresponds to a unit cell radius of 20.3 mm. In the peripheral zone this ratio was chosen to be 2.34, equivalent to a unit cell radius of 24.1 mm.

These ratios are given for the zero-void condition. If the fuel elements in both zones are placed in a triangular array, the element piches then become 38.1 mm for the central zone and 45.7 mm for the peripheral zone.

### 1.4.3. Thermal column arrangement

The thermal column is an iron structure lined on the inside with boral plates, the whole arrangement being contained within the concrete wall of the pool, facing the HOR-core (see Fig. 1.3). At the core side the column is separated from the pool water by an aluminium box. Entrance to the column is obtained by removing a heavy concrete door at floor level (horizontal access) or by lifting the hatch at the first floor around the reactor (vertical access). In the space obtained after removing the hatch the exponential assembly is placed on top of a cadmium shutter covered with lead, 10 cm thick. To satisfy the requirement of a high neutron source level, only the sides were covered with graphite. This combines a low neutron absorption in the column together with a reduction in neutron leakage from the column and absorption in the boral plates.

Experiments were performed to determine the thickness of graphite that would yield the highest neutron flux in the column per unit reactor power. Therefore the neutron flux was measured in various vertical planes in the column by activating gold, copper and indium foils. The results led to the conclusion that a thickness of 30 cm would be the best for this purpose. In order to increase the number of neutrons entering the tank an additional amount of graphite was placed in the column underneath the vertical entrance.

For the experiments it is desirable that the flux in LEAD due to source neutrons only, has a radial buckling distribution approximately that of neutrons born in the assembly. Although it should be recognized that the spatial buckling distribution is neutron energy dependent a matched buckling reduces the height over which the source influence is noticeable. The differing spectrum of the neutrons entering the assembly is a second order effect, since most of the neutrons are slowed down to thermal energies within the first 20 cm in the tank. Because the flux distribution in the assembly is required to be as flat as possible the same condition has to be met by the entering current.

Because the radial distribution and the number of neutrons entering the tank depend on the way the graphite is stacked underneath the assembly, measurements have been performed with various geometries. The best results were obtained with a staircase-type arrangement of graphite blocks as indicated in Fig. 1.3 [22]. Equivalent results have been obtained by MADNELL, *et al.* [23] for a graphite lined cavity at the Massachusetts Institute of Technology (MIT).

With this arrangement of the thermal column flux measurements were made near the bottom of the water-filled tank, prior to loading the fuel elements. The results are shown in Fig. 1.6. From this figure it can be

seen that the flux is fairly symmetrical about the axis of the assembly. The difference in the flux level at the sides as compared to the centre is on the order of 33 %. By irradiating some gold foils in the assembly which were then counted using a $4\pi(\beta, \gamma)$-coincidence technique the absolute value of the neutron flux level was measured with an accuracy of about 10 %. The maximum value amounts to $3.3 \times 10^7$ $n/cm^2 \cdot s$ at a reactor power of 100 kW.

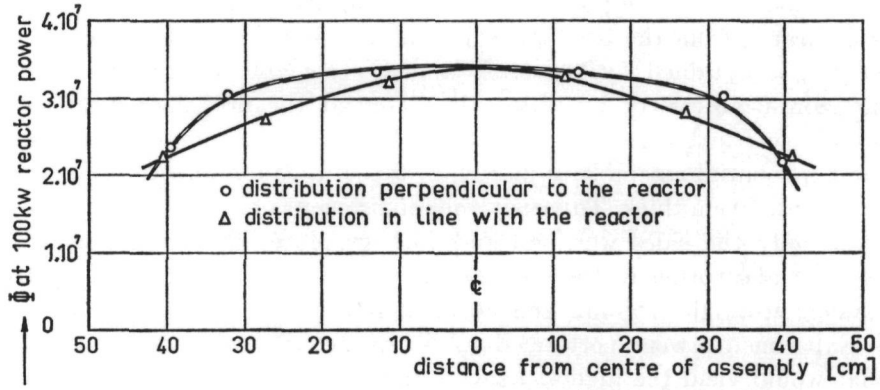


Fig. 1.6. Horizontal neutron flux distribution as a result of neutron leakage from HOR near the bottom of the aluminium tank, which is only filled with water.

### 1.4.4 Integral physical characteristics

For the purpose of reducing radiation levels a 5 Ci plutonium-beryllium neutron source was used during the initial fuel loading experiments rather than neutrons coming from the operating reactor. This source was positioned in the centre of the assembly and mounted on the upper grid plate. Using two $BF_3$-counters, data were obtained to make the conventional multiplication plots while loading fuel.

After loading the central zone a radial flux distribution was measured at a height of 50 cm from the bottom of the assembly. Here the source influence should be negligible. In addition the axial flux profile was determined. From these data $k_\infty$ for the central zone was calculated to be 0.91 resulting in a $k_{eff}$ of 0.62 ($\pm$ 0.05). Next the peripheral zone was loaded and the radial and axial flux measurements were repeated. The effective multiplication factor of the assembly had increased to 0.75 ($\pm$ 0.05). Then the neutron source was removed from the assembly and using reactor neutrons the flux distributions were measured once again. The results are presented in Fig. 1.7 and Fig. 1.8. The discrepancies in the curves for the 'source' distributions and the 'reactor' distributions are a result of the difference in source geometry. The reactor source resembles a plane source while the plutonium-beryllium source may be considered as a point source. The measurements with the plutonium-beryllium source were made with a small $BF_3$-counter. When the reactor was supplying the neutrons a less sensitive $^{235}U$-fission chamber was used. These detectors

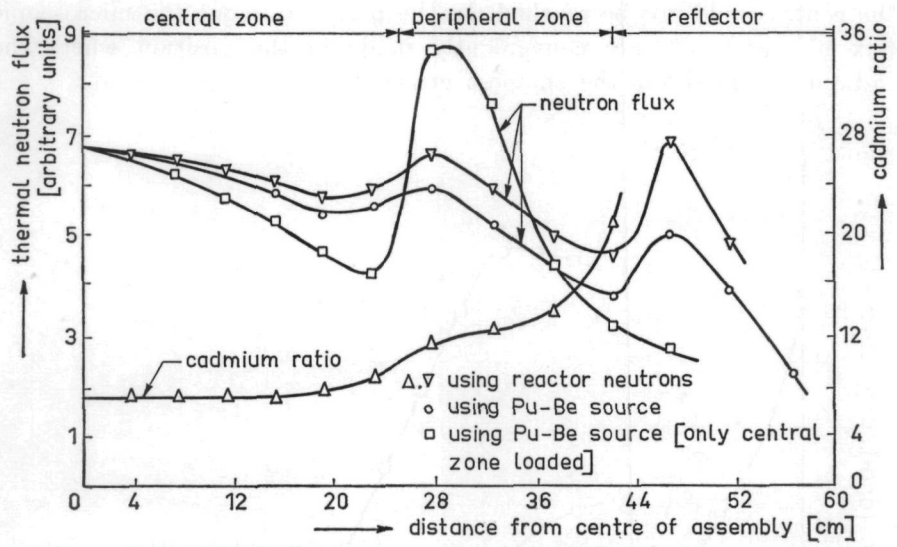


Fig. 1.7. Radial distribution of the neutron flux and the cadmium-ratio in LEAD.

were inserted inside the central gap of the fuel elements. As a consequence the fluxes have been measured in a depressed flux region of the unit cell. However the curve thus obtained hardly differs from the actual macroscopic thermal flux distribution.

Because the results of intracell measurements can be interpreted more correctly when they have been made at lattice positions where the spectral- and the macroscopic flux distribution do not vary, the cadmium-ratio was measured in axial and radial directions. The results of these measurements are also given in Fig. 1.7 and Fig. 1.8. From the cadmium-ratio data it can be seen that the axial equilibrium spectrum in the central zone is harder than the spectrum of the neutrons entering the assembly. As the equilibrium spectrum is reached at about 20 cm from the bottom, the location at which the intra cell measurements are to be performed should be taken at least above a height of 20 cm. However when voids are introduced in lattice sections the influence on the neutron spectrum of a heterogeneous distribution of air bubbles right after their injection results in additional disturbances, see Chapter 2. From vertical cadmium-ratio distributions with various voided conditions it was concluded that the height must be at least 40 cm or above. The fine structure measurements were made later at a height between 40 and 50 cm from the bottom (see Chapters 4 and 5). Furthermore it can be seen that the radial change in the spectrum is relatively small in the central zone. In view of the flat flux requirement, the intracell measurements should take place as close to the axis as possible. That the measurements were not made in the central unit cell itself is due to the fact that the top shield initially used consisted of two equal parts. In order to avoid time consuming manipulations necessary to remove both sections only one part was removed. As a consequence

the centre could not be reached. In the peripheral zone the microscopic flux measurements are conveniently made in the position where the cadmium-ratio shows the smallest gradient.

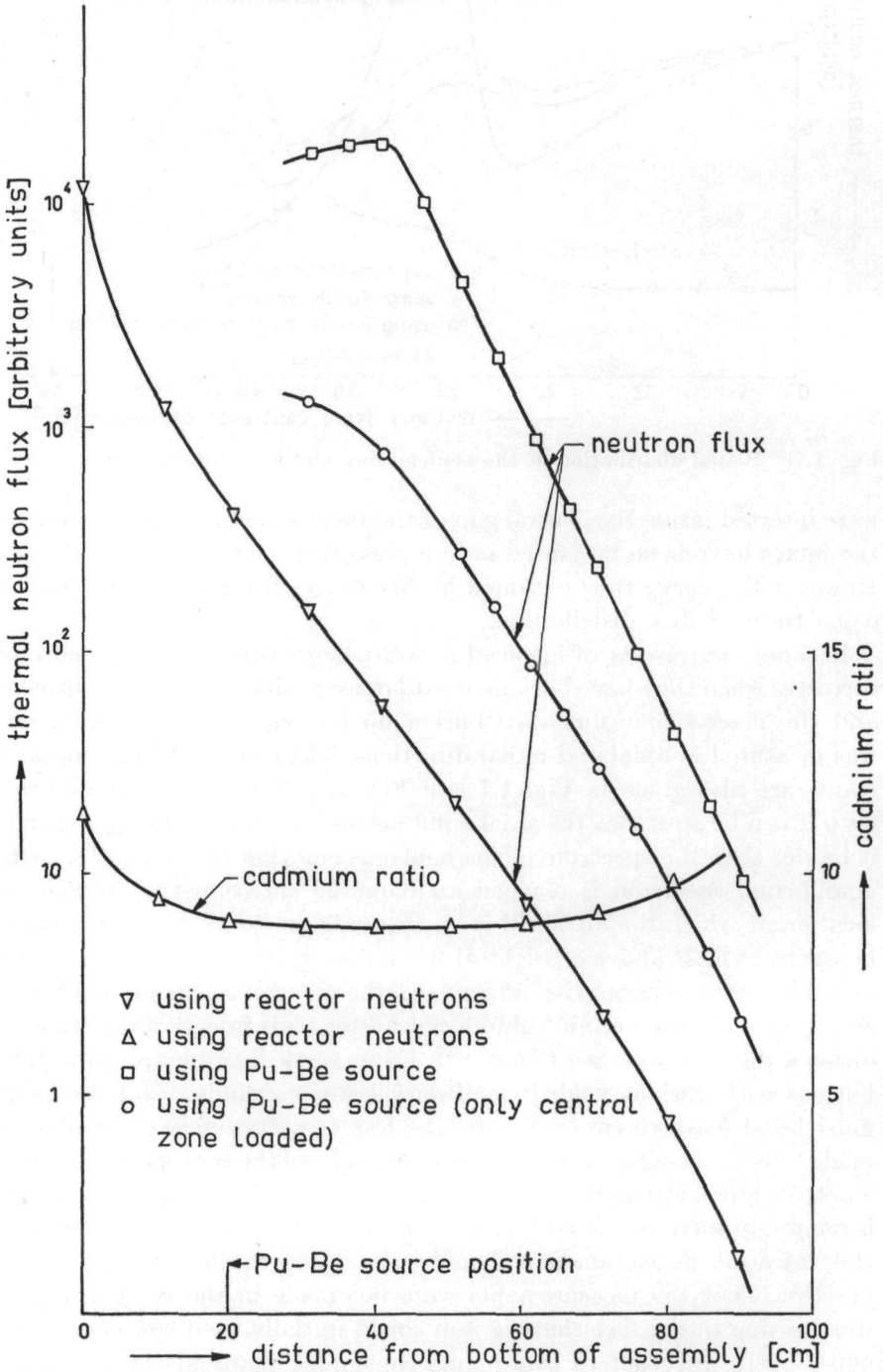


Fig. 1.8. Axial distribution of the neutron flux and the cadmium-ratio in LEAD.

### 1.4.5 Final remarks concerning the LEAD facility

The water-to-fuel volume ratios in the two zones of the LEAD-facility have been selected such, that a certain flattening occurs in the radial neutron flux distribution in the cold-clean condition when the void fraction in the water increases from zero on upwards to a specific value. Thereabove the thermal flux level in the centre may even become lower than near the outer boundaries. In an operating reactor having a uniform composition, the flux will have an additional tendency to flatten as a result of burn-up.

The initial idea was to simulate the effect of boiling of water in the proposed boiling water-reactor with integral superheat throughout the entire core. Then, by determining the macroscopic flux distribution the flattening effect might have been observed. However the technical problems associated with the creation of a homogeneous reduction in water density over the total core volume were such, that it was decided later to introduce voids only in a region of each of the core zones where the microscopic parameters were to be measured. Nevertheless it can be concluded from Fig. 1.7 which shows the radial flux distribution in the zero void condition, that a flattening of the flux would indeed have occurred at higher void fractions. In the central zone $k_\infty$ would decrease, which will lead to a reduction in thermal neutron production. In the peripheral zone $k_\infty$ will increase as a result of which the thermal flux level rises *). The combined effect then gives the expected result. It should be noted that a complete flat flux distribution can never be obtained in a simple two zone core.

The location of the assembly in the vertical access of the thermal column is favourable in regard to accessibility and from a technical point of view. However whereas the assembly is placed far from the HOR-core the flux levels in the assembly are relatively low. At 45 cm above the bottom the neutron flux in LEAD was found to be on the order of $5 \times 10^6$ $n/cm^2 \cdot s$ which led to poor counting statistics in the fine structure measurements. Positioning the exponential assembly inside the thermal column would have yielded considerably higher flux levels but also a number of technical difficulties. In that case it would have been necessary to place the fuel rods horizontally. Since the 0.75 mm thick aluminium outer cladding is not sufficiently rigid to support the fuel properly additional spacer material would have been required. Further the air injection method to create voids could not have been used. Still if the experiments were to be repeated in order to determine an accurate value of the microscopic reactor parameters rather than a trend, which is the object of this study, location in the thermal column would be seriously considered. Another point which would receive more attention is the positioning of the fuel rods especially in regard to their mutual distance. In the present construction the elements are kept in place by means of two grid plates

---

*) From experimental results described in Chapter 5 this supposition was shown to be wrong.

located at and 20 cm above the bottom of the assembly. A small gap (0.3 mm) is required between the outer diameter of the fuel elements and the holes in the grid plates because it was experienced that under the weight of the fuel rods the aluminium bottom plugs tend to blow up a little. In order to be able to remove the fuel elements from the core it was necessary in the course of the experiments to re-drill the holes in the grid plates. As a result the distance between two neighbouring fuel rods in the central zone at a height of 50 cm from the bottom, which is supposed to be 7.6 mm could have varied between 6.4 mm and 8.4 mm. This corresponds to a theoretical uncertainty in the water-to-fuel volume ratio between $-16$ % and $+12.5$ %. However in practice the error was about $\pm$ 4 % which is still serious.

The fact that natural uranium metal has been used in this experiment rather than slightly enriched $UO_2$, which is common for all water reactors, is of minor importance for the interpretation of the results. The microscopic reactor parameters $\varepsilon$, $p$ and $f$ depend more strongly on the neutron energy spectrum in combination with the water-to-fuel volume ratio than on the enrichment as long as the latter is small.

## REFERENCES


1. Naudet, R., Examen critique des méthodes de substitution, a CEN-Saclay reactor group report (EACRP–L32), (1963).
2. Graves, W. E., Analysis of the substitution technique for the determination of $D_2O$ lattice bucklings, DP–832 (EACRP–L22), (1963).
3. Casini, G. and J. Mégier, Critical analysis of the progressive substitution method for material buckling experiments, Paper SM–42/51, Proc. Symposium on Exponential and Critical Experiments, Vol. III, IAEA, Vienna (1964)
4. Blaeser, G., An application of heterogeneous reactor theory to substitution experiments, Paper SM–42/52, Proc. Symposium on Exponential and Critical Experiments, Vol. III, IAEA, Vienna (1964)
5. Weinberg, A. M. and E. P. Wigner, The physical theory of neutron chain reactors, The University of Chicago Press, Chicago (1958).
6. Meier, R. W., H. R. Lutz and E. Utzinger, MINOR, a subcritical facility for heavy water lattice studies, Paper SM–42/55, Proc. Symposium on Exponential and Critical Experiments, Vol. II, IAEA, Vienna (1964)
7. Meister, H., Pulsed-neutron experiments on subcritical heavy water reactors, Heavy Water Lattices, Second Panel Report, Technical Report Series 20, IAEA, Vienna, 163 (1964)
8. Küchle, M., Pulsed-neutron measurements on a heavy water reactor at zero energy, Paper SM–42/6, Proc. Symposium on Exponential and Critical Experiments, Vol. II, IAEA, Vienna (1964).
9. Ogura, S. *et al.*, Subcritical reactivity measurements by the pulsed-neutron source method, Paper SM–42/2, Proc. Symposium on Exponential and Critical Experiments, Vol. II, IAEA, Vienna (1964).

10. KERSTEN, J. A. H., Experiments with a subcritical reactor, in which an aqueous suspension of $UO_2$ particles is circulating, Reactor Science and Techn., 16, 15 (1962).
11. BECKURTS, K. H., Measurements with a pulsed-neutron source, Nucl. Science and Eng., 2, 516 (1957).
12. GARELIS, E., Theory of pulsing techniques, Nucl. Science and Eng., 18, 242 (1964).
13. UHRIG, R. E., The impulse response of an exponential assembly, Paper SM–42/43, Proc. Symposium on Exponential and Critical Experiments, Vol. III, IAEA, Vienna (1964).
14. ————, Neutron waves in a subcritical assembly, Trans. American Nucl. Soc. 22, 79 (1959).
15. KLEIJN, H. R., A. W. VAN DER HEIJDEN and H. VAN DAM, Subcritical experimental work at the Delft Reactor Institute, Paper SM–42/57, Proc. Symposium on Exponential and Critical Experiments, Vol. III, IAEA, Vienna (1963).
16. GLASSTONE, S. and M. C. EDLUND, The elements of nuclear reactor theory, D. Van Nostrand Company, Inc., NY., Chapter IX, 281, (1952).
17. KOUTS, H., Measurement of reactor constants, Nuclear Engineering Handbook (Ed. Etherington), Mc.Graw-Hill, 5–118 (1958).
18. PEAK, J. C., I. KAPLAN and T. J. THOMPSON, Theory and use of small subcritical assemblies for the measurement of reactor parameters, NYO–10204 (1962).
19. KAPER, H. G. and R. J. HANGELBROEK (private communication).
20. Argone National Laboratory, Reactor Physics Constants, ANL–5800, second ed., USAEC (1963).
21. HEIJDEN, A. W. VAN DER, RID internal report 131–63–05 (1963).
22. DURING, W. A., private communication.
23. MADELL, J. T., T. J. THOMPSON, A. E. PROFIO and I. KAPLAN, Spatial distribution of the neutron flux on the surface of a graphite-lined cavity, NYO–9657 (1962).

CHAPTER 2

# SIMULATION OF OPERATIONAL CONDITIONS

## 2.1 *General aspects*

As described in Chapter 1 the exponential facility LEAD has been used to study the thermal utilization factor and the resonance escape probability as a function of the liquid coolant void fraction in a simulated integral nuclear superheat lattice for the initial clean fuel condition. The latter addition includes that influences of burn-up have not been considered.

Due to laboratory restrictions, true boiling of water and consequent superheating of steam under operational pressure conditions (up to 60 at) cannot be practically realized in the assembly. However the actual boiling effect (bubbles) and the influence of the presence of steam on the diffusion of neutrons can be properly simulated under room-temperature conditions. The experiments performed in this way have the advantage over *real* experiments that other temperature effects are eliminated.

For instance, raising the water temperature reduces its density from 1 g/cm$^3$ at 4° C to 0.32 g/cm$^3$ at the critical temperature (374.15° C). Up to 175° C the reduction is about 10 % while at 280° C – a common operating temperature in the boiling region of a nuclear superheater – the density reduction is on the order of 25 %. Further by working under operational conditions, that include heating the fuel elements, the Doppler broadening in the resonance cross-sections affects the resonance escape probability. Consequently when one heats the assembly an overall effect is observed. These data are of course extremely important, but evaluation of the contribution of each of the individual effects is quite involved.

In order to observe and to interpret changes in the aforementioned lattice parameters as a result of various void fractions in the coolant it is not necessary to simulate boiling of water throughout the assembly. It will suffice to create the various void fractions in a relatively small core region containing the unit cell where the measurements will be performed. The distance from the outer boundary of this region to the unit cell should at least be a few scattering mean free paths of the thermal and epi-thermal neutrons. This condition has to be met so that the neutron energy spectrum in the unit cell approaches as close as possible its equilibrium condition. As such the experiment resembles a substitution technique, see Chapter 1.

The void fraction in a coolant channel of a typical boiling water-reactor varies from zero to about 70 % at the outlet. Simulating a distribution of voids throughout a channel equivalent to that in an operating reactor is rather difficult. Moreover such a distribution changes from reactor to

reactor and even within one reactor from channel to channel. Among other things it depends on the amount of subcooling which is applied. However it is again not necessary to simulate a void distribution over the total core height. It will be sufficient when various void fractions surround a proper selected measuring location up to a few scattering mean free paths. Data for other heights in a channel may then be deduced from the information thus obtained.

When selecting the range of void fractions to be simulated one should keep in mind that the average void fraction in a channel is usually close to 20 %. This means that a method offering simulation possibilities up to about 40 % void will cover a large fraction of the core height. From a reactor physics point of view the method should involve a reduction of the water density equivalent to the void fraction required. The average value of this reduction and its distribution over the water region should be fairly constant (better than 10 %) over the time that the neutron detectors are activated in the lattice. In addition the nuclear properties of the material used to simulate the voids should not differ greatly from the steam-water mixture. Since problems of heat transfer or problems of hydraulic nature are not the object of this study, the related effects inherent to two-phase flow need not be taken into account. Further it is emphasized that only static conditions will be examined.

Various methods have been considered to simulate voids according to the above-mentioned requirements. Expanded plastics, like Styrofoam, which are frequently used for simulating voids in a nuclear reactor when integral reactivity effects are to be determined [1, 2], could not be used in this case because of their high void fraction (98–99.5 %). However this fact makes this material particularly suitable for simulation of superheated steam conditions, see section 2.5. Filling the measurement region with mixtures of small plastic spheres of different sizes, where the empty space between the spheres represents the voids, leads to a difficult determination of the equivalent void fraction and moderating properties, and in addition, when applied in the LEAD facility, to complicated experimental techniques. DOWN, *et al.* [3] used small beads of highly expanded polystyrene with the interstices flooded with water. Actually this method is characterized by the same complexities that arise when solid spheres are used. Its advantage is that void fractions can be obtained ranging from 40 % to 60 % corresponding to the actual water density reduction (boiling and increase in temperature). Insertion of small sheets or rods of aluminium or magnesium to create a local reduced water density may be used for reactivity measurements but is not particularly suited for this experiment because the thermal spectrum is affected too locally. When only variations in the resonance escape parameter $p$ are to be observed this technique may be acceptable.

Another method which may be used is that of air injection near the bottom of the assembly. Although not free of intricacies and limitations

this technique was selected after a careful experimental examination. The prime difficulty associated with the use of air is the measurement of the void volume, which is related to the motion of air bubbles in the liquid.

The behaviour of a gas flow through a liquid has since long been the object of study in the field of chemical engineering, especially in relation to the performance of gas-liquid contactors. Early work of fundamental importance on the motion of single gas bubbles in a liquid has been reported by MIYAGI [4], and BOND, *et al.*, [5, 6]. VERSCHOOR [7] has given some aspects of the motion of a swarm of gas bubbles rising through a vertical liquid column. He showed that the gas content of a gas-liquid system increases with the overall gas flow rate up to a critical point, whereupon it decreases to pass a minimum and then gradually increases again on further increase of the gas flow rate. In addition VERSCHOOR's experiments – where air was injected through a porous plate – show coalescense of small bubbles emerging from the plate. This fact limits the minimum size of the bubbles. In recent publications of BEEK [8] and HINZE [9] problems associated with sieve plates on which liquid is fed and through which gas or vapour is blown are discussed. Depending on the system geometry two flow situations have been observed:

*a*) The bubbles, rising in streets force the liquid level to oscillate and the oscillating motion of the liquid forces the bubble streets into an alternating movement.

*b*) The bubbles rise in streets and create a row of stationary vortices along the length of the tank.

The liquid height considered in the experiments described just above is small in comparison to the height of LEAD.

Visual observations of a system described in section 2.4 showed that initially the gas content increased with increasing gas injection rate up to a point where large non-reproduceable air bubbles were formed, finally resulting in complete air channels.

### 2.2 *Methods to determine void fractions.*

Since the operation of the first boiling water reactor in 1952 many techniques have been tried to experimentally determine the void fraction in the reactor core. In many of these techniques actually the average density reduction of the water has been determined. Data on out-of-pile boiling loops have been reported by several authors [10, 11]. Gamma, X-ray and beta-ray attenuation techniques have reached a high degree of perfection in these facilities. However in that case there remains a correlation to be made to the in-pile void fraction. Therefore reliable in-pile measurements are to be preferred. One in-pile method involves the use of turbine flow meters as described by SCHENK [12]. From the differences between the fuel element inlet and outlet flow meter signals the exit void fraction in a channel can be determined, if the slip factor of the

bubbles is known. Recent developments on impedance-type void instruments are described by BJÖRKMAN, *et al.* [13], ØRBECK [14] and SPIGT, *et al.* [15]. In general the interpretation of in-core instrument readings is rather complicated. Moreover these methods, apart from the impedance technique, cannot be used in LEAD.

Assuming that – when blowing air in the assembly – the air temperature remains constant, the average air volume-fraction $\alpha$ at a given height in the water region of the unit cell can be approximated by:

$$\alpha = \frac{P_1 F}{P_2 v A} \tag{2.2.1}$$

where: $P_1$ = absolute pressure in the air inlet tube
$P_2$ = absolute pressure at the particular height in the element
$F$ = air flow rate
$v$ = bubble rise velocity
$A$ = unit cell cross-sectional water area

Applying this relation to obtain $\alpha$ should not give much precision because neither the bubble rise velocity $v$ and nor the pressure $P_2$ can be determined very accurately.

Another possibility for determining the average void fraction in a certain area of an operating reactor consists of measuring the static pressure differences in the water at various heights in the core. Actually this method has been tried to verify a nuclear technique described hereafter and which is more appropriate in regard to the experiment. However large and fast fluctuations in the differential pressure and in addition the lack of space in the cell to place proper pressure detectors caused the results to be too unreliable for a correct comparison with the results of the nuclear method.

This nuclear method is based on the fact that the local thermal-to-fast neutron flux ratio is approximately proportional to the amount of moderator in the immediate vicinity. A measure of this flux ratio is the cadmium-ratio minus one. Originally suggested by UNTERMEYER and tested by THIE, *et al.* [16] to determine void fractions in the EXPERIMENTAL BOILING WATER REACTOR (EBWR) this technique has been adjusted and simplified to determine void fractions in LEAD.

### 2.3 *Relation between the cadmium-ratio and the void fraction*

Assuming the validity of steady state two-group diffusion theory for the water region of the unit cell the neutron balance equations read:

$$D_f \nabla^2 \phi_f - \Sigma_r \phi_f = 0 \tag{2.3.1}$$

and

$$D_{th} \nabla^2 \phi_{th} - \Sigma_a \phi_{th} + \Sigma_r \phi_f = 0. \tag{2.3.2}$$

The subscripts $f$ and $th$ refer to the fast and thermal group respectively,

$D$ is the diffusion coefficient, $\Sigma_a$ is the thermal absorption cross-section. The removal cross-section $\Sigma_r$ is very nearly proportional to $(1-\alpha)$ (where $\alpha$ is the void fraction) on the assumption that shifts in the thermal spectrum do not affect the cross-section. Rewriting Eq. (2.3.2) leads to:

$$\frac{\phi_{th}}{\phi_f} = \frac{\Sigma_r}{\Sigma_a - \dfrac{D_{th}\nabla^2\phi_{th}}{\phi_{th}}} \tag{2.3.3}$$

or

$$\frac{\phi_{th}}{\phi_f} = (1-\alpha)\,Q \tag{2.3.4}$$

where:

$$Q = \frac{\Sigma_r/(1-\alpha)}{\Sigma_a - \dfrac{D_{th}\nabla^2\phi_{th}}{\phi_{th}}}.$$

The factor $Q$ will hardly be sensible to voids. Since $\Sigma_r$ is about proportional to $(1-\alpha)$ the numerator may be regarded independent of voids and the same is true for denominator when the influence of variations in the thermal absorption is neglected. In addition to being small in comparison to the leakage, the thermal absorption per unit volume varies approximately as $(1-\alpha)^2$ because both $\Sigma_a$ and $\phi_{th}$ are nearly proportional to $(1-\alpha)$ which makes the influence of voids on the absorption even less important. When void fractions are to be measured throughout the core it has to be kept in mind that where in general the core composition is space dependent $Q$ will vary as a function of position. However $Q$ may be regarded as a constant for measurements in the unit cell, with different values for the central zone and peripheral zone of the exponential assembly. The cadmium-ratio $R_{Cd}$ is given by:

$$R_{Cd} = 1 + \frac{\phi_{th}}{\phi_f} \cdot \frac{\overline{\Sigma}^d_{a_{th}}}{\overline{\Sigma}^d_{a_f}} \tag{2.3.5}$$

where $\overline{\Sigma}^d_{a_{th}}$ and $\overline{\Sigma}_f{}^d$ are the local spectral averaged thermal and epi-cadmium detector absorption cross-sections. For a $(1/v)$-detector the quotient of these cross-sections is independent of the void fraction and whereas it only refers to one particular place in each of the two zones in LEAD, the quotient may be regarded as a constant for each of the two unit cells. Elimination of the flux ratios from Eq. (2.3.4) and Eq. (2.3.5) leads to:

$$(1-\alpha) = A(R_{Cd}-1) \tag{2.3.6}$$

where the constant factors have been incorporated in the constant $A$ and thermal flux depression due to the detector has been disregarded. Experimentally the constant $A$ can be determined from the cadmium-ratio measured in the zero void condition ($R_{Cd_0}$). It follows that $A = 1/(R_{Cd_0}-1)$ and consequently:

$$\alpha = 1 - \left[\frac{R_{Cd}(\alpha)-1}{R_{Cd_0}-1}\right]. \tag{2.3.7}$$

Thus the method used to determine the void fraction in LEAD simply consists of:

*a*) The measurement of the cadmium-ratio for various air flow rates in the region where the fine structure parameters will be determined.

*b*) The calculation of the void fractions corresponding to the experimentally obtained cadmium-ratios using Eq. (2.3.7).

From these data it is possible to determine the relation that exists between the void fraction and the air flow rate, which is required for proper adjustment of the air injection system.

### 2.4 *Experimental determination of the void fraction*

To determine the radial dimensions of the region in which voids are to be created the scattering mean free paths of the epi-thermal and thermal neutrons in the air-water mixture were calculated for various void fractions.

From the results, which are given in Table II.1 it could be concluded that it would be acceptable to surround the unit cells in the two zones of the assembly in which the intracell flux plots were to be made with an area equivalent to the six neighbouring cells. This solution is to be regarded as a reasonable compromise between reactor physical requirements and technical problems that arise when the area is further increased.

TABLE II. 1.

Scattering mean free path of epi-thermal and thermal neutrons for various void fractions in water.

| Scattering mean free path (cm) | Void fraction | | | | |
|---|---|---|---|---|---|
| | 0 % | 10 % | 20 % | 30 % | 40 % |
| (thermal) | 0.28 | 0.31 | 0.35 | 0.40 | 0.47 |
| (epi-thermal) | 0.69 | 0.77 | 0.87 | 0.99 | 1.16 |

Prior to performing cadmium-ratio measurements in the exponential assembly an out-of-pile observation was made of the phenomena that occurred as a result of air injection in between the elements.

Two clusters of seven fuel elements with water-to-fuel volume ratios corresponding to those in the two zones of the exponential assembly were placed in a narrow fitting cylindrical tank of clear Perspex having a height equal to that of the elements. A hollow aluminium ring with six radially pointing arms, in the top of which small holes (0.4 mm diameter) were drilled – more in the arms than in the ring to compensate for the pressure drop – was brought around the centrally located element and in between the surrounding elements close to the bottom of the tank. A plastic hose connected one of the arms with the central pressurized air supply system of the laboratory. The tank was half filled with water. Air was inserted via the ring with the six arms and the following observations were made:

*a*) The air content of the water (void fraction) increased practically linearly with the air flow rate up to a void fraction of about 40 %. Up to this value, which also seemed to depend on the rate of increase of the air supply, the bubble distribution appeared homogeneous. The shape of the bubbles was not completely spherical but slightly flattened having a volume of approximately 0.1 $cm^3$, see Fig. 2.1. With further increases in the air flow rate a heavy coalescence of the bubbles occurred resulting in complete air channels and a stable system could not be retained. The air content of the water at which the unstability of the system began, started at a lower void fraction for the peripheral zone cluster (water-to-fuel ratio of 2.34) than for the central zone cluster (water-to-fuel ratio of 1.14).

*b*) The homogeneous and stable void distribution appeared to be established about 3 cm above the level of air injection.

*c*) A heterogeneous void layer occurred near the water surface. The thickness of this layer increased when the void fraction was increased but was less than 5 cm thick under stable void conditions.

From these visual observations the method of air injection to create voids was concluded acceptable although it would limit the obtainable void fraction to about 30 % to 40 %.

Next, the experimental arrangement for introducing air was adjusted to the exponential assembly. The air coming from the central pressurized air supply system was sent through a filter and then passed a pressure reducing valve, followed by a flow meter. The air pressure at the flow meter outlet was measured with a Bourdon-type pressure gauge. The outlet of the flow meter was connected to the same rings with arms as used in the Perspex tank. In Fig. 2.2 the experimental arrangement is shown.

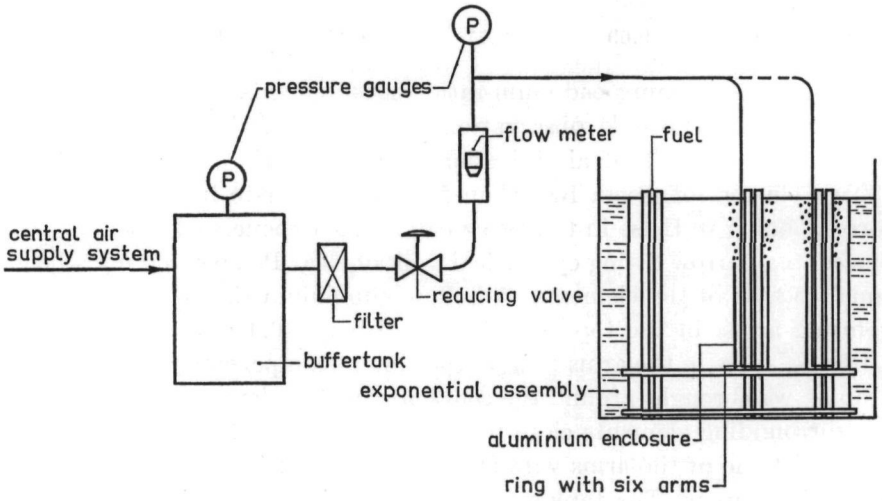


Fig. 2.2. Experimental arrangement for air injection.

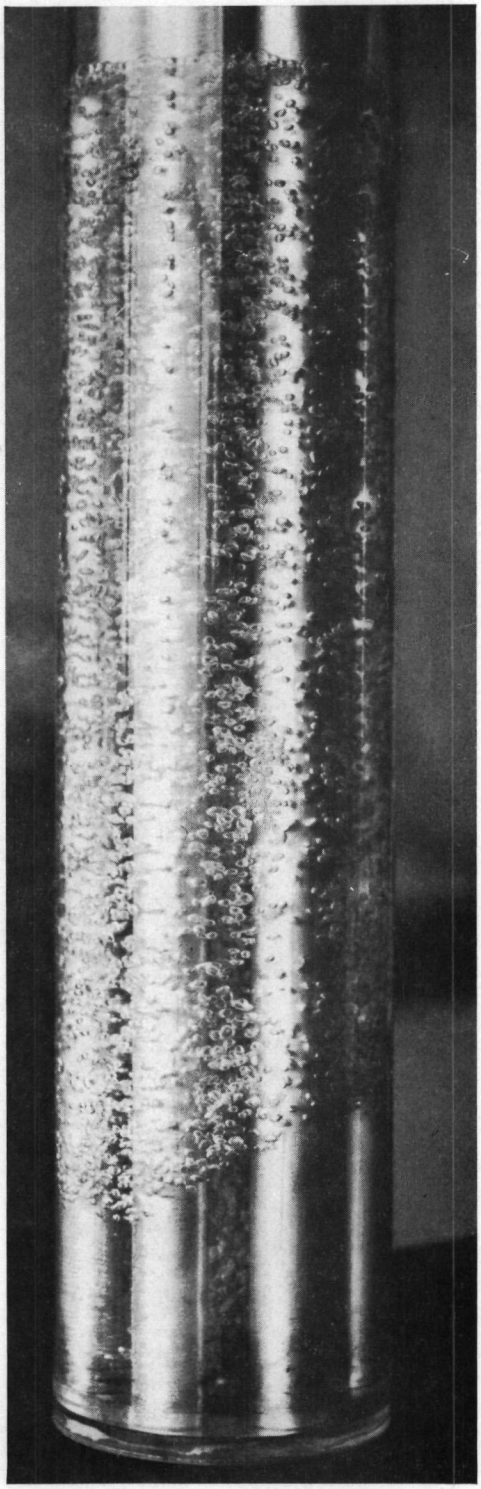

Fig. 2.1. Bubble formation as a result of air injection in the water region (void fraction about 5 %) in a seven-rod cluster placed in a Perspex tank.

To keep the voids in the exponential assembly in the proper regions aluminium enclosures (0.5 mm thick) were inserted around the two seven-rod combinations up to about 20 cm above the region where the intracell measurements were to be made. This allowed the air to stream freely into the surface region of the water, and prevented water from flowing over the fuel elements. In the exponential assembly the rings through which the air was introduced were fixed to the bottom of the aluminium enclosures. This combination was suspended from the top grid plate of the assembly, which is located 20 cm above the bottom. The variation in the void fraction was obtained by adjusting the reducing valve thereby changing the pressure in the air inlet tube. Therefore in addition to the flow rate, the pressure at the flow meter outlet had to be measured so as to be able to reproduce a particular void condition. The flow and pressure are of course related to the dimensions of the air injection system used.

Rather than determining the cadmium-ratios from foil activation methods the use of a proportional counter was preferred because of the immediate availability of data. In particular a $BF_3$-counter was used. Because of its size this detector could not be placed in the water space between the fuel elements where the changes in the thermal flux would be most noticeable. To overcome this difficulty the central fuel elements of the two seven rod clusters were replaced by empty thin-walled aluminium tubes with the same external dimensions as the fuel elements. In order to determine the height, where the axial spectrum would reach its equilibrium, measurements were made in these tubes along the vertical axis under various void conditions with a bare and with a cadmium covered counter. The results of the obtained cadmium-ratios as a function of the height in the tube for various flow rates are given in Fig. 2.3 for the central zone and in Fig. 2.4 for the peripheral zone.

Due to the fact that the central fuel rods were removed the neutron energy spectrum in the clusters is much softer than when these elements are present. Therefore the cadmium-ratio values cannot be compared with those given in Chapter 1. It can be concluded from Fig. 2.3 and Fig. 2.4

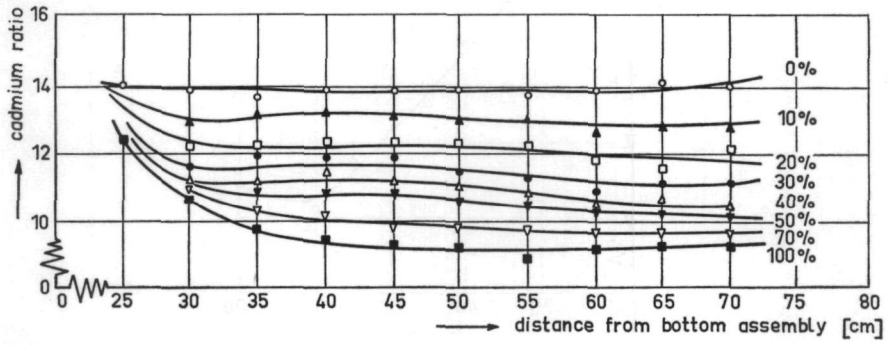


Fig. 2.3. Axial distribution of the cadmium-ratio in a cell of the central zone as a function of the air flow rate expressed in percent flow meter scale readings.

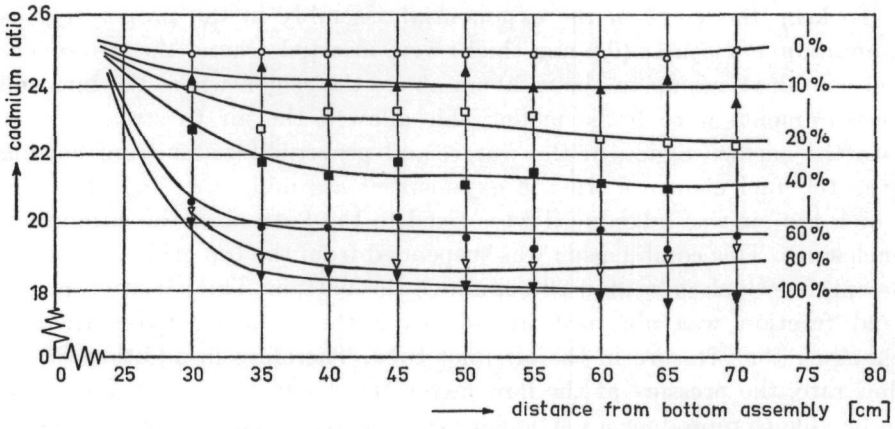


Fig. 2.4. Axial distribution of the cadmium-ratio in a cell of the peripheral zone as a function of the air flow rate expressed in percent flow meter scale readings.

that the equilibrium spectrum in the axial direction is reached at a height of about 40 cm from the bottom of the assembly. Therefore the fine structure measurements, the details of which are reported in Chapter 4 and Chapter 5, were made about 45 cm from the bottom of the assembly.

For proper calibration of the air injection system in regard to the adjustment of the void fraction another series of cadmium-ratio measurements were made at 45 cm from the bottom of the assembly for various flow rates. The results are shown in Fig. 2.5 and Fig. 2.6. From the plots given in these figures it can be seen that a minimum in the cadmium-ratio

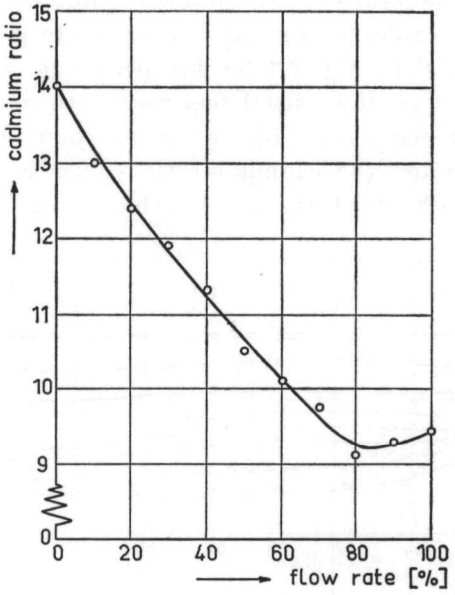


Fig. 2.5. Cadmium-ratio as a function of the air flow rate in the central zone at 45 cm above the assembly bottom.

occurs, which indicates the start of the 'channeling' effect. The data in Fig. 2.5 and Fig. 2.6 were used to obtain the actual calibration curves which are given in Fig. 2.7 where the void fraction is plotted as a function of the air flow rate. As can be seen, the maximum obtainable void fraction in the central region is approximately 36 % while in the peripheral zone the value is limited to 29 %. These values apply of course only to the measurement region.

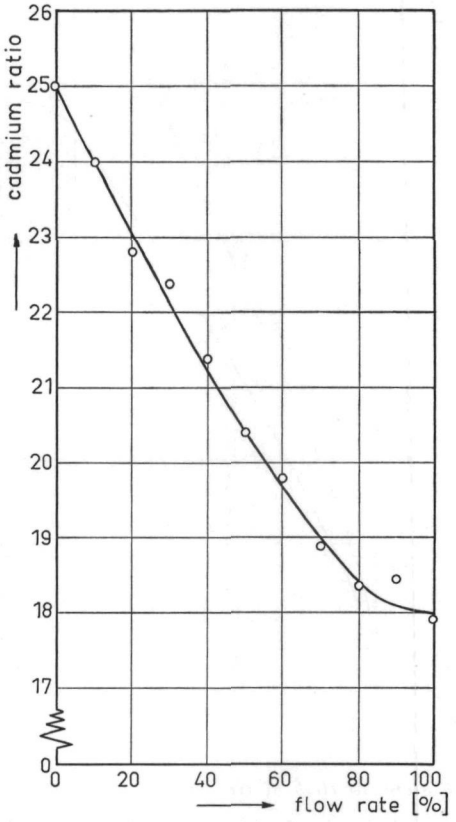


Fig. 2.6. Cadmium-ratio as a function of the air flow rate in the peripheral zone at 45 cm above the assembly bottom.

Although in principle dependent on counting statistics the obtainable accuracy in the void fraction is largely determined by the relation that exists between $\alpha$ and $R_{Cd}$.

The error in $\alpha$ decreases with increasing values of $\alpha$. When the count rates are measured with an accuracy of 1 % the error in a void fraction of 10 % is approximately 20 % while the error decreases to about 4 % for a void fraction of 36 %. Whereas the accuracy of the gamma-ray attenuation technique is said to be not better than $\pm$ 10 % and a $\pm$ 5 % accuracy is claimed for the turbine flow meter method, the cadmium-ratio method is certainly to be recommended for the measurement of void fractions in excess of 40 %. The fact that the void fraction at a particular

place shows a relatively large statistical variation does not affect the measurement of the microscopic reactor parameters, because the detectors used require long irradiation periods (2 to 8 hours).

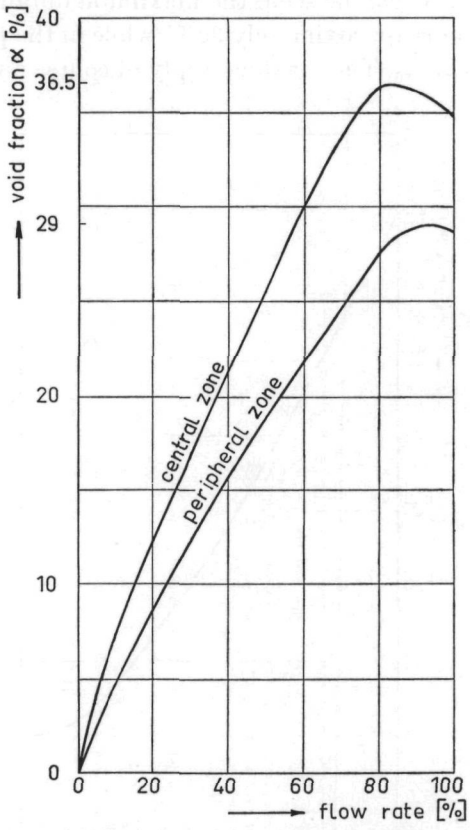


Fig. 2.7. Void fraction $\alpha$ as a function of the air flow rate.

2.5 *Simulation of superheated steam in view of neutron moderation.*

The exit steam conditions of current nuclear superheat reactors in the USA and Europe range from 440° C at a pressure of about $3.9 \times 10^6$ N/m$^2$ (40 at) in the PATHFINDER-reactor to the projected goal of 500° C and $5.9 \times 10^6$ N/m$^2$ (60 at) in the AEG-reactor (see Chapter 3). These conditions relate to steam densities of 0.0125 g/cm$^3$ and 0.0173 g/cm$^3$ respectively. As a result of the very low hydrogen density, neutron moderation due to superheated steam is of minor importance. However, whereas simulation of the moderating characteristics of superheated steam could easily be realized, it was incorporated in the experiment for the sake of completeness.

The moderating capacity of a material is in principle represented by its Fermi-age $\tau$. However it is not only moderation that determines the microscopic thermal flux profile. In addition the diffusion length $L$ is important. Because both the Fermi-age and the diffusion length of solid polystyrene do not differ much from those for water, expanded polystyrene

with a void fraction of 98 % is an excellent material to simulate from a neutron diffusion point of view superheated steam. Therefore all the internal fuel channels of the two seven-rod clusters were filled from top to bottom with Styrofoam. As a result a slight increase in the thermal neutron flux occurs in the 'steam region' of the elements, see Chapter 5.

## REFERENCES


1. SHONG, J. A. DE, JR., Styrofoam simulation of boiling and temperature effects in the EBWR cold critical experiments, ANL–5697 (1957).
2. KLEIJN, H. R., A. W. VAN DER HEIJDEN en H. J. RIJKS, Verslag van de initiële beproeving van de Hoger Onderwijs Reactor, RID 132–02 (1964).
3. DOWN, H. J., J. DICKIE and W. N. FOX, A method of simulating voids in experimental studies of boiling water-reactors, AEEW – M 14 (1963).
4. MIYAGI, O., Phil. Mag. VI, Vol. L, 112 (1925).
5. BOND, W. N. and D. A. NEWTON, Phil. Mag. VII, Vol. IV, 889 (1927).
6. ——— and ———, Phil. Mag. Vol. V, 794 (1928).
7. VERSCHOOR, H., Some aspects of the motion of a swarm of gas bubbles rising through a vertical liquid column, Trans. Ins. of Chem. Engrs. (London), 28, 52 (1950).
8. HINZE, J. O., Oscillations of a gas-liquid mixture on a sieve plate, Proc. Symposium on Two Phase Flow, Vol. II, Paper F 1, University of Exeter, Dept. Chem. Eng. (1965).
9. BEEK, W. J., Oscillations and vortices in a batch of liquid sustained by a gas flow, Proc. Symposium on Two Phase Flow, Vol. II, Paper F 4, University of Exeter, Dept. Chem. Eng. (1965).
10. HOOKER, H. H. and G. F. POPPER, A gamma-ray attenuation method for void fraction determination in experimental boiling heat transfer facilities, ANL – 5766 (1958).
11. PERKINS, H. C. JR., M. YUSUF and G. LEPPERT, A void measurement technique for local boiling, Nucl. Science and Eng. 11, 304–311 (1961).
12. SCHENK, K., HBWR turbine flow meters developed for nuclear application, ENEA Symposium on in-core instrumentation, paper D-7, Oslo (1964).
13. BJØRKMAN, J., *et al.*, Void measurements on the bases of impedance void meters, ENEA Symposium on in-core instrumentation, paper D–1, Oslo (1964).
14. ØRBECK, I., The impedance void meter, ENEA Symposium on in-core instrumentation, paper D–8, Oslo (1964).
15. SPIGT, C. L., *et al.*, The application of the impedance method for transient void fraction measurement and comparison with the gamma-ray absorption technique, ENEA Symposium on in-core instrumentation, paper D-2, Oslo (1964).
16. THIE, J. A., J. BEIDELMAN and B. HOGLUND, Void measurement in a boiling reactor, Nucl. Science and Eng. 11, 1–6 (1961).

CHAPTER 3

# SOME REACTOR PHYSICS ASPECTS OF NUCLEAR SUPERHEAT LATTICES

## 3.1 *Introduction*

Although physics and technological problems of nuclear superheat reactors have been described by NOVICK, *et al.* [1], KORNBICHLER [2], DOLLEZHAL, *et al.* [3], KLEIJN [4], SOKOLOV, *et al.* [5], DEUTSCH [6] and several other authors, it seems appropriate – in connection with the experiments described in this thesis – to include a condensed review of the boiling water-reactor (BWR) with integral superheat. A detailed review on the physics of nuclear superheat reactors developed in the USA is given by VALERINO and HARDING [7].

The operation of boiling water-reactors with integral nuclear superheat is such that the saturated steam, generated upon passage of water coolant through the boiler region, is made to re-enter the core – after removal of most of the entrained moisture – through the superheater region until the appropriate temperature is reached. At present two developments can be distinguished in this advanced concept of the boiling water-reactor. The first development, which comes from the USA, features a core composed of a separate boiler and superheater region, where the latter may be located centrally, annularly or at the periphery. In a second development, boiling and superheating take place throughout the entire core. More specifically in this case each fuel element together with its surrounding moderator contains a boiler and a superheater region. This concept, suitable for intermediate power levels, was proposed by KLEIJN [4] and has also been independently developed by the Allgemeine Elektrizitäts Gesellschaft (AEG) in Western Germany.

Examples of the first concept are the Boiling Nuclear Superheat reactor (BONUS) at Puerto-Rico, a General Nuclear Engineering Corporation (GNEC) design, and the PATHFINDER-reactor at Sioux Falls (USA) developed by Allis Chalmers Manufacturing Company (AC). BONUS has a centrally located forced circulation boiling region and a peripheral superheater. The reactor superheats steam up to 482° C at a pressure of $6.2 \times 10^6$ N/m$^2$ (63.3 at). The reactor is designed to produce 16.5 MWe. The PATHFINDER-reactor features a centrally located superheater which will produce steam of 440° C at a pressure of $4 \times 10^6$ N/m$^2$ (40.8 at). The power output of this reactor is 62 MWe. Both reactors are presently being commissioned.

The concept of boiling and superheating throughout the core is going to be realized in a 25 MWe prototype reactor designed by AEG. This

reactor is presently under construction at a site adjacent to the Kahl-reactor in Germany. The exit steam conditions are aimed at 500° C at a pressure of $5.9 \times 10^6$ N/m$^2$ (60 at). In the literature as well as in reports available, only scarce information could be found about the physics characteristics of this reactor.

The reactor physics experiments reported in this thesis are relevant to lattices based on this concept.

### 3.2 *General reactor physics aspects*

Fuel elements and lattices intended for use in nuclear superheat reactors are radically different from those in boiling and pressurized water-reactors. In general, nuclear superheat fuel elements are larger in geometrical cross-section so that for a given water-to-fuel volume ratio, greater thicknesses of water surround the elements. Because of the small transport mean free path in water, flux peaking will even be more pronounced than in conventional boiling water-reactors. Accordingly the thermal flux depression in the fuel region is large and the thermal spectrum varies considerably across the fuel element lattice cell. As a consequence disadvantage factors can be calculated accurately only by using transport theory methods with sophisticated approximations. The calculation of $^{238}$U resonance capture effects is difficult due to the complicated fuel element geometry, especially for the case that internal steam coolant passages are flooded. Because of the greater degree of heterogeneity associated with superheat lattices, the homogeneous treatment of the fast fission factor which is used successfully for boiling and pressurized water lattices may not be a good approximation in superheat systems. In this respect experimental checks are very essential, because detailed data are still scarcely available.

Table III.1 lists the main properties of some superheat fuel elements. In Fig. 3.1 geometrical cross-sections of a few superheater fuel elements are given, used in US-reactors, while in Fig. 3.2 a cross-section is shown of the element proposed for the AEG-reactor. In addition a geometrical cross-section of a LEAD fuel element is shown in this figure.

The operation of a nuclear superheat reactor with a separate boiler and superheater section introduces a number of physics problems which are not found in other water-reactors, such as:

*a*) Upon start-up of the reactor, the steam channels in the superheater region usually contain water. It is necessary as a safety measure to design the system so that the reactivity changes associated with the removal of water remain below a pre-assigned value. Furthermore the reactivity change associated with an accidental flooding of the superheater under operational conditions should not be permitted to exceed a specified value. The main factors affecting the reactivity upon flooding are:

1. A positive effect due to decreased neutron leakage.

TABLE III. 1.

Main properties of some superheat fuel elements.

| Reactor | Fuel material | Enrichment | Type | Cladding |
|---|---|---|---|---|
| BONUS | $UO_2$ | 3.41 % | rods | 316 SS (0.47 mm) later Inconel |
| Borax-V | $UO_2$+304B SS (cermet) | highly enriched | plates | 304 SS (0.25 mm) |
| Pathfinder | 1e $UO_2$+304 SS (cermet) | 93.3 % | double annular | 304 SS |
| | 2e $UO_2$ | 3.5 % and 7 % | rods / rods | (0.34 mm) 316 SS |
| AEG (under construction) | $UO_2$ | 3 % | annular rods | proposed: inside Inconel outside 16–16 SS |

2. A change in the thermal utilization factor as a result of the softening of the spectrum. Whether this results in a positive or negative effect depends on the water-to-fuel volume ratio. In practical cases the construction will be made in such a way that the net effect is generally a negative reactivity addition.

3. The resonance absorption in $^{238}U$ in the superheater region changes due to increased moderation which is a positive effect and an increased surface absorption, a negative effect. The combination may result in a positive reactivity effect.

One solution would be a construction which prevents flooding of the steam channels. However it should be kept in mind that shut-down cooling of the superheater fuel elements requires the use of some water, since steam is no longer available under these circumstances.

*b*) The boiler is required to produce a specific amount of steam that is then raised to the appropriate superheat temperature in the superheater. An adequate control system is necessary to regulate the power output of each region under steady state and transient conditions. This control system must – together with eventual burnable poisons – also maintain the proper split in power for the lifetime of the core. Further it should keep the spatial power distribution flat so as to achieve a high burn-up. Because the reactivity change with fuel burn-up may vary from region to region, the control system will be more complex.

*c*) In general, both the enrichment of the fuel and the water-to-fuel volume ratio of the unit lattice cells in the boiler region and in the superheater region are not equal. As a result local distortions of the fluxes may occur, which give rise to local peaking factors that may be larger than

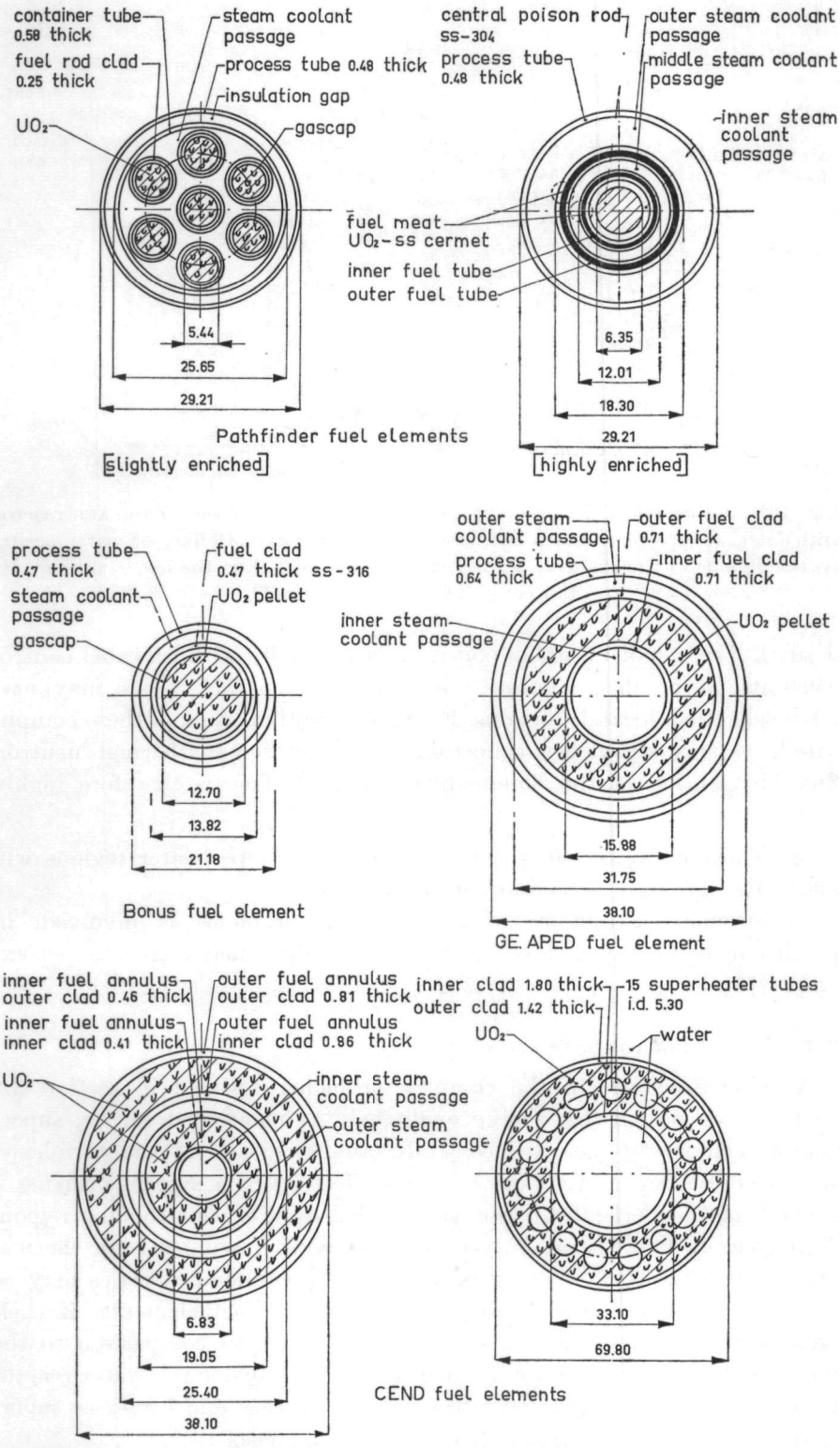


Fig. 3.1. Geometrical cross-sections of some fuel elements under construction or in use in superheater regions of water-reactors with *separated* boiling and superheater zones. (Dimensions in mm).

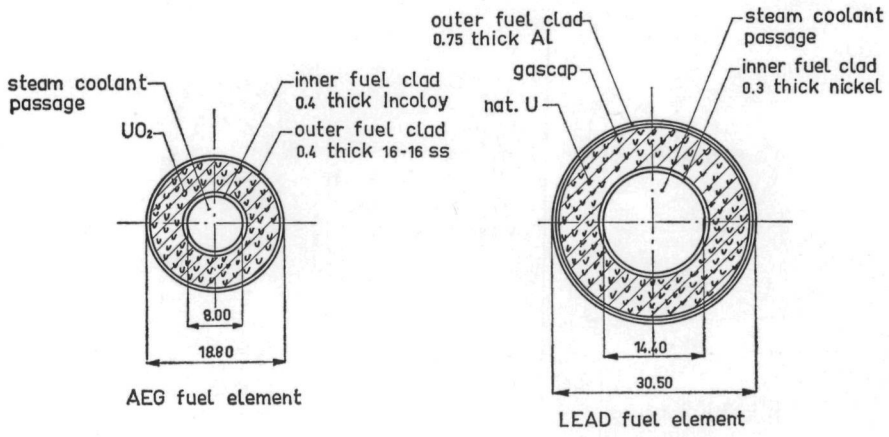


Fig. 3.2. Geometrical cross-sections of a fuel element proposed for the AEG-reactor with integral superheat and a fuel element used in LEAD. Boiling of water occurs on the outside of the elements while steam is superheated on the inside throughout the core. (Dimensions in mm).

desired. The use of burnable poisons and manually withdrawable control elements to regulate lifetime and operating characteristics may also adversely effect local distortions. For further optimization of these complicated systems knowledge concerning the microscopic thermal neutron flux distribution at the boiler-superheater interface is therefore highly desirable.

*d*) The nuclear coupling between boiler and superheater regions will affect the dynamic behaviour of the reactor.

Furthermore a number of technological problems is involved, in particular in regard to the selection of cladding materials, see for example [8].

### 3.3 *Core-design considerations*

As a consequence of the complex problems outlined in section 3.2 various core designs have been evaluated. As mentioned earlier, superheater regions were selected centrally, annularly and at the periphery. Also studies were undertaken (General Electric) of a system utilizing a central 'fast' superheater region surrounded by a thermal boiling region. This concept has the advantage that materials having a high thermal absorption cross-section but good corrosion resistance properties may be used as cladding materials for the superheater fuel elements, if their cross-sections in the fast energy region are small in comparison to the fuel and blanket material cross-sections in that region. A water-reactor in which water enters the core in a subcooled state and leaves as supercritical steam is being evaluated by Westinghouse.

Arguments for selecting the superheater region at the periphery of the core are:

*a*) Steam, just like gases, is a poor heat transfer medium relative to boiling water. It is therefore advantageous to utilize steam cooling in the outer part of the core where power densities are less.

*b*) Most of the materials which can withstand high temperature steam environment, such as nickel alloys, have high neutron absorption cross-sections, as shown in Table III.2. This poisonous material has a less adverse effect on the neutron economy if placed in the peripheral region of the core.

*c*) The reactivity effects associated with flooding of the superheater elements are smaller and, therefore, less hazardous when the elements are near the outside of the core.

TABLE III. 2.

Thermal macroscopic absorption cross-sections of some cladding materials.

| Cladding Material | $\Sigma_a(2200)$ [cm$^{-1}$] |
|---|---|
| Al | 0.015 |
| Zr | 0.008 |
| Fe | 0.222 |
| Ni | 0.420 |
| Cr | 0.255 |

However the major disadvantage is, that for a peripheral superheater location a large core is needed in order to obtain an acceptable burn-up because of the low specific power in the superheater region. For a central superheater location there is a reduction in core size resulting from a higher average power density but at expense of poorer neutron economy due to the cladding of the superheater fuel elements. Because neutron leakage from large size reactors is relatively small, a centrally located superheater would appear more appropriate for these reactors whereas a peripheral superheater region is preferable for smaller reactors. From these considerations it might be argued that the concept of boiling and superheating throughout the entire core is recommendable for power levels in the intermediate range (50 MWe – 100 MWe).

A combination of boiling and superheating throughout the entire core may be obtained by using annularly shaped fuel elements as used in the exponential assembly described in Chapter 1. Water can be converted to steam on the outside of the elements, and the steam then superheated inside the elements. In comparison with a reactor featuring a separate boiler and superheater region this concept has the following merits:

*a*) Only one type of element is required, resulting in manufacturing convenience and a reduction in fabrication costs.

*b*) The combined boiling-superheat element facilitates easy emergency and shut-down cooling. The residual heat after shut-down is transferred to the boiler region and the elements do not become excessively over-

heated. As a result, flooding can be prevented by proper construction without any risks resulting from decay heat.

*c*) Due to inside and outside cooling of the fuel elements the average fuel temperature is relatively low. Consequently it is expected that practically no fission gases will be released from $UO_2$-elements.

*d*) Problems of neutron flux adjustments between different zones do not exist or, at least, are of minor importance.

*e*) In principle most of the neutron moderation has to be effected with the water. Consequently the water channels have to be wider than in conventional water-reactors. This would result in lower velocities and steam content of the water than in a boiling water-reactor with the same specific load. Therefore potentially higher specific loads are possible in these reactors.

*f*) The requirements in regard to neutron absorption for the cladding material used on the inside of the fuel elements are not very stringent. An alloy containing a high percentage of nickel such as Incoloy or Inconel may be used in a self-supporting structure because even then only small amounts are used, due to the small internal diameters of the fuel elements.

*g*) It is sufficient to control the integral reactor power. No separated control of boiler and superheater section is required because the power ratio is determined by the geometry and dimensions of the fuel element itself.

*h*) Criticality and reactivity calculations are less complicated since there are no separate zones.

The concept of combined boiling and superheating in one fuel element also has a number of inherent disadvantages such as:

*a*) The complicated construction of the elements, which makes them difficult to fabricate and therefore more expensive.

*b*) The complicated piping and header arrangements for proper steam guiding.

*c*) The difficulties involved in obtaining the desired heat-split to the boiler part and the superheating part of the element.

*d*) The thermal expansion of inside and outside cladding of the element which will be different, due to the differences in temperatures and material composition. The inner cladding may reach temperatures of about 600° C while the cladding on the boiling side will not exceed 300° C.

### 3.4 *Calculation methods* (compiled from ref. [7])

Some of the laboratories and industries involved in nuclear superheat reactor design have developed calculation methods for engineering design

purposes, especially for determining integral reactivity effects. These schemes, based upon techniques used for normal BWR and PWR type reactors, are in all cases closely related to the geometry and the enrichment of the superheat fuel elements. They appear to give reasonably accurate predictions of experimental results obtained from cold-clean critical experiments. How reliable the calculation methods are for operating temperature conditions will be learned when the reactors have been commissioned.

In general criticality calculations are performed using two and three-group diffusion theory. In the latter case the assumption is sometimes made that in $^{235}U$ only thermal fission takes place. Fast fission and epi-thermal absorption are restricted to $^{238}U$. For slightly enriched fuels and a large water-to-fuel ratio such an approximation seems very reasonable but it may lead to less accurate results when highly enriched uranium is used in combination with a small water-to-fuel ratio.

Each of the calculation techniques utilizes an assortment of digital computer codes to determine the individual lattice parameters. Most of the fast group constants are obtained using the nuclear code MUFT-4 [9]. The thermal group constants and the resonance capture are treated differently in the various schemes. This is necessary because these parameters are very sensitive to the fuel element geometry, its composition and to the water-to-fuel ratio. In order to determine these constants, cylindrical lattice cell approximations according to Wigner and Seitz are widely used. In how far such an approach is acceptable depends on the array in which the fuel elements are placed and on the fuel element geometry.

For rod-type $UO_2$-fuel elements designed by GNEC for use in the BONUS reactor (see Fig. 3.1) the macroscopic cross-sections in the thermal region are obtained from microscopic values. The latter have been averaged over a 'hardened' Maxwellian spectrum, corresponding to the most probable neutron temperature $T_n$ given by:

$$T_n = T\left(1 + 0.75\,\frac{\Sigma_a}{\xi\,\Sigma_s}\right)^2 \tag{3.4.1}$$

where $T$ is the moderator temperature in electron volts, $\Sigma_a$ is the absorption cross-section at the temperature $T$ and $\Sigma_s$ is the scattering cross-section just above thermal energy. In this relation both $\Sigma_a$ and $\Sigma_s$ are calculated for the homogenized cell composition. The microscopic absorption cross-sections are corrected for deviations from a $(1/v)$-dependence; the microscopic transport cross-sections are assumed to be independent of temperature and spectrum except for hydrogen, which is approximated by a $(1/v)$-dependence. Consequently this cross-section is treated as equivalent to absorption cross-sections. The microscopic thermal cross-section for the unit lattice cell is obtained by weighting the macroscopic cross-section of the individual constituents of the cell by their volume factions and by the relative thermal flux 'seen' by the constituents.

The ratios of the relative thermal fluxes, referred to as disadvantage factors, are obtained by $P_3$-calculations. This method requires correction when the thickness of water spaces between the fuel elements is large in terms of neutron mean free path. In that case a considerable 'softening' of the spectrum occurs in the water region.

In a scheme used by Combustion Engineering Nuclear Division (CEND) for double annular fuel elements (see Fig. 3.1) the thermal utilization factor is calculated by a $P_3$ approximation using plain Maxwellian cross-sections corresponding to the ambient water temperature. In some cases an improved method is used. The macroscopic Maxwellian absorption cross-section for the homogenized cell is then modified by the following empirical scheme:

*a*) A hardened neutron temperature $T_n$ is obtained according to Eq. (3.4.1).

*b*) A macroscopic Maxwellian absorption cross-section is determined for materials of the cell that are outside the fuel element ($\Sigma_{a\,\mathrm{out}}$).

*c*) The modified Maxwellian absorption cross-section for the unit cell is then taken as:

$$\Sigma_{a\,\mathrm{mod}} = \Sigma_{a\,\mathrm{Max}} + \left(\frac{1-F}{F}\right)\Sigma_{a\,\mathrm{out}} \tag{3.4.2}$$

where:

$$(1-F) = \frac{V_{\mathrm{out}}}{2}\sqrt{\frac{T}{T_n}}\left[1 - \sqrt{\frac{T}{T_n}}\right]$$

and $V_{\mathrm{out}}$ is the volume fraction of the total material within the cell but outside the fuel element.

More practical and of a less empirical nature is a method applied by General Electric Atomic Power Equipment Department (GE-APED) to a single annular fuel element geometry (Fig. 3.1). Here the thermal group cross-sections are obtained by dividing the unit cell into two zones of uniform, but dissimilar spectra. The boundary between the two zones is chosen at one scattering mean free path from the fuel element surface, as evaluated for thermal neutrons in water at the ambient moderator temperature. The spectrum within the inner zone is determined by a WILKENS spectral calculation [10]. The thermal parameters for the discrete composition regions within this inner zone are averaged over this spectrum and are referred to as 'hard' parameters. Parameters obtained for a pure water Wilkens spectrum are called 'soft parameters'. The thermal parameters for the discrete composition regions within the outer zone (usually normal water unless spacer materials are present) are determined by the relation:

$$\Sigma_{\mathrm{outer\,zone}} = \left[\Sigma_{\mathrm{soft}} - (\Sigma_{\mathrm{soft}} - \Sigma_{\mathrm{hard}})\exp - \frac{(Ct)}{\lambda_s}\right] \tag{3.4.3}$$

in which $t$ represents the thickness of the outer zone, while $C$ is an empirical constant equal to 1.1.

The methods described above clearly indicate that many different schemes are used for the calculation of the thermal utilization factor. To each of the unit lattice cells spectral corrections are to be made, the nature of which depends on the fuel element geometry. Equivalent problems arise with respect to the epi-thermal capture cross-section for $^{238}U$. The relations used for room-temperature conditions are frequently based on the measurements of HELLSTRAND [11] and include a $(1/v)$-component of the $^{238}U$ effective absorption cross-section of 1.1 barn. The cross-section for $UO_2$ is then taken as:

$$\Sigma_a{}^{238} = \frac{V_{UO_2} \cdot N_{UO_2}}{\triangle u} \left[ 5.25 + 26.6 \sqrt{\left(\frac{S}{M}\right)_{eff}} \right] \cdot 10^{24}. \tag{3.4.5}$$

The term between the brackets is the resonance integral for $UO_2$. Further is $V_{UO_2}$ the $UO_2$ volume, $N_{UO_2}$ the number of $UO_2$ atoms per $cm^3$ and $\triangle U$ is the epi-thermal lethargy interval. The factor $(S/M)$ is the fuel element surface-to-mass ratio. The effective surface-to-mass ratio depends of course on the fuel element geometry. For solid rods $(S/M)_{eff}$ is taken as the physical surface-to-mass ratio $(S/M)$ of the fuel. In the GNEC determination of $(S/M)_{eff}$ for single or double annular fuel elements in the voided condition, $S$ is taken as the perimeter of the outer $UO_2$ surface and $M$ is taken as the mass of the fuel per unit length of the fuel element. This is equivalent to treating the element as a solid rod with the same outer surface but the given mass of fuel uniformly distributed within the surface. This approach involves a fictive reduced fuel density as a result of which the spectrum in the fuel is softened. Consequently the pure resonance absorption and the $(1/v)$-absorption are accounted for in a shifted proportion.

Various methods are used to account for epi-thermal self-shielding between neighbouring fuel elements. The GNEC-method does not account for this effect. CEND uses a correction developed by BELL [12], while GE-APED applies the DANCOFF-GINSBURG relations [13].

When water is contained in the internal spaces of the element (i.e. flooded condition) there is an increase in the effective surface-to-mass value. As suggested by CRITOPH [14] and by HELLSTRAND [11] a fraction of the inner surface is to be added to the outer surface to calculate the total $(S/M)_{eff}$ value. The actual inner surface exposed to the water is reduced in proportion to the probability of an epi-thermal neutron escaping from the water to the element surface. For a cylindrical central hole, this probability may be taken from the PLACZEK-tabulation [15]. The expression for the effective inner surface then becomes:

$$S_{i,eff} = S_i \cdot r\Sigma_s{}^r P_0(\Sigma_s{}^r r). \tag{3.4.6}$$

where $\Sigma_s{}^r$ is the macroscopic scattering cross-section for the internal

medium (generally water) at the resonance energy; $r$ is the internal radius and $P_0$ is the Placzek escape probability in cylindrical geometry. The effective surface to be used in Eq. (3.4.5) is:

$$S_{eff} = S_{i,eff} + S_0. \tag{3.4.7}$$

For similar conditions, that is a flooded fuel element steam section, GE-APED uses the following expression for the effective surface-to-mass ratio:

$$\left(\frac{S}{M}\right)_{eff} = \frac{1}{M}\left(S_0 DG_0 + \frac{\phi_i S_i DG_i}{\phi_0}\right) \tag{3.4.8}$$

where:

$M$ = mass of fuel per cm length of fuel

$S_{0(i)}$ = outer (inner) fuel element surface area per cm

$DG_{0(i)}$ = appropriate Dancoff-Ginsburg factors

$\phi_{i(0)}$ = resonance flux at respective surfaces.

The method of obtaining $DG_{0(i)}$ is given by SPINRAD, *et al.* [16].

Comparing the various results of one or two-dimensional analyses with those of experiments (see also reference [17]) the conclusion may be that:

*a*) Predictions of $k_{eff}$ can generally be made within $\pm$ 1.5 %.

*b*) Element wise power distributions can be predicted to about 15 % depending on the heterogeneities present.

*c*) Azimuthal power peaking in large fuel elements adjacent to wide water channels is grossly overestimated.

*d*) Control rod reactivities can generally be determined to within 10 % to 25 %.

A consequence of the inaccuracies in the calculations is that the actual obtainable power level may be considerably higher than the design output. This fact may be verified by measuring the true power distribution in a critical assembly using proven experimental techniques. Furthermore the inaccuracies in the control rod reactivity calculations may affect the proposed core lifetime, and certainly require the rod values to be experimentally checked.

## REFERENCES


1. NOVICK, M., *et al.*, Developments in nuclear superheat, A/Conf. 28/P/215 (1964).
2. KORNBICHLER, H., Superheat reactor development in the Federal Republic of Germany, A/Conf. 28/P/535 (1964).
3. DOLLEZHAL, N. A., *et al.*, Development of superheating power reactors of the Beloyarsk nuclear power station type, A/Conf. 28/P/309 (1964).
4. KLEIJN, H. R., Problemen bij nucleaire oververhitting van stoom, Atoomenergie en haar toepassingen, 5, 100–112 (1965).

5. Sokolov, I. N., *et al.*, Experimental pressure vessel reactor for studies in boiling and steam superheating, A/Conf. 28/P/206 (1964).
6. Deutsch, R. W., Nucl. Science and Eng., 13, 110–131 (1962).
7. Valerino, M. F., *et al.*, State of the art physics of nuclear superheat reactors, GNEC–282 (1963).
8. Spalaris, C. N., Nucleonics, 21, No. 9, p. 41–49 (1963).
9. Bohl, H. Jr., E. N. Gelbard and G. H. Ryan, Muft-4 Fast neutron spectrum code for IBM-704, WAPD–TM–72 (1957).
10. Argone National Laboratory, Reactor physics constants, ANL–5800 second edition, par. 3.1.4.3, USAEC (1963).
11. Hellstrand, E., J. of Appl. Physics, 28, 1493 (1957).
12. Bell, G. I., Nucl. Science and Eng., 5, 138 (1959).
13. Dancoff, S. M. and M. Ginsburg, Surface resonance absorption in a close-packed lattice, CP–2157, U. of Chicago (1944).
14. Critoph, E., Canadian report CRRP–655 (1955).
15. Case, K. M., F. de Hoffmann and G. Placzek, Introduction to the theory of neutron diffusion, Vol. I, U.S. Government Printing Office, Washington, D.C. (1953).
16. Spinrad, B., *et al.*, Resonance capture in uranium and thorium lumps, A/Conf. 15/P/1847 (1958).

CHAPTER 4

# RESONANCE ESCAPE PROBABILITY

## 4.1 *Introduction*

Capture of neutrons in $^{238}U$ leads to the formation of $^{239}Pu$ according to the following nuclear reaction:

$$^{238}U(n,\gamma)\,^{239}U \xrightarrow[23.5\ \text{min}]{\beta^-(1.21\ \text{MeV})} {}^{239}Np \xrightarrow[56.3\ \text{h}]{\beta^-(0.72\ \text{MeV}),\,\gamma} {}^{239}Pu \xrightarrow[24\times10^3\ \text{a}]{\alpha}$$

where the energies indicated refer to the maximum energy of the beta-particles emitted in the respective decays.

In an operating reactor, fueled with slightly enriched uranium, neutrons captured in $^{238}U$ are lost for a further fission-slowing down cycle. As a result the reactivity of the core is negatively affected, which has a direct bearing on the core size and the reactor vessel dimensions when the enrichment of the fuel is kept constant. Consequently, like all parasitic neutron absorptions in a reactor, neutron capture in $^{238}U$ is increasing the capital costs of a nuclear power plant installation. Whereas in general neutron capture in $^{238}U$ is also met by increasing the fuel enrichment, the rise in capital costs is partially compensated, but at expense of a small increase in the operational costs. However the resulting $^{239}Pu$ is again fissionable by thermal neutrons and adds to the fissile fuel investment and ultimately to the attainable burn-up. Indirectly therefore, neutron capture in $^{238}U$ contributes to a reduction of operating cost.

The isotopes $^{240}Pu$ and $^{241}Pu$ are also produced as a result of neutron capture. The half-lives of the parent nuclei differ as do the half-lives of the plutonium isotopes. Therefore their relative yield is time and power dependent.

The isotope $^{240}Pu$, which has a threshold energy for fission of less than 500 keV, contributes to the fast fission factor. Further it is a valuable fertile material. The isotope $^{241}Pu$ is again fissionable by thermal neutrons.

Due to the fact that $^{239}Pu$ and $^{241}Pu$ are fissionable by thermal neutrons their formation influences the microscopic neutron distribution as well as the reactivity balance.

Neglecting the influence of temperature the probability of a $^{238}U$ nucleus absorbing a neutron depends upon the energy of the neutron. Above 6 eV this probability shows a number of large peaks, as a result of which a

considerable fraction of the plutonium produced is due to so-called resonance absorption. In thermal reactors fueled with natural or slightly enriched uranium the resonance peaks are important up to an energy of about 200 eV. Generally, the peak closest to the thermal region (at 6.68 eV) accounts for about 50 % of the epi-thermal neutron absorption. The absorption mean free path of the resonance neutrons in uranium is on the order of one hundred microns and therefore they will only just penetrate the surface of a fuel rod. The remaining part of the fuel in the rod is 'shielded' against these resonance neutrons. Of course, other than resonance neutrons will be absorbed throughout the entire fuel volume. This effect is frequently referred to as $(1/v)$-absorption. Consequently capture over the entire neutron spectrum may be divided into a surface effect and a volume effect. The fraction of neutrons having higher than thermal energies not leaking from the reactor and escaping capture in $^{238}U$ is defined as the resonance escape probability $p$.

In general the neutron flux and the neutron energy spectrum in a reactor are spatially dependent. Therefore the production rate of the forementioned plutonium isotopes will vary over the core. As the fuel burn-up rate is also not homogeneous throughout the core both the energy and spatial distribution of the neutrons are in addition time dependent. Thus the fuel composition in a reactor will be a complicated function of space and time.

In view of the foregoing discussions it is clear that the attainable burn-up in slightly enriched lattices is very sensitive to the ratio of the number of plutonium atoms produced per uranium atom destroyed. Neglecting for the time being the formation of plutonium isotopes with mass numbers exceeding 239, this ratio is expressed in the conversion-ratio $CR$, which is defined as:

$$CR = \left[\frac{\text{number of neutrons captured in } ^{238}U}{\text{number of neutrons absorbed in the fuel } (^{235}U + ^{238}U)}\right].$$

This ratio, which is a function of the burn-up, is to be determined over the entire energy spectrum. As long as burn-up is not very high, this definition may be simplified to:

$$CR = \frac{\text{number of neutrons captured in } ^{238}U}{\text{number of neutrons absorbed in } ^{235}U}.$$

The latter definition of the conversion-ratio can be expressed as:

$$CR(t) = \frac{\int_0^\infty \int_{\text{fuel vol.}} \Sigma_c{}^{238}(E, \mathbf{r})\, \phi(E, \mathbf{r}, t)\, dE\, d\mathbf{r}}{\int_0^\infty \int_{\text{fuel vol.}} \Sigma_a{}^{235}(E, \mathbf{r})\, \phi(E, \mathbf{r}, t)\, dE\, d\mathbf{r}}. \tag{4.1.1}$$

SPINRAD, *et al.* [1] indicates, that for a light water-reactor where a burn-up of 10,000 MWday/ton is expected, an increase of 1 % in the initial-conversion-ratio (that is for a clean core) will give an increase of 5 % in attainable burn-up.

Boiling of the liquid coolant in a water-reactor reduces the slowing down density in the moderator and consequently affects the neutron energy spectrum. Therefore the conversion absorption will also be related to the void fraction in the coolant. In order to test the validity and possibly to improve existing calculation methods for BWR-type reactors it is necessary to experimentally determine the relationship between various void fractions and the conversion absorption. Such experiments can be carried out in relatively small assemblies.

In the absence of external sources the neutron energy spectrum in a neutron multiplying system at a particular time depends on the physical properties of the materials involved, the geometrical arrangement and the size of the system. Microscopic spatial changes in this spectrum are a consequence of the heterogeneous composition of the system. Macroscopic changes in the spectrum result from different neutron leak rates for different neutron energies and are related to the size of the core, or are due to the application of regions with different material compositions. When the macroscopic distribution shows no gradient the spectrum is said to be at equilibrium. An equilibrium spectrum occurs far from boundaries or discontinuities (three to five scattering mean free paths). It is obvious that for mutual comparison of experimental data in regard to fine structure parameters on one hand, and for verification of theoretical results on the other it is essential that all data implicitly refer to an equilibrium spectrum.

In principle the resonance escape probability $p$ is determined by the same factors that stipulate the neutron energy spectrum. In fact $p$ may – within certain limits – be considered as an indication for the hardness of the spectrum. When the spectrum gets softer $p$ increases and vice versa.

When by one means or another one succeeds in creating the right spectrum in a small subcritical lattice section to be examined, it is completely unimportant whether this test lattice is part of a critical, subcritical or exponential facility. Whereas it is possible to obtain equilibrium spectra in exponential assemblies, these facilities can be very useful for the experimental determination of microscopic reactor parameters.

From Fig. 1.7 and Fig. 1.8 in Chapter 1 it can be seen that in light water moderated exponential assemblies not the spectrum but the exponential decay of the neutron flux level is a problem. In addition it can be concluded from these figures that in a large section of the LEAD central zone the equilibrium spectrum exists. In the peripheral zone there is no equilibrium spectrum because the region is too small. On the inner side it is adjacent to a region with a harder spectrum, while in the surrounding reflector the spectrum is considerably softer. Consequently the measurements in the peripheral zone have not been performed under ideal circum-

stances. Since the regions which could be voided are somewhat small, it may be expected that the fine structure measurements at higher moderator void fractions have been performed in a somewhat softer spectrum than the equilibrium spectrum, leading to a too high value for $p$. An attempt to measure the neutron temperature as a means of verification failed because of the low neutron flux level.

Although the experiments described in this thesis only refer to two different moderator-to-fuel volume ratios, it would have been possible to measure both the resonance escape probability and the thermal utilization factor (see Chapter 5) for any other ratio, provided a sufficiently large test lattice would have been introduced in the LEAD facility. For such measurements it would have been preferable to construct a one zone core optimized in neutron multiplication.

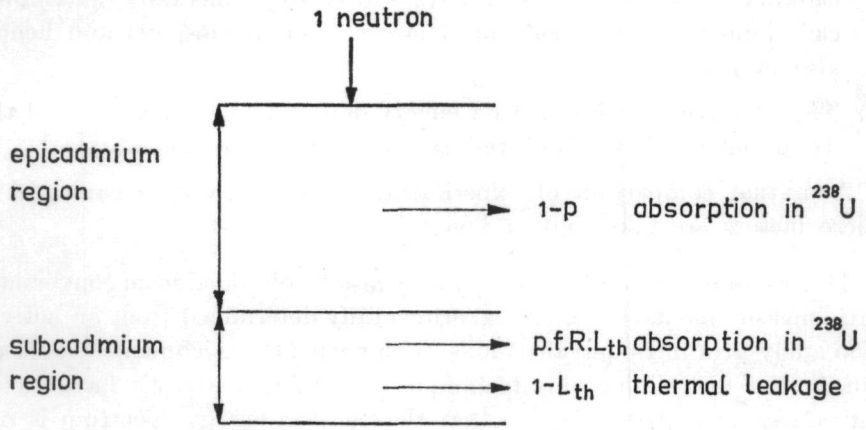


Fig. 4.1. Neutron balance in view of cadmium-ratio measurements.

4.2 *Experimental methods to determine the resonance escape probability*

As indicated in section 4.1 the value of the resonance escape probability is of direct importance in reactor design calculations. Experimentally this parameter is frequently determined from the epi-cadmium absorption rate in the fuel, particularly in $^{238}$U. Measurements of this kind have for example been reported by KRASIK, *et al.* [2] and KLEIN, *et al.* [3]. As can be concluded from Fig. 4.1 the relationship between the resonance escape probability $p$ and the cadmium-ratio $R_{Cd}$ is given by

$$p = \frac{1}{1 + \left[\frac{fRL_{th}}{R_{Cd} - 1}\right]}. \tag{4.2.1}$$

In Eq. (4.2.1), which is implicitly based on a two group approach, $f$ stands for the thermal utilization factor, $R$ is the ratio of the number of thermal neutrons absorbed in $^{238}$U to the number of thermal neutrons absorbed in the fuel ($^{235}$U + $^{238}$U) per unit time, and per unit volume in the sub-

cadmium region. The factor $L_{th}$ accounts for the thermal leakage and is referred to as the thermal non-leakage probability.

The cadmium-ratio method to determine $p$ is simple from an experimental point of view and does not require expensive instrumentation. However it has the following disadvantages:

*a*) The use of cadmium will cause perturbations in the resonance capture as a result of spectral shifts.

*b*) The results depend on the thermal utilization factor, which is either obtained from calculations or experiments. Any error in $f$ will automatically affect the accuracy in $p$, while further the threshold between the thermal and epi-thermal energy regions must be equal for $f$ and $p$.

*c*) In general water lattices are undermoderated so that, relatively, the cadmium-ratio will be low. An error in an experimentally determined cadmium-ratio will result in a larger error in $(R_{Cd}-1)$ and hence, also in $p$.

*d*) The effective cadmium cut-off energy depends on the thickness of the cadmium covers used as well as on the neutron temperature.

A mutual comparison of experimental results is only meaningful if these factors are taken into account.

The resonance escape probability may also be obtained from conversion-ratio measurements which are experimentally determined from an activation analysis of fuel-equivalent foils (with regard to enrichment) irradiated within the fuel. Using this technique no foreign materials have to be introduced into the lattice, so that the neutron energy spectrum is not affected. Consequently conversion-ratios can be determined rather accurately. A description of this technique is given below:

Applying a two energy group approach to well-thermalized, slightly enriched systems (see Fig. 4.2) the general formulation of the initial-

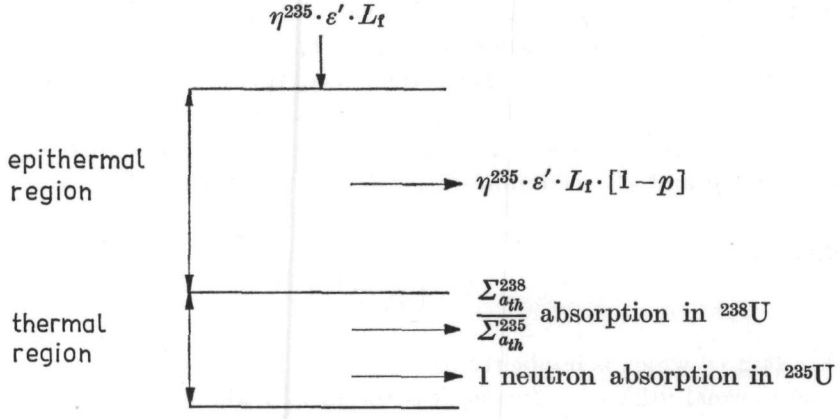


Fig. 4.2. Neutron balance in respect of the conversion-ratio based on a two-energy group approach.

conversion-ratio $ICR$ (at time of start-up) as given in Eq. (4.1.1) can be modified into:

$$ICR = \frac{\Sigma^{238}_{a_{th}}}{\Sigma^{235}_{a_{th}}} + \eta^{235}\varepsilon'(1-p)\,e^{-B^2\tau}. \tag{4.2.2}$$

The first term on the right side of Eq. (4.2.2) accounts for the conversion in the thermal energy region. The absorption cross-sections are the effective cross-sections over the thermal spectrum up to a selected cut-off energy (see also Chapter 5). On the average the thermal conversion accounts for about 70 % of the total conversion. The second term represents the epi-thermal conversion primarily determined by the resonance absorption in $^{238}$U. The contribution to the conversion-ratio of neutrons having energies higher than 1 MeV, the fission threshold of $^{238}$U, is on the order of 1 % and is therefore not separately specified in Eq. (4.2.2). Actually this effect is accounted for by the resonance escape probability $p$. The factor $\varepsilon'$ is the total-to-thermal fission-ratio, which accounts for fast fission in $^{238}$U and epi-thermal fission in $^{235}$U. In fact $\varepsilon'$ is equal to the fast fission factor used in the four factor formula. In this chapter $\varepsilon$ will be used to indicate the contribution to the fission neutron yield due to fission of $^{238}$U only. Fast leakage is corrected for by the factor $e^{-B^2\tau}$ which is based on Fermi-age theory. In large size, slightly enriched water lattices fast leakage is on the order of a few percent or less.

For experimental convenience it is necessary to introduce the concept of the modified-conversion-ratio ($MCR$), which is defined as:

$$MCR = \frac{^{238}\text{U-capture}}{^{235}\text{U-fission}} = \frac{\Sigma^{238}_{a_{th}}}{\Sigma^{235}_{f_{th}}} + \nu^{235}\varepsilon'(1-p)\,e^{-B^2\tau}. \tag{4.2.3}$$

Comparing Eq. (4.2.3) with Eq. (4.2.2) one observes that $^{235}$U-capture has been omitted. The reason is that the half-life of the $\alpha$-active $^{236}$U which results from neutron capture in $^{235}$U is very long ($2.4 \times 10^7$ a). Therefore the $^{236}$U activity cannot be detected from clean foils with any accuracy.

In order to avoid problems involved with absolute counting it is advantageous to normalize the $MRC$-measurements to a reference spectrum. If one is primarily interested in the conversion properties of a lattice, this reference spectrum should preferably be a plain Maxwell-spectrum because from a conversion point of view the conditions for normalization are thus properly defined making a mutual comparison with other experimental data possible. However when one wants to determine the resonance escape probability the parameter to determine for normalization purposes is the modified-conversion-ratio in a thermal spectrum equivalent to that in the fuel rods in the lattice. It should be realized that this spectrum hardens when the moderator void fraction in a reactor is increased. For the LEAD-peripheral zone an increase of about 80° K in the neutron

temperature was calculated for a void fraction varying from zero to about 30 %. A reference spectrum approaching the thermal spectrum in the fuel rod may be found in a suitable medium surrounding a neutron multiplying system at some distance from the system-medium interface. It is obvious that this reference spectrum will introduce a systematical error in the experiment which is readily accepted in view of the problems that arise when absolute counting techniques have to be used. By normalizing the lattice *MCR*-data to this thermal reference spectrum one obtains the relative-modified-conversion-ratio *RMCR*:

$$RMCR = \frac{\left[\frac{^{238}\text{U-capture}}{^{235}\text{U-fission}}\right]_{\text{lattice spectrum}}}{\left[\frac{^{238}\text{U-capture}}{^{235}\text{U-fission}}\right]_{\text{thermal spectrum}}}.$$

Consequently the experiments to be performed for the determination of $p$ basicly consist of:

*a*) The detection of fission in $^{235}U$

*b*) The detection of capture in $^{238}U$

Problems related to conversion-ratio experiments have been described by BROWN, *et al.* [4].

Because the *RMCR*-method is potentially more accurate and more instructive than the cadmium-ratio method, it was selected to determine the resonance escape probability as a function of various void fractions in LEAD.

A further refinement in the experiment known as the differential technique made it possible to measure the spatial distribution of fissions in the fuel and neutron capture in $^{238}U$. For this purpose a number of foils has been placed across specific fuel rods, see Fig. 4.6.

### 4.3 *Detection methods for fission and neutron capture in* $^{238}U$.

#### 4.3.1 Detection of fission

The integrated number of fissions that have occurred in an irradiated fuel sample may be determined from the fission product activity. In principle four different methods have been reported:

*a*) DETECTION OF GROSS FISSION PRODUCT GAMMA-RAY ACTIVITY

The gamma activity, above a certain threshold energy, of a complete mixture of fission products in an irradiated fuel sample provides a means to determine the relative number of fissions that have taken place [5, 6]. For this purpose a NaI(Tl) scintillation crystal in combination with a single-channel analyser may be used. The threshold is required to eliminate perturbations caused otherwise by bremsstrahlung as a result of beta-decay activity of $^{239}U$ and $^{239}Np$ respectively. Shortly after irradiation the

threshold is to be set slightly above 1.2 MeV to discriminate against the most energetic beta-rays emitted by $^{239}U$, see section 4.1. A few hours after the end of an irradiation the threshold may be reduced to 0.7 MeV which then eliminates pulses caused by beta-rays from $^{239}Np$. Since the energies of the fission product gamma-rays thus detected are in excess of at least 0.7 MeV the gamma-ray self-absorption in the foils is quite small (on the order of 1 %) and no stringent requirements have to be set on the foil surface. However due to the sensitive relationship between the integral gamma activity as a function of the gamma-ray energy the stability of the counting equipment must be rather high. The foils cannot be re-used for a couple of weeks so that the activity may decay sufficiently. In order to compare integral fission densities in different foils the relative yield of fission products should be the same in all samples. Only then will the gamma-ray spectra be equivalent. To obtain an equal fission product yield the irradiation periods of all foils should be the same and in addition the irradiation intensity should be constant over that period. Changes in this yield due to variations in the neutron energy spectrum can be ignored.

*b*) Detection of gamma-rays from a specific fission product

A method to determine the absolute integral fission density is to measure the gamma-ray activity of a specific fission product [7]. This fission product should meet two conditions; in the first place its half-life must be sufficiently long and secondly it should emit nevertheless high energy gamma-rays. The daughter product of $^{140}Ba$ (12.8 d), $^{140}La$ (40.2 h) has proved to be very useful for this purpose. It yields in 88 % of all disintegrations gamma-rays with an energy of about 1.6 MeV. For completeness it should be noted here, that $^{140}Ba$ is the decay product of $^{140}Cs$ (66 s) which results from the decay of the fission product $^{140}Xe$ (16 s). The advantage of this method is that especially when a large number of foils is to be counted, the irradiation and counting times of the various foils are not required to be equal because of the pure exponential build-up and decay of the gamma-ray activity. Time differences can be very simply accounted for. A disadvantage is the low counting yield. In order to obtain accuracy in the results the neutron flux at the detector position in the lattice should be at least $10^8$ n/cm$^2$·s.

*c*) Gross beta or gamma-ray counting of fission fragments in catcher foils

A third technique to determine the number of fissions that have occurred in irradiated fuel samples is based on catching recoiled fission products [8, 9]. For this purpose the fuel foils are surrounded by thin aluminium foils while being irradiated. Fission products that escape from the fuel foils are caught in the aluminium foils which are later counted on beta or gamma-ray activity. Although this method has the advantage that simple

counting equipment can be used and fuel foils are quickly re-usable it has also some disadvantages. The aluminium foils need to be very pure to guarantee that no impurities are activated. A further drawback inherent in the method is that foreign material is introduced in the fuel which may affect the neutron-energy spectrum and therefore the local fission density. Since the fission product range in uranium is very short (less than 10 $\mu$) the ejection rate of fission fragments is low. Consequently the counting yield will be relatively small.

*d*) CHEMICAL SEPARATION OF A PARTICULAR FISSION PRODUCT

Chemical techniques to separate a particular fission product require chemical facilities and staff. The method has the advantages that the requirements with regard to foil dimensions are not stringent and simple counting equipment can be used [3, 10]. It is obvious that a fuel foil can only be used once so that the amount of fuel consumed is relatively high.

The methods *a*) to *d*) described above determine fissions that have occurred both in $^{235}U$ and $^{238}U$. In order to obtain the number of fissions that have occurred only in $^{235}U$, results have to be corrected for fast fission of $^{238}U$. This correction can either be calculated as has been done in the experiments described in this chapter or it may be obtained from an activation analysis of irradiated depleted foils. Comparing merits and disadvantages of the various fission detection methods, and taking into account available facilities and equipment, the technique described under *a*), detection of gross fission product gamma-ray activity, was selected to determine the number of fissions that have occurred in $^{235}U$.

### 4.3.2 Neutron capture in $^{238}U$

A quantity proportional to the number of neutrons captured in $^{238}U$ might be obtained by determining the amount of $^{239}U$, $^{239}Np$ or $^{239}Pu$ produced. Because in general the fuel foils used are less than 1 gram in weight and the integrated thermal neutron flux over the irradiation time does not exceed $10^{12}$ $n/cm^2$, the amount of plutonium produced in a foil is only on the order of $10^{-13}$ g. Since its half-life is $24 \times 10^3$ years, counting the $\alpha$-activity would not yield any information in a practical period of time. Therefore the techniques used for the determination of capture in $^{238}U$ rely on the detection of $^{239}U$ or $^{239}Np$ by means of various counting techniques. The main problem that arises, comes from the disturbing activities resulting from:

*a*) The fission product activity, which is particularly great in the lower gamma-ray energy range.

*b*) The natural activity of $^{238}U$ which consists primarily of 93 keV gamma-rays from its decay product $^{234}Th$.

*c*) The natural activity of $^{235}U$ which becomes more important as the enrichment of the fuel is increased. The activity consists mainly of

gamma-rays with an energy of 186 keV. Whereas only natural uranium foils are used the results should not be influenced very much by this activity.

Depending on the method through which the unwanted activities are suppressed three basicly different techniques can be distinguished.

*a*) Use of depleted uranium foils

When depleted uranium foils are used one can either determine the $^{239}U$ content from beta or gamma-ray activity measurements or the amount of $^{239}Np$ by counting the characteristic 106 keV gamma-rays or the 104 keV X-rays; see method *c*) below [5, 8, 11]. It is obvious that even when using highly depleted foils a significant fission product contribution remains, not only as a result of fast fission in $^{238}U$ but in particular from fission in $^{235}U$ which is still present in these foils. Furthermore the use of depleted foils causes local perturbations in the fission density while the foils are being irradiated. Consequently also the capture in $^{238}U$ is affected. Detecting the amount of capture by counting the $^{239}U$ activity is attractive because of its relatively short half-life (23.5 min) which will lead to acceptable counting statistics. However the self-absorption for the 74 keV gamma-rays from $^{239}U$ is larger than that of the 104 keV X-rays or 106 keV gamma-rays following the decay of $^{239}Np$.

*b*) Chemical or chromatographical separation techniques

Sophisticated chemical and chromatographical techniques have been developed to separate either $^{239}U$ or $^{239}Np$ from the other constituents of irradiated foils [12, 13, 14]. Although these techniques are quite complex the counting equipment can be very simple. They have not been used because a method described in the next paragraph, based on a physical approach, would be more appropriate.

*c*) Application of coincidence techniques for detecting $^{239}Np$.

Coincidence techniques are widely used for suppressing unwanted activities while counting discrete nuclear effects [15]. For the detection of $^{239}Np$ two fundamentally different coincidence methods may be used. In one method the background is suppressed by means of time discrimination while the other is based on energy discrimination.

From the decay-scheme of $^{239}U$ presented in Fig. 4.3 it can be seen that one of the excited states of $^{239}Pu$, which follows about 45 % of the $^{239}Np$ decays, has a half-life of 0.193 $\mu$s, which is relatively long. No fission products are known with the same combination of half-life and abundance, so that by counting coincidences between beta-particles and delayed gamma-rays a very good suppression of all other activities may be obtained. However this technique requires a fast coincidence system with a resolving time of less than $10^{-8}$s, hence calling for rather specialized electronic equipment [16]. Therefore this method was *not* selected.

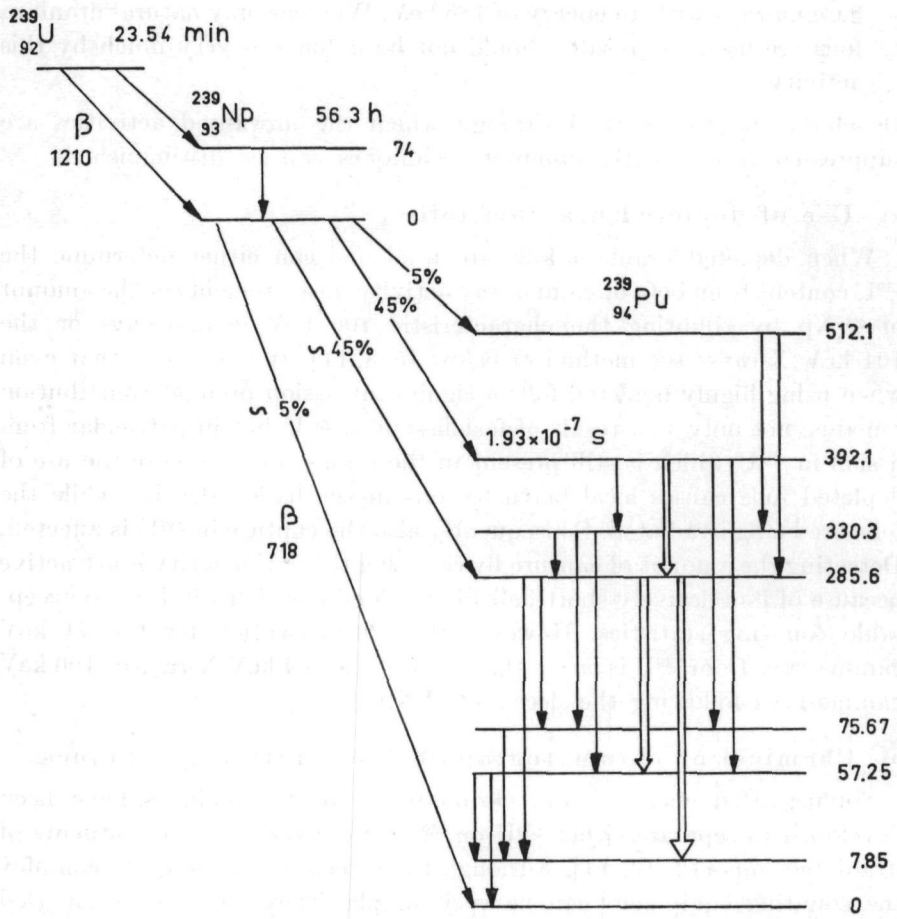


Fig. 4.3. Simplified decay scheme of $^{239}U$. The dubble lines indicate the 106 keV, 228 keV and 278 keV coincident gammy-rays. (All energies are expressed in keV.)

The energy discrimination method reported originally by SHER [17] and further developed by TUNNICLIFFE [18] is more attractive. A lower excited state of $^{239}Pu$ decays by emission of either 228 keV or 278 keV gamma-rays. These gamma-rays have large internal K-conversion coefficients which give rise to 104 keV X-rays. The X-rays are of comparable intensity to 106 keV gamma-rays, which follow from the decay of the previously mentioned excited state of $^{239}Pu$. The gamma-rays and the X-rays are coincident in time. The coincident gamma-rays are shown in Fig. 4.3 in double lines. Applying a gamma-X-ray coincidence counting technique the suppression of unwanted activity is very effective. As a matter of fact *this* technique was selected to determine the amount of neutron capture in $^{238}U$.

## 4.4 *Experimental accessories*

### 4.4.1 Counting equipment

*a*) INTEGRAL FISSION DENSITY

The integral fission density was determined from the gross fission product gamma-ray activity. A cylindrical NaI(Tl) crystal 5 cm in diameter and 5 cm high was used in combination with a single-channel analyser. Since counting of the fuel foils started one hour after the end of an irradiation, the discriminator level was set slightly above 1.2 MeV to eliminate pulses resulting from the 1.2 MeV beta-particles emitted by $^{239}$U. The energy calibration of the discriminator was obtained by using $^{137}$Cs (0.662 MeV) and $^{60}$Co (1.17 MeV and 1.33 MeV) gamma-ray sources. In view of the required stability of the electronic equipment special care was taken in selecting the various instruments and components. Further the temperature in the room where the electronic equipment was used was kept as constant as possible ($\pm$ 1° C). In order to suppress perturbing background effects both the crystal and photomultiplier were shielded with 5 cm thick lead blocks.

*b*) COINCIDENCE COUNTING EQUIPMENT

For counting the time-coincident 106 keV gamma-rays and the 104 keV X-rays following the decay of $^{239}$Np two single-channel analysers were used. The detectors, cylindrical NaI(Tl) crystals (5 cm in diameter and 0.5 cm high) were mounted on to EMI-photomultipliers, type 9536 A. The complete combination was shielded with 5 cm lead. Since the absorption coefficient for 100 keV gamma-rays in NaI is about 7 cm$^{-1}$ the thin crystals were selected to suppress high energy contributions in the coincidence yield. In addition the detection of possible coincidences from cosmic radiation was reduced. The energy calibration of the differential analysers was obtained with a $^{144}$Ce source (34, 81, 94, 100 and 134 keV). The relationship between the energy and the pulse height was found to be linear. The discriminator level of the two analysers was set between 90–116 keV and 89–119 keV respectively. These values were selected in view of reproduceability as they correspond to integers (voltages) on the pulse height and channel-width selectors. Because of the resolving power of the crystal-photomultiplier combination (relative half-width 16 % at 88 keV) the $K\alpha_1$-line of 103.65 keV will be detected together with the $K\alpha_2$-line at 99.46 keV and the $K\beta_1$-line at 117.15 keV. For isotopes with an atom number around 92 the intensity ratio $K\alpha_1/K\alpha_2$ is about 2 and $K\alpha/K\beta$ is of the order of 2.5 so that the major fraction of X-rays is emitted with an energy of 103.6 keV. As all the measurements are normalized to a thermal spectrum the wide window (channel) does not affect the counting results and no coincidences are lost as a result of energy discrimination.

The arrangement of instruments was such that the standardized output pulses of the differential analysers were fed into a transistorized coinci-

dence circuit. Counts could be taken from each individual channel and from the coincidence circuit output. A block diagram is shown in Fig. 4.4 while a cross-sectional drawing of the crystals which are mounted opposite to each other is presented in Fig. 4.5. When located in its measuring position between the crystals the foil is surrounded by a lead shield in order to avoid coincidences due to Compton-scattering from one crystal into the other.

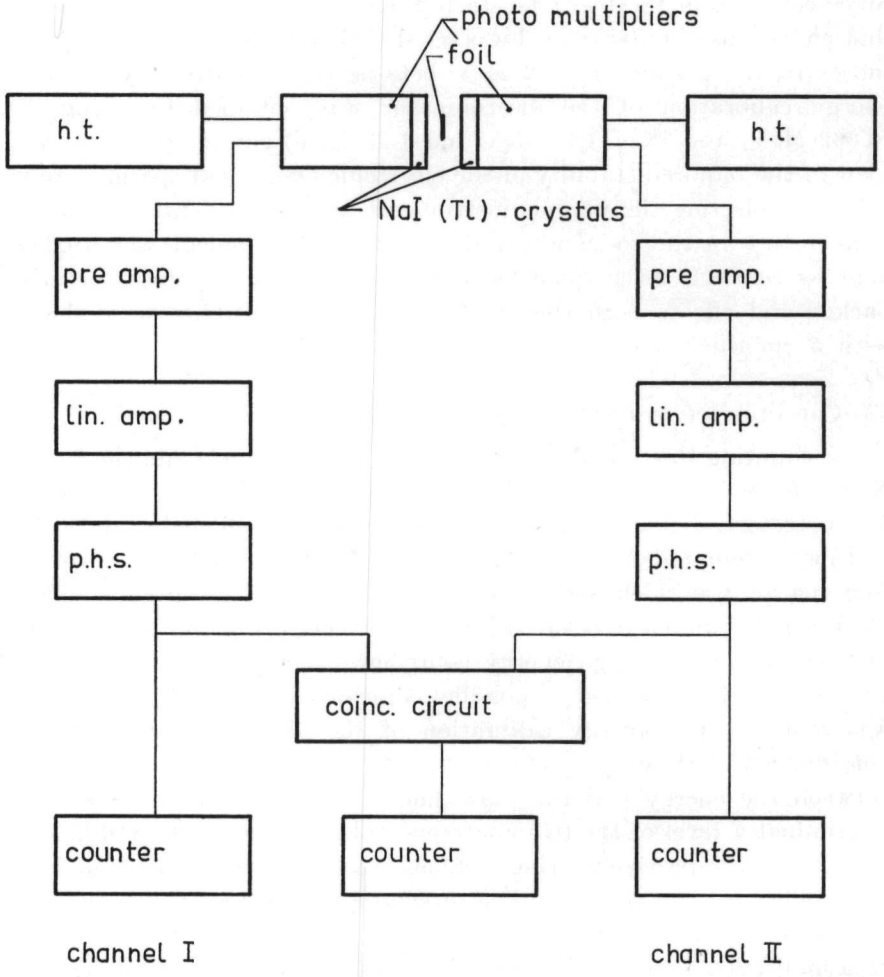


Fig. 4.4. Block diagram of the instruments used for coincidence measurements.

The resolution time of the coincidence equipment used is mainly determined by the length of the input pulses ($\sim 10^{-6}$ s) to the coincidence circuit proper and was measured to be $(0.78 \pm 0.01) \times 10^{-6}$ s. The stability was checked, by determining the statistical spread in the number of counts obtained from a source having a relatively long half-life, over a period of 24 hours. The deviations were not larger than those of regular decay statistics following a Poisson-distribution.

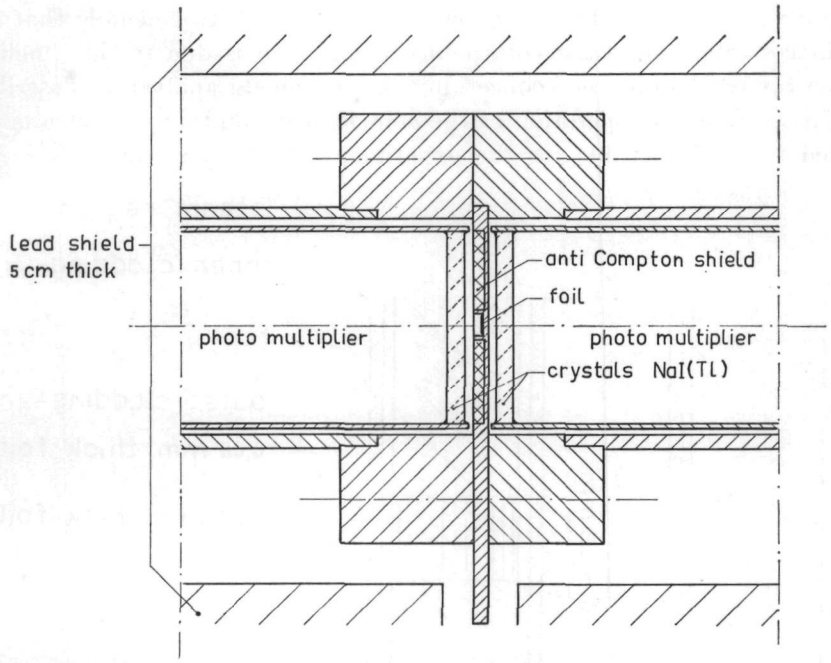


Fig. 4.5. Geometry of NaI(Tl)-crystals and photomultipliers with respect to a uranium foil for the detection of coincident photons resulting from neutron capture in $^{238}U$.

A number of measurements was made with a non-irradiated natural uranium foil giving the following results:

| | | | | |
|---|---|---|---|---|
| Channel I | 2400 | $\pm$ | 15 | cpm |
| Channel II | 1950 | $\pm$ | 15 | cpm |
| Coincidence output | 3.85 | $\pm$ | 0.07 | cpm |

Without a foil the output of the coincidence circuit was measured to be ($0.9 \pm 0.1$) cpm, which is due to cosmic rays or other background sources. In analysing the counting results of all the irradiated foils the coincidences due to background radiation were subtracted. The relatively large number of background coincidences probably arises from uranium and its decay products. In the energy range under consideration coincidences may occur from the decay of $^{234}Pa$ (125–99 keV), $^{235}U$ (74–110 keV) and $^{231}Th$ (84–81 keV). Measurements with foils of various enrichments may give more detailed information about these effects, which are believed to be mainly due to $^{234}Pa$. The coincidence decay curve was determined from measurements with an irradiated fuel foil (integrated thermal neutron flux $2.10^{12}$ $n/cm^2$). A half-life of 57.3 h was found when no corrections were applied for background coincidences, which now may also result from the decay of radioactive fission products.

Since the half-life of $^{239}Np$ is 56.3 h it seems safe to conclude that the main contribution to the coincidence count rate is due to this nuclide. From the results obtained concerning the equipment analysis as described in this section, the operation of the coincidence counting system was believed to be acceptable for the experiments to be performed.

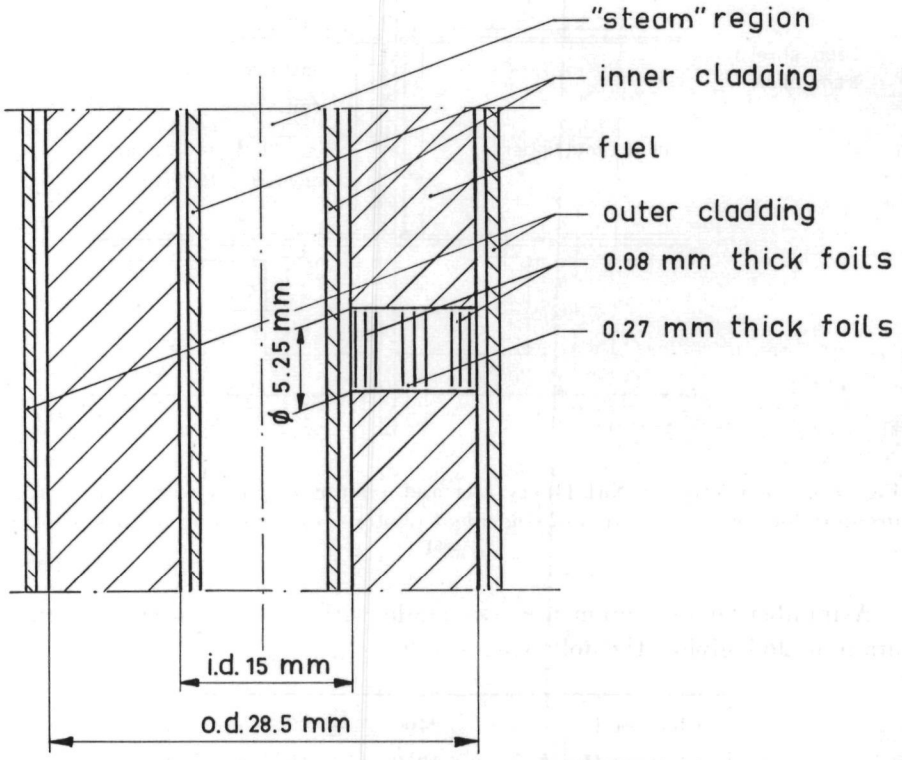


Fig. 4.6. Positioning of natural uranium foils in a fuel element.

### 4.4.2 Foils

The spatial distribution of the fission density and neutron capture in $^{238}U$ through a LEAD fuel rod was obtained from an activation analysis of natural uranium foils outlined earlier in this chapter. During irradiation these foils were positioned in a fuel rod as indicated in Fig. 4.6. In the interior region of the rod 0.27 mm thick foils were used while, because of the steep slope in the pure resonance conversion distribution, 0.08 mm thick foils were placed near the internal and external rod surfaces. The diameter of all foils was 5.15 mm. The hole in the fuel rod was 5.25 mm in diameter. Although the weight of the 0.27 mm thick foils varied between 97.8 mg and 106.9 mg a major fraction weighted between 102.5 mg and 105 mg. These differences were due to variations both in diameter and in thickness. For the purpose of foil intercalibration, correction factors had to be determined. Corrections because of a spread in diameter are simply proportional to the weight of the individual foils. Variations in thickness

affect the gamma-ray self-absorption. When fission densities are determined the gamma-rays measured have an energy in excess of 1.2 MeV. The 1.2 MeV photons have a total mean free path of about 9 mm in uranium. Therefore a small spread in foil thickness will not affect the counting results. When determining the capture rate in $^{238}U$, the photon energy is on the order of 100 keV (see section 4.3) for which the total mean free path in uranium is about 0.5 mm. It is obvious that in this case the influence of self-absorption may be quite appreciable. In order to estimate how serious a variation in thickness influences the counting results, the coincidence yield was approximatively calculated as a function of the foil thickness. The coordinate system and geometry used in this calculation are given in Fig. 4.7.

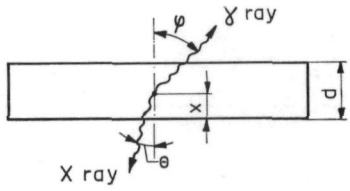


Fig. 4.7. Coordinate system used in the calculation of the coincidence yield.

The probability $P$ of a photon, born at some point in the plane at $x$ being emitted in the solid angle between $\theta$ and $\theta+d\theta$ is

$$P(\theta\rightarrow\theta+d\theta) = \frac{\sin\theta\, d\theta}{2}$$

and the probability $W$ that this photon will not undergo an interaction in the foil is

$$W = \mathrm{e}^{-\frac{x}{\cos\theta}\cdot\frac{1}{\lambda}}$$

where $\lambda$ is the photon total mean free path. The probabilities $P'$ and $W'$ for the coincident photon are obtained in an analogous way. Since no angular correlation is present here, the total probability $I$ that both coincident photons will escape from the foil and be counted is:

$$(4.4.1) \qquad I = \tfrac{1}{4}\int_0^d\int_0^{\pi/2}\int_0^{\pi/2} \sin\theta\sin\varphi\, \mathrm{e}^{-\frac{x}{\lambda\cos\theta}}\, \mathrm{e}^{-\frac{(d-x)}{\lambda\cos\varphi}}\, dx\, d\theta\, d\varphi.$$

where $d$ is the thickness of the foil.

Numerically the value of $I$ has been calculated for a number of $d/\lambda$ values. The results are shown in Fig. 4.8. The maximum is found to be around $d=0.5\,\lambda$ which corresponds to a foil thickness of about 0.25 mm. It should be noted that the required correction factor for photon self-absorption is proportional to the probability $I$. From Fig. 4.8 it can be

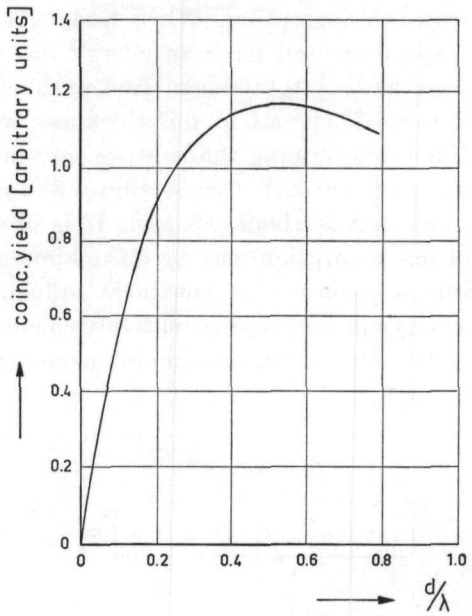


Fig. 4.8. Coincidence yield as a function of $d/\lambda$, where $d$ is the foil thickness and $\lambda$ the total mean free path.

seen that even a 10 % variation in thickness in a 0.27 mm thick foil results in a less than 1 % change in the correction factor. As the differences in thickness were all far less than 10 % no correction has been applied for this effect. Further it can be seen that when the foil thickness is small in comparison with the mean free path, the corrections are proportional to the foil thickness. Therefore the corrections made to inter-calibrate the foils were simply proportional to their weights. The fact that the coincident X-ray and gamma-ray have about equal energy has not been taken into account in the derivation for $I$. As a result of this coincidence, both single channel analysers will detect the coincident X-rays and gamma-rays and consequently the coincidence yield will be about twice as high as is indicated by Eq. (4.4.1).

### 4.5 *Experimental procedures*

The experimental work in connection with the determination of the conversion-ratio consisted of the following actions:

For manipulation convenience it was necessary that each of the fuel slugs obtained its own inner cladding. Therefore one of the existing LEAD fuel elements was modified in such a way that the inner nickel cladding was completely separated in between each of the five slugs. In one of these slugs a radial hole was drilled 5.25 mm in diameter running from the outer to inner surface, prior to inserting its closely fitting inner cladding. For each of the irradiations in LEAD, this hole was filled with natural uranium

foils. About eight 0.08 mm thick foils were used near each of the surfaces, while in the central part 0.27 mm thick foils were placed. In total about 30 foils were closely packed over 6.75 mm length of the fuel rod cross-section. After the hole was filled it was sealed with thin adhesive plastic tape. Next this fuel slug together with four others was placed inside the aluminium tube which functioned as the outer cladding. Before closing the element the central channel was filled with expanded polystyrene which was used to simulate superheated steam (see Chapter 2). The axis of the hole in the fuel slug in which the foils were positioned was located at 45 cm from the lower end of the element. Thereupon the prepared element was placed in the middle of one of the two seven-rod clusters in LEAD which could be voided. The element was positioned in such a way that the stack of foils was located tangentially with regard to the centre line of the assembly. In the central zone irradiations were performed with 0 %, 10 %, 20 %, 30 % and 36 % moderator void corresponding to water-to-fuel volume ratios of 1.14, 1.03, 0.91, 0.80 and 0.73 respectively. In the peripheral zone the irradiations were carried out with 0 %, 10 %, 20 % and 29 % moderator void, equivalent to water-to-fuel volume ratios of 2.34, 2.10, 1.87 and 1.66.

A standard practice for each irradiation was to start the HOR, which functioned as the neutron source for LEAD, with a period of 30 seconds to a power level of 200 kW, which corresponds to a neutron flux of about $5 \cdot 10^6$ $n/cm^2 \cdot s$ at the foil location in LEAD. All irradiations lasted eight hours and were concluded by a rapid insertion of the HOR control rods. At the end of the irradiations the special fuel element was removed from LEAD and placed in a lead container. The radiation level near the bottom of the element was on the order of 1.5 R/h. In a laboratory adjacent to the reactor building the outer cladding was removed by remote handling equipment and the irradiated foils were taken from the fuel slug.
Together with these foils a natural uranium reference foil was activated in the lattice, which was later used to normalize the fission density measurements. Exactly one hour after finishing an irradiation, counting of the foils was started. Because of the fast decay of the fission product gamma-rays the gross gamma activity was first counted. These measurements started by first counting the reference foil during $t$ seconds to give $N$ counts. Thereafter all other foils were counted one after another, each foil simultaneously with the reference foil (two single-channel analysers were used for this purpose) over a period necessary to obtain again $N$ counts from the reference foil. Thus all counting results were corrected for decay and normalized at one hour after the end of the irradiation period. Next the coincidence measurements were performed to determine the amount of neutron capture in $^{238}U$.

These measurements were normalized to the time at which the reactor was shut down, by making the usual corrections for radioactive decay.

The most suitable neutron spectrum available for the determination of

the thermal reference $(MCR)_{th}$, necessary to obtain the relative-modified-conversion-ratio was a hardened spectrum at some distance from the HOR-core in the water reflector. From cadmium-ratio measurements radial to the core, the point was determined where the neutron spectrum would reach its equilibrium value. Based on these data and the flux level in the reflector two natural uranium foils were irradiated, one bare, the other cadmium covered, at a distance of 70 cm from the core. Here a cadmium-ratio of 70 was measured with copper foils, which indicates that the spectrum at this point is certainly not a plain Maxwell-spectrum. Just as for the other foils, this irradiation lasted eight hours. By subtracting the counting results of one foil from those of the other, the sub-cadmium modified-conversion-ratio was obtained which is due to neutrons having energies less than 0.45 eV.

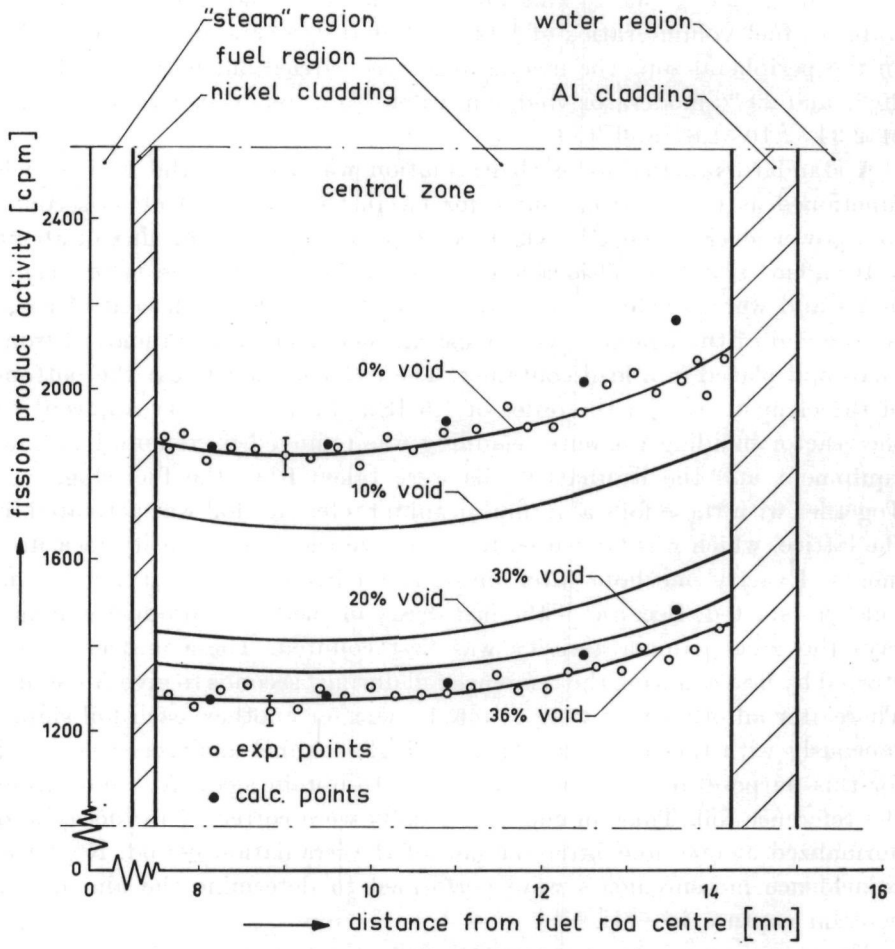


*a*) central zone

Fig. 4.9. Fission density distribution in a

## 4.6 *Data reduction and results*

### 4.6.1 Measurements

The counting results of the spatial fission density measurements are plotted in Fig. 4.9a for the central zone and in Fig. 4.9b for the peripheral zone. The experimentally obtained points have been given for 0 %, 29 % and 36 % moderator void only. The experimental points associated with the lines for 10 %, 20 % and 30 % void have been omitted for clearness. The data presented in these figures, which have been corrected for differences in weight of the various foils and for decay, result from fission both in $^{235}U$ and in $^{238}U$.

In the graphs drawn for 0 %, 29 % and 36 % void, points are shown of the calculated product $\Sigma_f \phi_{th}$, the number of thermal fissions per unit

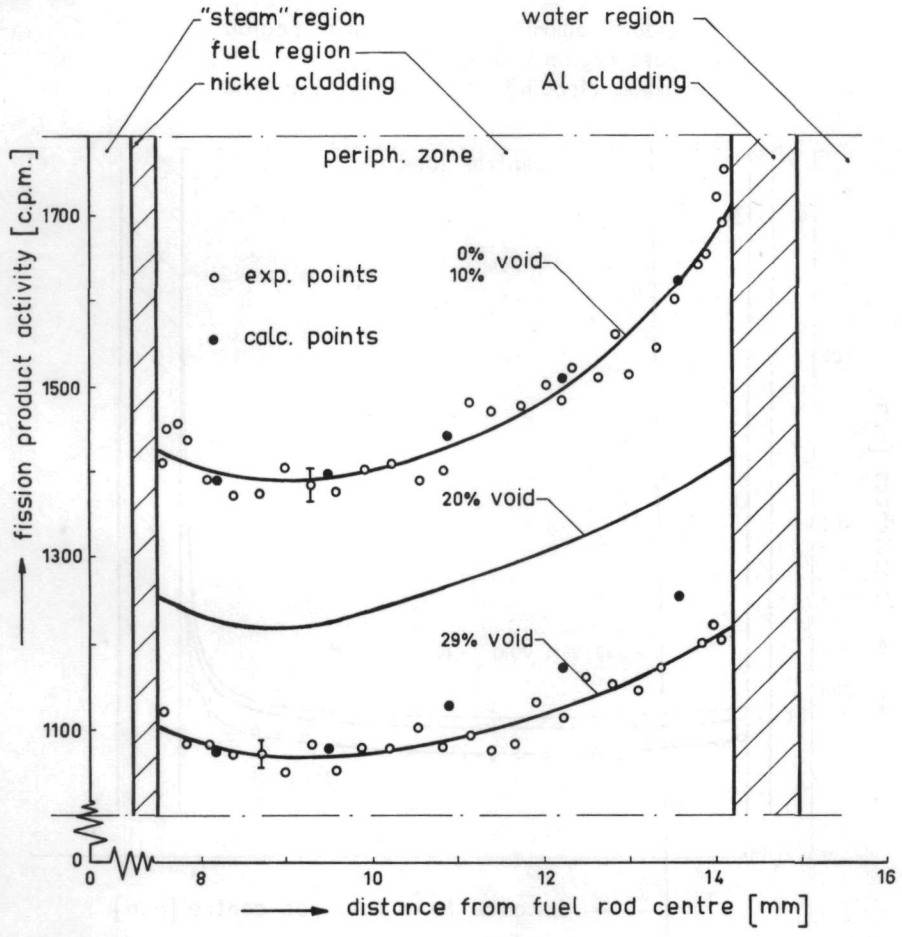


*b*) peripheral zone

fuel rod for various moderator void fractions.

volume and per unit time. These values, obtained from a K7-THERMOS calculation (see Chapter 5), are normalized to the experimental data near the inner fuel rod surface. They are based on a thermal cut-off of 0.625 eV. Hence, epi-thermal fission is not included.

The results of the coincidence measurements are presented in Fig. 4.10a for the central zone and in Fig. 4.10b for the peripheral zone. Here the experimental points are only given for the zero void condition, while the experimental points associated with the lines for higher void fractions have again been omitted for clearness.

In order to determine the modified-conversion-ratio from these data, the average values of the fission densities and the coincidences over the fuel rod cross-section had to be calculated. They were obtained from a numerical integration of the relation:

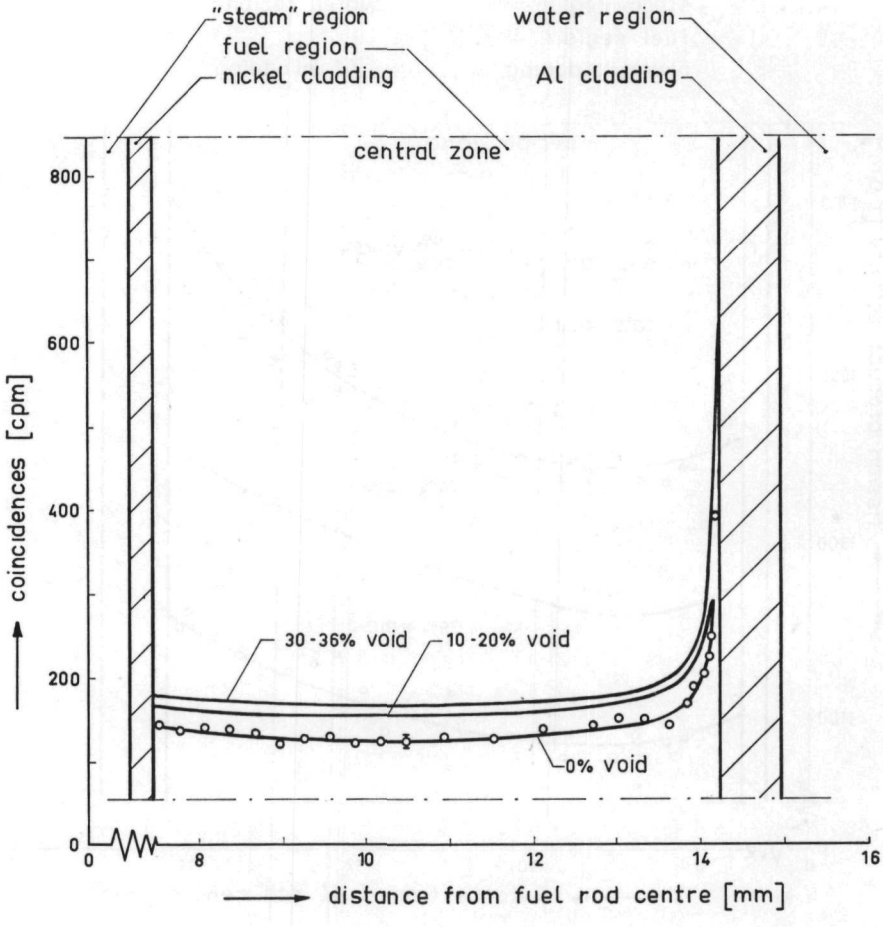


*a*) central zone

Fig. 4.10. Distribution of the neutron absorption in $^{238}U$ (expressed in

$$\bar{A}_{f,c}(r) = \frac{2\pi \int_{7.5}^{14.25} A_{f,c}(r)\, dr}{2\pi \int_{7.5}^{14.25} r\, dr} \tag{4.6.1}$$

where $A_{f,c}(r)$ represents either the spatial distribution of the fission densities or the coincidences following the decay of $^{239}$Np. Thereafter the average values of the fission densities were corrected for fast fission in $^{238}$U.

From cadmium-ratio measurements performed with fuel foils in the HOR-reflector a factor proportional to the thermal contribution of the modified-conversion-ratio was determined to be $5.85 \times 10^{-2}$. This value does not correspond with the actual thermal modified-conversion-ratio, since it contains the detector efficiency which is unknown. The factor is

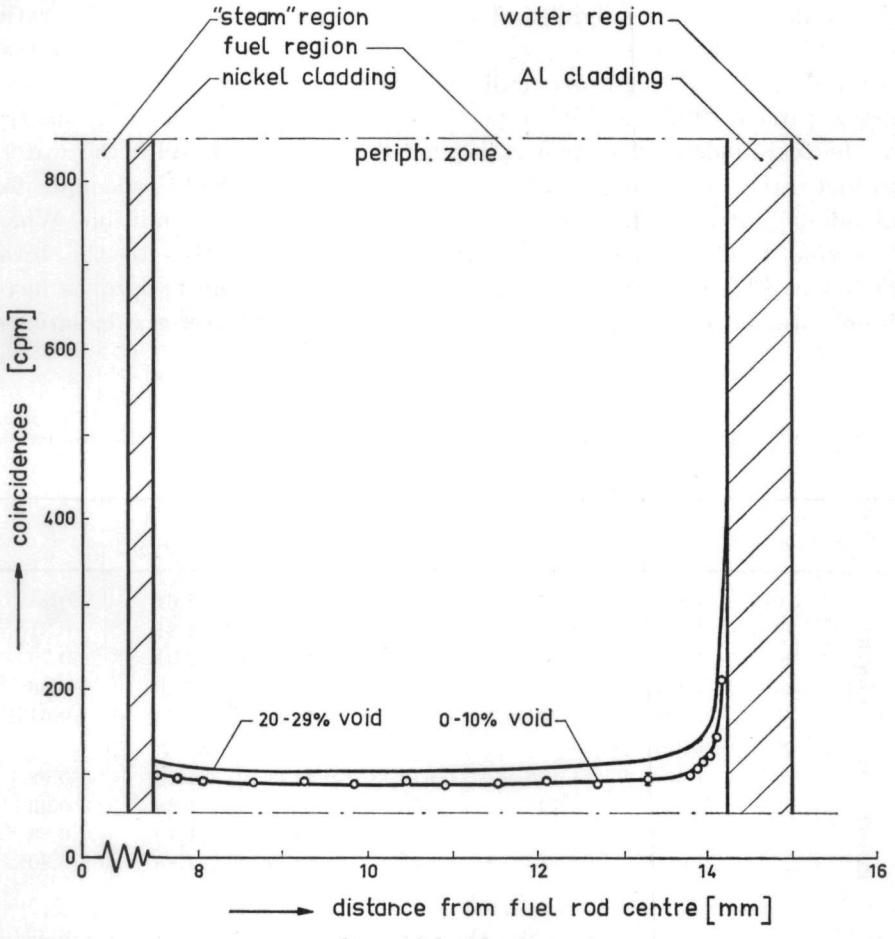


*b*) peripheral zone

terms of coincidences) in a fuel rod for various moderator void fractions.

necessary to obtain the relative-modified-conversion-ratio *RMCR*. It has been corrected for the difference between the neutron temperature in the equilibrium water spectrum and the fuel rod thermal spectrum by using the WESTCOTT-convention [19].

From Eq. (4.2.3) it follows, that the resonance escape probability $p$ can be obtained from the relation:

$$p = 1 - \left[\frac{MCR_{th}(RMCR-1)\,(1+B^2\tau)}{\varepsilon'\,\nu^{235}}\right]. \tag{4.6.2}$$

The value of *RMCR* was determined experimentally while the parameters $\varepsilon'$ and $\nu^{235}$ have been calculated from the best available values in the literature [20, 21]. Although the fast nonleakage probability $1/(1+B^2\tau)$ decreases with increasing void fraction, no corrections have been made for fast neutron leakage because – as is discussed in section 4.7 – the influence is negligible. The total fast-to-thermal fission-ratio $\varepsilon' = 1+\{[\nu^{238}-(1+\alpha^{238})]/\nu^{235}\}\,\delta_{235}^{238}$, where $\alpha$ is the capture-to-fission cross-section ratio of the isotope indicated. Further $\delta_{235}^{238}$ is the ratio of the fission rates in $^{238}$U and $^{235}$U respectively. In this parameter the geometry of the fuel-moderator system is implicitly incorporated. With the water-to-fuel ratios under consideration epi-thermal fission in $^{235}$U accounts for about 8 % of the total fission in $^{235}$U in the zero void condition. When the void fraction increases the epi-thermal contribution to the total fission in $^{235}$U increases too. The $MCR_{th}$ values for the two zones have been obtained for various void conditions from K7-THERMOS calculations.

TABLE IV.1

Values of parameters used in the experimental determination of the resonance escape probability $p$.

| ZONE | $\alpha$ (%) | $\varepsilon$ | $\varepsilon'$ | $MCR_{th}$ (calc.) | $\nu^{235}$ | RMCR (meas.) | $p$ |
|---|---|---|---|---|---|---|---|
| CENTRAL | 0 | 1.102 | 1.170 | 0.680 | 2.4493 | 1.61 | 0.84 |
| | 10 | 1.108 | 1.182 | 0.681 | 2.4493 | 1.81 | 0.81 |
| | 20 | 1.115 | 1.193 | 0.682 | 2.4493 | 2.31 | 0.79 |
| | 30 | 1.126 | 1.211 | 0.684 | 2.4493 | 2.48 | 0.66 |
| | 36 | 1.132 | 1.221 | 0.686 | 2.4493 | 2.71 | 0.61 |
| PERIPHERAL | 0 | 1.069 | 1.116 | 0.672 | 2.4493 | 1.12 | 0.98 |
| | 10 | 1.074 | 1.124 | 0.673 | 2.4493 | 1.28 | 0.93 |
| | 20 | 1.079 | 1.132 | 0.674 | 2.4493 | 1.49 | 0.88 |
| | 29 | 1.085 | 1.143 | 0.675 | 2.4493 | 1.85 | 0.80 |

In Table IV.1 all data used for the determination of $p$ are summarized. The values of $p$ obtained are plotted in Fig. 4.11a for the central zone and in Fig. 4.11b for the peripheral zone.

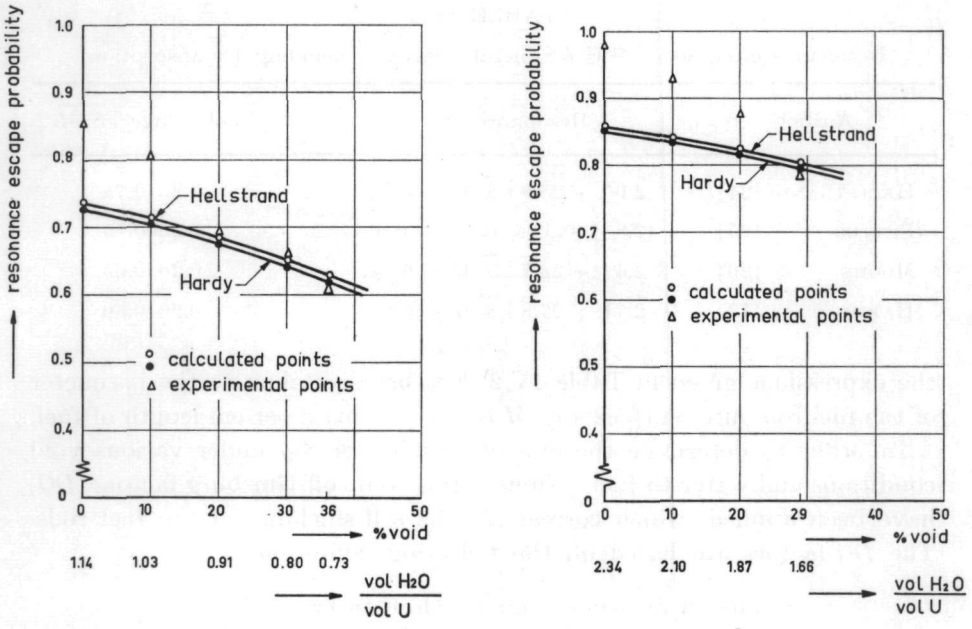


Fig. 4.11. Experimentally and theoretically determined resonance escape probabilities as a function of the moderator void fraction, *a*) for the central zone and *b*) for the peripheral zone.

### 4.6.2 Calculation of the resonance escape probability using an engineering method

It is of interest to compare the experimental values of the resonance escape probability and those obtained from a widely used standard engineering design-method, see Chapter 3. In the latter the resonance escape probability $p$ is calculated by means of Eq. (4.6.3) [20, 21]:

$$p = \exp - \left[\left(\frac{N_u \cdot V_u}{\xi \Sigma_{s_{H_2O}} \cdot V_{H_2O}}\right) \cdot \left(\frac{\overline{\phi}_u}{\overline{\phi}_{H_2O}}\right) \cdot (RI)_{eff}\right] \tag{4.6.3}$$

where $N_u$ is the number of $^{238}U$ nuclei per cm$^3$. The factors $V_u$ and $V_{H_2O}$ are the volume fractions of $^{238}U$ and $H_2O$ in the unit cell under consideration. The ratio $(\overline{\phi}_u/\overline{\phi}_{H_2O})$ is the resonance disadvantage factor; it is calculated in the same way as the corresponding thermal quantity, see Chapter 5. The parameter $(RI)_{eff}$ is the effective resonance integral, which is a complicated function of geometry and composition of the lattice. A number of experimentally determined relations for the resonance integral exists that involve both a volume effect and a surface term (see, for instance, WEINBERG and WIGNER [22] and CHERNICK, *et al.* [23]). Results of measured resonance integrals for natural uranium metal rods used in the engineering calculations are given in Table IV.2. In

TABLE IV.2

Resonance integrals of $^{238}U$ for metal rods, not including $1/v$ absorption.

| Author | Resonance Integral | Val. range $\sqrt{S/M}$ |
|---|---|---|
| HELLSTRAND [24] | $2.95 + 25.8\sqrt{S/M} \pm 5\ \%$ | 0.25–0.75 |
| PETTUS [25] | $(2.8 \pm 0.5) + (27.1 \pm 0.9)\sqrt{S/M}$ | 0.25–0.75 |
| MOORE [26] | $2.42 + 28.7\sqrt{S/M} \pm 6\ \%$ | 0.26–0.63 |
| HARDY [13] | $2.71 + 27.8\sqrt{S/M} \pm 0.6$ | 0.20–0.60 |

the expressions given in Table IV.2, $S$ is usually taken as the perimeter of the fuel rod outer surface and $M$ is the $^{238}U$ mass per cm length of fuel.

In order to determine the effective perimeter $S_{eff}$ under various void conditions and water-to-fuel volume ratios, Dancoff-Ginsburg factors ($DG$) have been applied, which correct for the self-shielding of the fuel rods. The $DG$-factors are based on the following definition:

$$DG = \frac{\begin{array}{l}\text{number of resonance neutrons which on first flight}\\ \text{in the adjacent moderator strike the fuel surface}\end{array}}{\begin{array}{l}\text{number of resonance neutrons which would on first flight}\\ \text{strike the fuel surface if an infinite volume of}\\ \text{unshielded moderator were adjacent to the fuel surface}\end{array}}.$$

For fuel rods of the size used in the LEAD facility positioned in a triangular array with light water as a moderator, $DG$ is calculated from:

$$DG = 1 - \left[2.432 \times K_i\left(f(d/R) \cdot \frac{R}{\lambda_s}\right) \times \arcsin(R/d)\right] \tag{4.6.4}$$

where $d$ is the centre-to-centre distance between the fuel rods, $R$ is the fuel rod outer radius, and $\lambda_s$ is the scattering mean free path of the resonance energy neutrons in the water region of the unit cell. The functions $f(d(R)$ and $K_i\left(f(d/R) \cdot \frac{R}{\lambda_s}\right)$ are tabulated [20, 21].

The expanded polystyrene, which is contained in the central hole in the LEAD fuel element to simulate superheated steam, will not affect the energy spectrum in the resonance region. Therefore $M$ could be taken as the actual mass per cm length of fuel; this is equivalent to treating the fuel rod as a solid with the given mass of fuel uniformly distributed within the surface. In the effective resonance integrals used a correction of 1.2 barns has been incorporated to account for the $1/v$ absorption in $^{238}U$.

In the calculations a $\xi\Sigma_s$ value has been used of $40.5 \times 10^{-2}$ cm$^{-1}$ per $H_2O$ molecule. The results of sub-calculations are summarized in Table IV.3. The values obtained for $p$ using this engineering scheme are plotted in Fig. 4.11a for the central zone and in Fig. 4.11b for the peripheral zone together with the experimental results. In these figures only the results

TABLE IV.3

Results of sub-calculations and parameters used for the engineering calculation of the resonance escape probability.

| ZONE | $\alpha$ | $\frac{\text{Vol}H_2O}{\text{Vol U}}$ | $N_u$ $\times 10^{-24}$ | $V_u$ | $N_{H_2O}$ $\times 10^{-24}$ | $V_{H_2O}$ | $\bar{\phi}_u/\bar{\phi}_{H_2O}$ | $DG$ | $\sqrt{\left(\frac{S}{M}\right)_{eff}}$ | Hellstrand | | Pettus | | Moore | | Hardy | |
|---|---|---|---|---|---|---|---|---|---|---|---|---|---|---|---|---|---|
| | | | | | | | | | | $RI_{eff}$ | $p$ | $RI_{eff}$ | $p$ | $RI_{eff}$ | $p$ | $RI_{eff}$ | $p$ |
| | % | | Nuclei per cm³ | | Mol per cm³ | | | | cm.g$^{-\frac{1}{2}}$ | barns | | barns | | barns | | barns | |
| CENTRAL | 0 | 1.14 | 0.0478 | 0.367 | 0.0335 | 0.419 | 0.832 | 0.896 | 0.304 | 11.99 | 0.735 | 12.24 | 0.730 | 12.34 | 0.728 | 12.36 | 0.725 |
| | 10 | 1.03 | 0.0478 | 0.367 | 0.0301 | 0.419 | 0.832 | 0.873 | 0.301 | 11.91 | 0.712 | 12.16 | 0.707 | 12.23 | 0.705 | 12.28 | 0.704 |
| | 20 | 0.91 | 0.0478 | 0.367 | 0.0268 | 0.419 | 0.832 | 0.851 | 0.297 | 11.81 | 0.684 | 12.05 | 0.679 | 12.14 | 0.677 | 12.17 | 0.676 |
| | 30 | 0.80 | 0.0478 | 0.367 | 0.0235 | 0.419 | 0.832 | 0.827 | 0.293 | 11.71 | 0.651 | 11.94 | 0.645 | 12.03 | 0.642 | 12.06 | 0.642 |
| | 36 | 0.73 | 0.0478 | 0.367 | 0.0215 | 0.419 | 0.832 | 0.794 | 0.287 | 11.65 | 0.626 | 11.77 | 0.623 | 11.86 | 0.620 | 11.98 | 0.618 |
| PERIPHERAL | 0 | 2.34 | 0.0478 | 0.255 | 0.0335 | 0.596 | 0.845 | 0.977 | 0.317 | 12.23 | 0.856 | 12.59 | 0.852 | 12.72 | 0.850 | 12.72 | 0.850 |
| | 10 | 2.10 | 0.0478 | 0.255 | 0.0301 | 0.596 | 0.845 | 0.966 | 0.316 | 12.30 | 0.840 | 12.56 | 0.837 | 12.69 | 0.835 | 12.69 | 0.835 |
| | 20 | 1.87 | 0.0478 | 0.255 | 0.0268 | 0.596 | 0.845 | 0.957 | 0.314 | 12.26 | 0.822 | 12.52 | 0.819 | 12.65 | 0.817 | 12.65 | 0.817 |
| | 29 | 1.66 | 0.0478 | 0.255 | 0.0238 | 0.596 | 0.845 | 0.943 | 0.312 | 12.20 | 0.803 | 12.46 | 0.800 | 12.57 | 0.798 | 12.58 | 0.798 |

are shown when resonance integrals as obtained by HELLSTRAND and HARDY are used. As can be seen from Table IV.3 the values obtained for $p$ when using the resonance integrals due to MOORE and PETTUS are in between. Note that $p$ has been determined on the assumption of an infinite lattice.

### 4.7 *Discussion of the results*

In this study the resonance escape probability $p$ was obtained as a function of the moderator void fraction $\alpha$ by using experimentally determined relative-modified-conversion-ratios (*RMCR*) in addition to nuclear data taken from the literature.

The accuracy in $p$ depends on the accuracy of each of the parameters which have been used in the final calculation. In the zero void condition an error of 1 % in the *RMCR*-value corresponds to an error in $p$ of approximately 0.5 %, while a 1 % error in the $MCR_{th}/\varepsilon' \nu^{235}$ ratio results in a 0.2 % error in $p$. At higher void fractions the consequence of an error in the value of these factors becomes more important. However in the void ranges under consideration the error in $p$ for a LEAD unit cell composition will always be less than the error in either the *RMCR*-value or the ratio $MCR_{th}/\varepsilon' \nu^{235}$.

Whereas the product $B^2\tau$ for the assembly is very small ($10^{-2}$ in the zero void condition) $1/(1+B^2\tau)$ does not differ noticeably from unity and changes in the void fraction will hardly influence this factor. When voids are introduced in the moderator the Fermi-age $\tau$ increases approximately proportional to $1/(1-\alpha)^2$ while the buckling $B^2$ shows a tendency to decrease. Assuming $B^2$ to remain constant, the decrease in the fast non-leakage probability will be about 3 % at a void fraction of 36 %, leading to a decrease of about 1 % in $p$.

Although potentially relative-modified-conversion-ratios can be determined more accurately than cadmium-ratios, because no foreign materials have to be introduced in the lattice, the fact that more additional corrections have to be incorporated and use must be made of other parameters, such as the fast fission factor, gives the *RMCR*-method to determine $p$ a drawback.

A first look at the results, which have been shown in Fig. 4.11a and Fig. 4.11b indicate that there is little agreement between the experimental results and those obtained from the semi-empirical engineering calculation, in particular when the void fractions are very small. In the zero void fraction the experimental values are about 14 % higher than the calculated values; the discrepancies decrease at higher void fractions. For the central zone the reduction in $p$ is about 27 % for the experimental values and 15 % for the calculated values, when the void fraction is increased from zero to 36 %. In the peripheral zone these fractions are about 18 % and 6 % respectively when going from zero to 29 % void.

To understand these differences both the experimental and calculated results have to be analysed in more detail in regard to the effects that determine the level and the gradient. First the experimental values will be examined.

The experimental $p$-values have been obtained using Eq. (4.6.2). Going from zero to 36 % void the ratio $MCR_{th}/\varepsilon' \nu^{235}$ decreases with about 3.5 %, while the $RMCR$-value increases with approximately 170 %. Consequently the change in $p$ due to the introduction of voids is mainly determined by the increase in the $RMCR$. The experimentally obtained thermal reference factor used to calculate the $RMCR$ from the experimental data corresponding to the $MCR$, has been taken equal for all void fractions. As can be seen from Table IV.1 which also gives the calculated $MCR_{th}$-values, this approximation is justified. Therefore the slope in the $(p-\alpha)$-relationship shown in Fig. 4.11 is largely a consequence of the change in the experimentally obtained $MCR$ which in turn follows from the data plotted in Fig. 4.9 and Fig. 4.10.

It can be seen from Fig. 4.9a that the fission density level in the peripheral zone decreases by about 30 % when the void fraction is increased from zero to 36 %. Due to the introduction of voids the removal cross-section is decreased proportional to $(1-\alpha)$ leading to an equivalent reduction in the thermal slowing down density. Whereas the neutron energy spectrum hardens when the void fraction increases, the contribution to the fission density level of epi-thermal fission in $^{235}$U increases with increasing void fraction. Combining these effects a reduction of about 30 % in the fission density level is not unexpected. The same reasoning may be given for the peripheral zone where the fission density level decreases with 25 % when going from zero to 29 % void.

The data presented in Fig. 4.10 refer to the capture of neutrons in $^{238}$U over the entire energy spectrum. Going from zero to 36 % void a net increase of about 30 % is obtained in the central zone. In the peripheral zone the increase is roughly 20 % when the void fraction is increased from zero to 29 %.

Taking into account the hardening of the neutron energy spectrum as a result of voids – the neutron temperature in the fuel in the central zone cell increases about 100° K – the thermal contribution to the total capture in $^{238}$U must have decreased by fractions somewhat less than 30 % and 25 %.

Consequently the rise in capture level is solely due to epi-thermal and fast neutrons. It is surprising to note that the epi-thermal neutron capture extends so far in the rod. As a first guess one would have expected the increase in the surface effect, but a decrease in the $(1/v)$-absorption. The latter effect would then have led to a less rapid decrease of $p$ as a function of the void fraction $\alpha$. Thus the large increase in epi-thermal and fast neutron capture in $^{238}$U over the entire fuel rod volume is responsible for the pronounced slope.

In contradiction with the $p$-values obtained from the engineering calculations all experimental values are obtained completely independent of each other. Although some factors of uncertainty are involved, which may, to a certain extent, influence the slope of the experimentally obtained $(p-\alpha)$-relationship, a complete agreement with the calculated curve cannot be reached. The accuracy in the experimental results is primarily affected by the following random errors:

*a*) The statistical spread in the count rates. The reproduceability in the count rates measured was on the order of 3 %. However, because these data have been integrated over the fuel element cross-sectional area the error in the average values will be considerably less.

*b*) A possible discrepancy from the correct water-to-fuel volume ratio, due to a misaligment in radial direction of the fuel rod in which the data have been measured.

*c*) The influence of temperature on the characteristics of the crystal-photomultiplier combination. It was observed that 1° C temperature difference in the counting room led to a 1 % to 2 % change in the count rates. Therefore the temperature in the room was kept as constant as possible ($\pm$ 1° C). In experiments recently performed at the Winfrith-centre in England, the photomultiplier environment temperature was kept constant by using a temperature-controlled enclosure.

The factors mentioned above and also the values of all other parameters used, affect the level of the resonance escape probability. However they do not seriously influence the gradient.

A systematical error is introduced at high void fractions. In that case the dimensions of the regions which could be voided are somewhat too small to reach an equilibrium spectrum corresponding to the particular voided condition, see Chapter 2. As a consequence the measurements at high void fractions have been performed in a too soft spectrum resulting in higher values for $p$ than when the correct spectrum would have been present. Accordingly the slope in the experimental $p$–$\alpha$ curve would have been even more pronounced.

The curves obtained with the semi-empirical calculations show that there results not much difference from the use of various resonance integrals. A decrease is found in the resonance integral of about 3 % in the central zone when the void fraction rises from zero to 36 %. Consequently the slope of the calculated $p$-values is primarily determined by the reduction of the macroscopic scattering cross-section in the water region and in addition by the value of the resonance escape probability in the zero void condition as may be seen from the following analysis:

The relationship between $p$ and $\alpha$ can be approximated by:

$$p(\alpha) \approx e^{-\left[\frac{N_u V_u \bar{\Phi}_u}{\bar{\xi} \Sigma_s (1-\alpha) V_{H_2O} \bar{\Phi}_{H_2O}} \cdot RI\right]} \tag{4.7.1}$$

or

$$p(\alpha) \approx p(0)^{1/(1-\alpha)}. \tag{4.7.2}$$

The gradient of the $(p-\alpha)$-curve follows from differentiating Eq. (4.7.2)

$$\frac{\partial p(\alpha)}{\partial \alpha} = \frac{p(0)^{1/(1-\alpha)}}{(1-\alpha)^2} \ln p(0) \tag{4.7.3}$$

or

$$\frac{\partial p(\alpha)}{\partial \alpha} = \frac{-C}{(1-\alpha)^3} p(0)^{1/(1-\alpha)} \tag{4.7.4}$$

where $C = \left[\frac{N_u V_u \bar{\phi}_u}{\xi \Sigma_s V_{H_2O} \bar{\phi}_{H_2O}} \cdot RI\right]$.

From Eq. (4.7.4) it can be seen that the slope in the calculated curves depends also on the initial value of the resonance escape probability.

Consequently when the value calculated for $p$ in the zero void condition is larger, the gradient of the $(p-\alpha)$-curve will increase. Observing the importance of the epi-thermal volume contribution to neutron capture in $^{238}U$ it is very likely that the difference between the experimental and calculated values of $p$ result from an underestimation of the volume absorption in the resonance integrals when applied to fuel rods equivalent to those used in LEAD. Although the relations given for the resonance integrals in Table IV.2 are claimed to be valid for a $\sqrt{S/M}$-range between 0.25 and 0.75 it is clear that for LEAD fuel rods ($\sqrt{S/M} \approx 0.3$) no agreement can be obtained.

When the volume capture contribution is accounted for by applying an increased effective mass-term the value of the resonance integral is decreased, which in turn will lead to an increase in the resonance escape probability. In order to obtain closer agreement between experimental and calculated results the $\sqrt{S/M}$-value used in the resonance integrals should be replaced by $\sqrt{S/4M}$ in which case also the gradient of the calculated curve is adjusted. It is recommended that this proposal should be further experimentally examined for fuel rods with $\sqrt{S/M}$-values lower than 0.3.

## REFERENCES


1. B. I. SPINRAD, J. C. CARTER and C. EGGLER, Reactivity changes and reactivity lifetimes of fixed fuel elements in thermal reactors, Proc. Intern. Conf. Peaceful Uses Atomic Energy, **5**, 125 (1955).
2. S. KRASIK and A. RADKOWSKY, Pressurized water critical experiments, Proc. Intern. Conf. Peaceful Uses Atomic Energy, **5**, 203 (1955).
3. D. KLEIN, J. HARDY JR., G. G. SMITH and S. STEIN, Effective $^{238}U$ resonance captures integrals in rods and lattices, Technical Report Series No. 12, Light Water Lattices, IAEA, Vienna, 211, (1962).
4. W. A. V. BROWN and D. J. SKILLINGS, The measurement of relative conversion-ratio in low enrichment oxide lattices, UKAEA Reactor Group Report AEEW–R 340 (1964).

5. R. AXTMAN and J. STUTHEIT, ANL–HDY–715 (1952).
6. A. Z. KRANZ, WAPD-report No 134 (1955).
7. J. R. WOLBERG, T. J. Thompson and I. KAPLAN, Measurement of the ratio of fissions in $^{238}U$ to fissions in $^{235}U$ using 1.6 MeV gamma-rays of the fission product $^{140}La$, Proc. Symposium on Exponental and Critical Experiments, IAEA, Vienna, Vol. II, 147 (1964).
8. C. G. CAMPBELL and M. D. CARTER, BNL–433, 26 (1956).
9. H. KOUTS, G. PRICE, K. DOWNES, R. SHER and V. WALSH, Exponential experiments with slightly enriched uranium rods in ordinary water, Proc. Intern. Conf. Peaceful Uses Atomic Energy, **5**, 183, (1955).
10. T. J. BARENDRECHT and M. BUSTRAAN, Determination of neutron capture-to-fission ratio in different uranium samples, Proc. Intern. Conf. Peaceful Uses Atomic Energy, **5**, 55, (1955).
11. G. G. SMITH, J. HARDY, D. KLEIN and J. A. MITCHELL, Experimental studies of $^{238}U$ responance neutron capture in $UO_2$ fuel rods, Nucl. Science and Eng., **9**, 421, (1961).
12. E. CREUTZ, *et al.*, J. of Applied Physics, **26**, 271 (1955).
13. J. HARDY, G. G. SMITH and D. KLEIN, The effective $^{238}U$ resonance capture integrals of uranium metal and $UO_2$ rods, Nucl. Science and Eng., **14**, 358 (1962).
14. J. THOMASSEN and H. H. WINDSOR, Measurement of resonance absorption in $^{238}U$ using a chemical separation technique for isolation of $^{239}Np$, Kjeller Report No. KR–44 (1963).
15. W. H. G. LEWIN, Determination of nuclear decay energies and conversion coefficients using coincidence techniques, Dissertation, Technological University Delft (1965).
16. L. S. BELLER, Nanosecond scintillation coincidence spectrometer system with high reliability, Rev. Sci. Instr. **34**, 1001, (1963).
17. R. SHER, $\gamma$–$\gamma$ coincidence methods for measuring resonance escape probabilities in $^{238}U$ lattices, Nucl. Science and Eng., **7**, 479 (1960).
18. P. R. TUNNICLIFFE, D. J. SKILLINGS and B. G. CHIDLEY, A method for accurate determination of relative initial conversion ratios, Nucl. Science and Eng., **15**, 268 (1963).
19. C. H. WESTCOTT, Effective cross-section values for well-moderated thermal reactor spectra, Atomic Energy of Canada Limited, Report No. 1101, (1960).
20. M. F. VALERINO and R. S. HARDING, State of the art physics of nuclear superheat reactors, GNEC, Report No. 282, (1963).
21. H. ETHERINGTON (Ed.), Nuclear Engineering Handbook, McGraw-Hill Book Company Inc., New York, (1958).
22. A. M. WEINBERG and E. P. WIGNER, The physical theory of neutron chain reactors, The University of Chicago Press, Chapter XIX, (1958).
23. J. CHERNICK and M. M. LEVINE, Developments in resonance absorption, A/Conf. 28/P/262, (1964).
24. E. HELLSTRAND and C. LUNGREN, The resonance integral for uranium metal and oxide, Nucl. Science and Eng., **12**, 435, (1962).
25. W. G. PETTUS, Atomic Energy Division Report BAW–1244, Babcock and Wilcox Co. (1962).
26. P. G. F. MOORE, S. K. PATTENDEN and R. B. TATTERSALL, UKAEA Reactor Group Report AEEW–R 57, (1961).

CHAPTER 5

# THERMAL UTILIZATION FACTOR

## 5.1 *Introduction*

One of the four factors that determine the infinite multiplication factor $k_\infty$ of a fuel-moderator system is the thermal utilization factor $f$, which is generally (and, therefore, as will be illustrated, somewhat arbitrarily) defined as the ratio of the neutron absorption rate in the fuel to the total neutron absorption rate in the system, below a certain thermal cut-off energy $E_{th}$.

For a heterogeneous reactor $f$ frequently refers to the respective absorption rates in a unit cell, preferably to one which is part of an infinitely large lattice so that the integral neutron spectrum is at equilibrium. For the heterogeneous case the following general formulation can be given for the thermal utilization factor:

$$f = \frac{\text{thermal neutron absorption rate in the fuel region of the cell}}{\text{total thermal absorption rate in the cell}}$$

$$f = \frac{\int_0^{E_{th}} \int_{\substack{\text{fuel vol.}\\ \text{cell}}} \Sigma_{a_f}(E)\, N_f(E,\mathbf{r})\, v\, dE\, d\mathbf{r}}{\int_0^{E_{th}} \int_{\substack{\text{fuel vol.}\\ \text{cell}}} \Sigma_{a_f}(E)\, N_f(E,\mathbf{r})\, v\, dE\, d\mathbf{r} + \int_0^{E_{th}} \int_{\substack{\text{mod. vol.}\\ \text{cell}}} \Sigma_{a_m}(E)\, N_m(E,\mathbf{r})\, v\, dE\, d\mathbf{r}} \tag{5.1.1}$$

where the subscripts f and m refer to the fuel and to the moderator respectively. The space dependence is given by $\mathbf{r}$, and $E$ denotes the neutron energy. Further $N$ stands for the neutron density and $v$ for the neutron velocity corresponding to the energy $E$. The product of $N$ and $v$ is the neutron flux $\phi(E)$. The absorption cross-sections $\Sigma_{a_f}$ and $\Sigma_{a_m}$ are to be selected for the proper neutron temperature which differs in general from the physical temperature of the system. The influence of fuel rod claddings and construction materials can be taken into account by adding the appropriate term to the denominator in Eq. (5.1.1). In principle the thermal utilization factor is also time-dependent, because the flux distribution and the energy spectrum throughout the unit cell are related to the burn-up. However in this presentation effects resulting from burn-up will not be considered.

The upper limit of the energy integral – the thermal cut-off energy $E_{th}$ – depends basicly on the composition and geometry of the unit cell. In calculations the value for $E_{th}$ has always been selected such that it falls within the $1/E$-tail of the spectrum. Thus, errors associated with the joining of the thermal and epi-thermal fluxes will be minimized. For uranium-water systems HONECK [1, 2, 3] has used a value of 0.785 eV. In STAMM'LER's K7-THERMOS code [4] the cut-off is selected at 0.625 eV, while a value of 0.632 eV is chosen by TAS [5] in his code MICRO-FLUX. As can be seen from the measurements of POOLE [6] all these values lie well within the $1/E$-part of the spectrum. The actual value chosen frequently depends on the capacity of the digital computer for which the particular computer program has been written. However, in order that calculated results may be properly compared with those of experiments, without making questionable corrections, it is recommended here that the cut-off energy is selected equal to the value stipulated by the experimental technique applied, (see a paragraph below).

It is obvious that also the calculations of other parameters such as the slowing-down length and the resonance escape probability must be adapted to the selected cut-off energy in order to obtain the proper neutron cycle. Furthermore it should be recognized that the thermal spectrum in the unit cell is spatially (and time) dependent and that noticeable differences exist between the fuel and the moderator spectrum. In systems with water-to-fuel volume ratios between 1 and 2 a difference of about 80° K to 50° K occurs in the average effective neutron temperature between the water and fuel regions, the highest temperature being found of course in the fuel region [7, 8].

In case of an experimental determination of the thermal utilization factor, which is frequently based on the measurement of neutron reaction rates using activation detectors, the cut-off energy follows from the absorption cross-sections of the detectors used in combination with the techniques applied. In fact not a well defined real sharp cut-off energy is obtained with such measurements. Because of the statistical nature of the neutron interaction processes the threshold is smeared-out over a certain energy range, depending for instance on the thickness of the cover foils used, (see section 5.2). It is clear that especially as a result of different cut-off energies corrections are necessary when one tries to correlate theoretical and experimental values of thermal utilization factors. The presentation of data without an indication of the application of such corrections is not meaningful.

When the moderator absorption cross-section follows a $(1/v)$-dependence the general formulation given in Eq. (5.1.1) may be simplified to:

$$f = \frac{\Sigma^0_{a_f} g_f \bar{N}_f V_f}{\Sigma^0_{a_f} g_f \bar{N}_f V_f + \Sigma^0_{a_m} \bar{N}_m V_m} \tag{5.1.2}$$

where the superscript zero indicates 2200 m/s values of the absorption cross-sections, $g_f$ is the non$(1/v)$-factor for the fuel absorption cross-section, and $V_f$ and $V_m$ are the fuel and moderator volume fractions in the unit cell. The factors $\bar{N}_f$ and $\bar{N}_m$ are the spectrum averaged thermal neutron densities up to the cut-off energy in the fuel rod and in the moderator region respectively. They are found from:

$$\bar{N}_f = \frac{1}{V_f}\int_0^{E_{th}} \int_{\substack{\text{fuel vol.}\\ \text{cell}}} N_f(E,\mathbf{r})\, dE\, d\mathbf{r} \tag{5.1.3}$$

and

$$\bar{N}_m = \frac{1}{V_m}\int_0^{E_{th}} \int_{\substack{\text{mod. vol.}\\ \text{cell}}} N_m(E,\mathbf{r})\, dE\, d\mathbf{r}. \tag{5.1.4}$$

In relation to the thermal utilization factor the following quantities are defined:

the neutron *density* disadvantage factor: $\delta_N = \dfrac{\bar{N}_m}{\bar{N}_f}$

the neutron *flux* disadvantage factor: $\delta_\phi = \dfrac{\bar{\phi}_m}{\bar{\phi}_f}$.

From the definition of $\phi$ it follows, that $\delta_\phi = \dfrac{\bar{v}_m}{\bar{v}_f} \cdot \delta_N$, where the average neutron speeds $\bar{v}$ are obtained from:

$$\bar{v} = \frac{\int_0^{E_{th}} N(v)\, v\, dv}{\int_0^{E_{th}} N(v)\, dv}. \tag{5.1.5}$$

The neutron flux disadvantage factors are mostly used in those cases where the $(1/v)$-approximation for the absorption cross-sections may not be applied. In addition the following two quantities are sometimes used:

the *fuel* disadvantage factor $\delta_f = \dfrac{\text{neutron density at the fuel surface}}{\text{average neutron density in the fuel}}$

which may be considered as a reciprocal fuel self-shielding factor and

the *moderator* disadvantage factor $\delta_m = \dfrac{\text{average neutron density in the moderator}}{\text{neutron density at the fuel surface}}$.

It is obvious from these definitions that $\delta_f \cdot \delta_m = \delta_N$. In the following discussions only the neutron density and flux disadvantage factors will be referred to.

Introducing the density disadvantage factor in Eq. (5.1.2) yields:

$$f = \frac{1}{1 + \dfrac{\Sigma^0_{a_m} V_m}{\Sigma^0_{a_f} g_t V_f} \cdot \delta_N}. \tag{5.1.6}$$

Using the proper values for $\Sigma^0_{a_m}$, $\Sigma^0_{a_f}$, $g_t$ and $\delta_N$, the thermal utilization factor can be calculated. The problem of obtaining $f$ is now shifted towards experimental or calculation methods to obtain $g_t$ and $\delta_N$, which requires knowledge of the spatial and energy distribution of the thermal neutrons in the unit cell under consideration.

## 5.2 *Experimental methods to determine the thermal utilization factor*

The reported experimental methods employed to determine the thermal utilization factor are, apart from some exceptions, directed towards the measurement of disadvantage factors and based on neutron activation techniques in unit cells. Actually a reaction rate $R$ is obtained, where:

$$R = \int_{E_1}^{E_2} \Sigma_a(E)\, N(E)\, v\, dE. \tag{5.2.1}$$

The limits of the integral depend on conditions such as for instance, covering of the detector with cadmium. In case $(1/v)$-detectors are used, $R = \Sigma^0_a v^0 \bar{N}$, where the superscript zero indicates the rather arbitrarily selected 2200 m/s values. In principle two types of experiments can be distinguished:

### *a*) The integral method

In the integral method single foils of selected shape and composition are activated in the fuel and the moderator region. The advantage of this technique is, that it can be conveniently used for lattices with small moderator-to-fuel volume ratios (light water lattices) where the determination of the spatial neutron distribution by means of foils is rather tedious. Further the foil activations obtained are directly related to the average neutron densities in the two regions. It should be noted that the alignment of the foil in the moderator region with respect to the foil in the fuel region is required to be very accurate.

### *b*) The differential method

In the differential method the detailed spatial distribution of the neutron density is measured by activation of small foils (or wires as described in section 5.3) placed throughout the moderator and the fuel region. From the flux distribution thus obtained, the average values for the two regions are determined by proper integration methods. The advantage of the differential technique lies in the fact that it yields the detailed flux distribution throughout the cell. Consequently the results give a better

insight in the neutron behaviour and provide more information for checking experiments and for correlating the results with those of calculation models.

In general it will be necessary to correct the results from either of the two experimental methods for epi-thermal activation. Frequently this is done with cadmium-ratio measurements. Consequently the experimental thermal cut-off energy is related to the effective cadmium cut-off energy, which depends on the thickness of the cadmium covers used. It will be furthermore necessary to correct the results for a macroscopic neutron density variation across the unit cell (correction for leakage).

In graphite and $D_2O$ moderated systems, where the centre-to-centre distance between the fuel elements is large in comparison to light water lattices a combination of the two experimental techniques may be used: the integral method in the fuel and the differential method in the moderator region. A few examples of experiments are presented below:

Using the PHYSICAL CONSTANTS TESTING REACTOR [9] the density disadvantage factor was obtained from flux traverses measured with bare and cadmium covered strips of a $^{235}U$–Al alloy inserted into a cell of a test lattice of the EXPERIMENTAL GAS COOLED REACTOR. The isotope $^{235}U$ exhibits a $(1/v)$-cross-section up to about 0.1 eV and necessitates an epi-thermal activation correction. In lattice studies at Chalk River [10] using the zero power $D_2O$-moderated lattice test reactor ZED-2 the microscopic neutron density distribution was measured with 0.10 mm thick Mn–Ni foils placed between fuel pellets and also at various positions in the coolant and the moderator. The activities obtained were corrected for the 340 eV Mn resonance activation. The experimental values of the moderator-to-fuel neutron density ratios are thought to be accurate to $\pm$ 2 %.

In the zero-power reactor NORA at Kjeller, where lattice studies have been performed on 3 % enriched $UO_2$ elements moderated with mixtures of $D_2O$ and $H_2O$ [11] the techniques used for measuring intracell density distributions consisted of irradiating Cu-wires 1.0 mm in diameter along the principle traverse axis of a reactor cell. Thereafter the wires were flattened, extended to about three times their original length and counted on beta-ray activity. The measured activation profile was corrected for an epi-thermal contribution by using the result of one cadmium-ratio measurement in the moderator, assuming its magnitude to be radially invariant. The differences between theoretically and experimentally obtained values for the disadvantage factors varied between 8.5 % for a 10 cm pitch lattice to 7 % for a 1.9 cm pitch lattice, with the theoretical values being larger than the experimental ones.

In light water moderated lattices, where the water-to-fuel volume ratios are small, the measurement of flux distributions becomes more complicated due to the short distance between neighbouring fuel elements. Further

as a result of the small $\lambda_{tr}$ in water, which leads to pronounced flux peaking, one must be very selective when introducing foreign material in the lattices in view of possible perturbations caused in the neutron distribution.

Many of the publications dealing with the measurement of microscopic parameters in light water lattices are either from the experimental group at Westinghouse/Bettis [12, 13, 14, 15] which uses the TRX facility, a zero-power testing reactor, or from the experimental group at Brookhaven National Laboratory (BNL) [16, 17, 18]. The latter group uses an exponential facility which can be located in the BNL graphite reactor. Although both groups have used the integral and differential technique the integral method is favoured at Westinghouse while the differential method is preferred by the BNL-group. In the integral technique the average neutron densities have been measured with 0.12 mm thick uranium-aluminium sector foils positioned as shown in Fig. 5.1. The uranium used

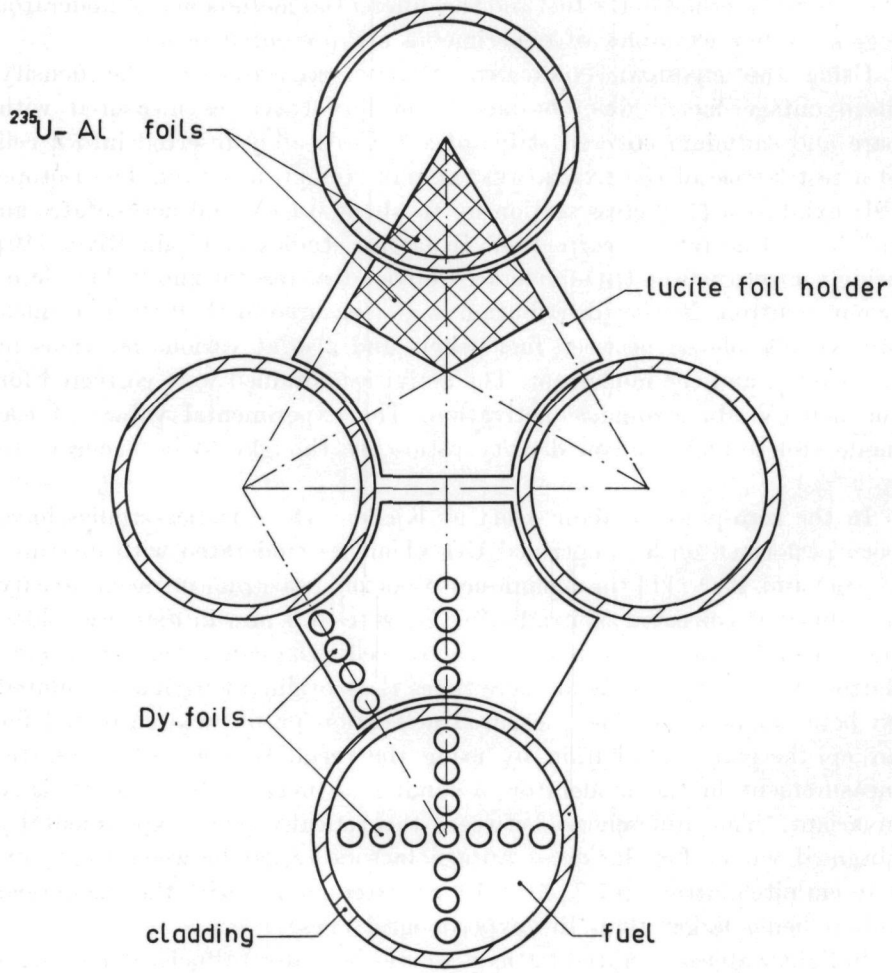


Fig. 5.1. Positioning of U—Al sector foils and dysprosium foils in integral and differential experiments performed at Westinghouse and BNL.

was enriched to more than 90 wt% and alloyed with 10 wt% 2S aluminium, making the $^{235}U$ atomic density in the foil approximately equal to that in the fuel. Epi-thermal activation was corrected for by using measured cadmium-ratios. In the differential technique very small dysprosium foils, 1.5 mm in diameter and 0.25 mm thick, were used. Dysprosium is an ideal detector because it makes cadmium-ratio measurements unnecessary. Originally methyl methacrylate plastic was used as a base for the foils; later polyethylene was applied and more recently aluminium has been selected simply for mechanical reasons.

Several systematic difficulties in these measurements have been observed, caused by foil holders, fission-product contamination, self-shielding effects, etc. Aluminium foil holders which were used in the early experiments were found to be detrimental due to local perturbations caused in the neutron flux. Subsequently plastic foil holders such as Lutice were widely used on the assumption that their nuclear properties are almost identical to those of water. Recently however, TUNNEY [19] has observed significant perturbations due to Lutice foil holders by measuring disadvantage factors as a function of Lutice thickness and extrapolating the results to zero thickness.

Comparing the experimental results with those obtained from THERMOS-calculations [25] it was observed that TUNNEY's measured results are within 1.5 % of the computed curves whereas the original values were low by about 4 %. Both the integral and differential techniques described above have also been used by Allis Chalmers in lattice studies concerning the PATHFINDER-reactor [20] and by Combustion Engineering in regard to the BONUS-reactor [21].

For the study of the thermal neutron density distribution in the LEAD-exponential facility at Delft the differential technique was selected, using *wires* composed of dysprosium-oxide and polyethylene. The details of this technique are described in the following sections. Apart from the light water experiments performed at BNL and heavy water experiments carried out at MIT most of the fine structure measurements have been made in critical facilities. As is demonstrated in this thesis a less costly exponential assembly may be used just as well.

## 5.3 *Experimental accessories*

### 5.3.1 Dysprosium wires

In order to determine disadvantage factors under various conditions of simulated boiling in the water region of LEAD lattice cells, the differential method was selected because of its advantages mentioned in the preceding section.

Rather than activating foils to determine the spatial distribution of the thermal neutrons, a wire activation method was preferred. Especially in tightly packed lattices – as is the case in the central zone of LEAD – this

technique has several merits. The wire, which is to traverse the fuel rod can be positioned in any direction perpendicular to the fuel rod axis in a simple and reproducible way. Furthermore when a proper scanning method is used, more experimental points per unit length may be obtained than when foils are used. An experimental curve thus determined, closer resembles the true neutron distribution throughout the cell, when the induced activity of more local parts of the wire is measured. Of course the presence of the wire in the reactor cell results in local perturbations of the neutron flux. However by activating wires of various thickness and extrapolating the counting results to zero thickness, the effects of flux depression and self-shielding can be eliminated and the true distribution of thermal neutrons may be approximated quite closely. As a matter of fact wires with four different diameters ranging from 1.2 mm to 0.3 mm have been used in the experiments. In order to obtain a low statistical spreading in the counting results a high activity is required of each individual part of the wire to be counted. In view of the available neutron flux at the measuring positions in the LEAD lattice (about $5 \times 10^6$ $n/cm^2 \cdot s$) the detector material must have a high thermal neutron activation cross-section. In addition the product formed should decay with a reasonable half-life. Further the energy dependence of the detector absorption cross-section in the thermal region should be proportional to $1/v$ and not exhibit any resonance capture peaks, so that neutron density disadvantage factors can be measured.

Materials meeting these requirements are $^{235}U$ and dysprosium. In case $^{235}U$ is utilized the decay activity of the fission products must be determined. The fission cross-section for neutrons with a speed of 2200 m/s is about 587 barns. Counting the induced activity of a small section of a $^{235}U$-wire is rather difficult, because of the energetic fission product gamma-rays. Furthermore when $^{235}U$ is used with an atomic density different from that of the fuel, the fission density is locally affected, which in turn influences the measuring results. Moreover a cadmium-ratio measurement would be required to correct for epi-thermal neutron activation.

In section 4.3 a method is described by which the distribution of fissions throughout a fuel rod has been measured with fuel equivalent foils in order to obtain the resonance escape probability. From the fission distribution the neutron density distribution may be obtained when the proper values of the fission cross-sections are known. For experiments concerning the disadvantage factor it was preferred to use dysprosium, which has a $\sigma_a(2200)$ of about 950 barns. Natural dysprosium contains 28.2 % $^{164}Dy$ which has a $\sigma_a(2200)$ of approximately 2500 barns, and therefore accounts for most of the low neutron energy cross-section of dysprosium. Neutron absorption in $^{164}Dy$ results in the formation of $^{165}Dy$ which decays by emission of beta-particles (and gammas) with a half-life of 139 minutes. Although it is frequently assumed that the $^{164}Dy$ absorption cross-section varies as $1/v$ up to about 1 eV, it can be seen from Fig. 5.2 that the total

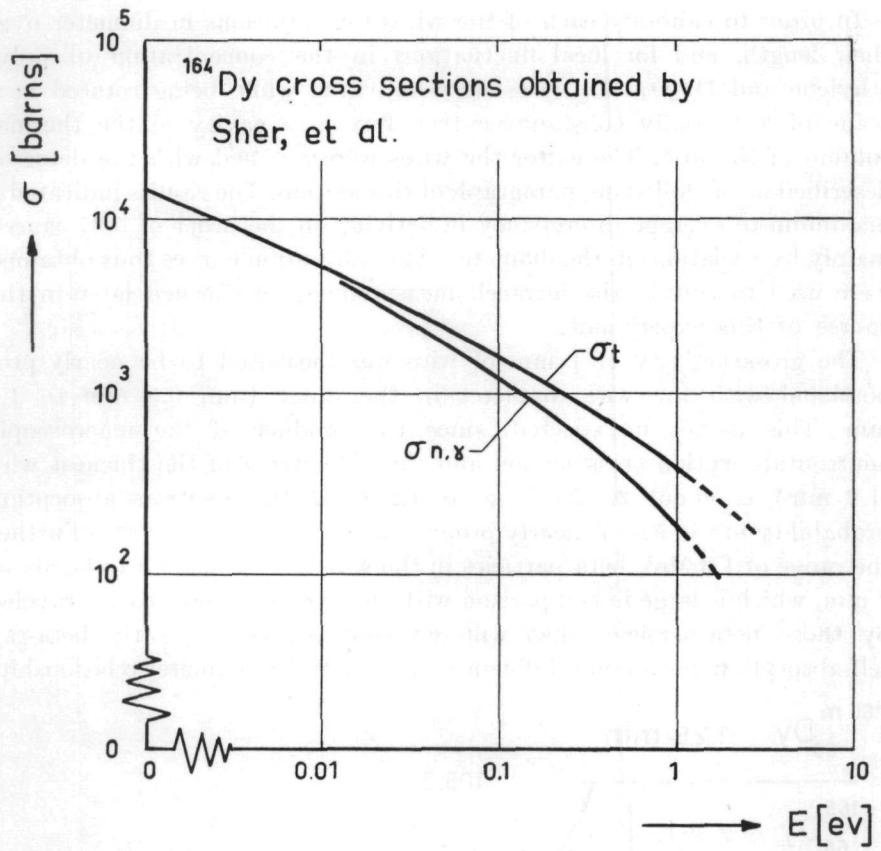


Fig. 5.2. Microscopic cross-sections of $^{164}$Dy in the thermal energy range.

and capture cross-section of $^{164}$Dy show a certain departure from the $1/v$ behaviour above one tenth of an electron volt. The only known resonance in the absorption cross-section of $^{164}$Dy occurs at 150 eV which gives rise to a thermal contribution of only 5 barns [22]. The contribution to the thermal cross-section of natural dysprosium by resonances of other dysprosium isotopes, mainly $^{162}$Dy and $^{163}$Dy with resonances at 5.44 eV and 1.72 eV respectively, may be neglected.

Making wires of small diameters from pure dysprosium is extremely difficult if not impossible at the present time. Therefore the oxide $Dy_2O_3$ which is available in powdered form was selected. It can be easily mixed with other substances to make homogeneous foils or wires. In this case polyethylene was selected as a base material. Wires were extruded which contained about 70 vol % $Dy_2O_3$ having diameters of 1.2 mm, 0.9 mm, 0.6 mm and 0.3 mm. In order to determine the purity of the wires various parts were irradiated and spectrally analysed using a 400-channel spectrometer. In addition the half-life was determined. The results of both checks indicated that no activated impurities were detectable so that the wires were indeed sufficiently pure.

In order to calibrate each of the wires for variations in diameter over their length, and for local fluctuations in the concentration of polyethylene and $Dy_2O_3$, the wires were activated while being rotated in a plane of a spatially constant neutron flux in a cavity in the thermal column of the HOR. Thereafter the wires were scanned with the detector described in the following paragraph of this section. The results indicated a maximum-to-average discrepancy in activity on the order of 5 % caused mainly by variations in the diameter. The calibration curves thus obtained were used to correct the intracell measurements performed later in the course of this experiment.

The gross activity of 1 mm of wire was measured to be nearly proportional with the wire diameter in the range from 0.3 mm to 1.2 mm. This is not unexpected, since the product of the macroscopic neutron absorption cross-section and the diameter $d$ of the thickest wire (1.2 mm) is about 2. As long as $(\Sigma_a d) < 2$ the neutron absorption probability in the wire is nearly proportional to the diameter[23]. Further the range of 1.3 MeV beta-particles in the wire was calculated to be about 2 mm, which is large in comparison with the average length to be traveled by those beta-particles that will get counted. Consequently beta-ray self-absorption has a minor influence on the activity-diameter relationship.

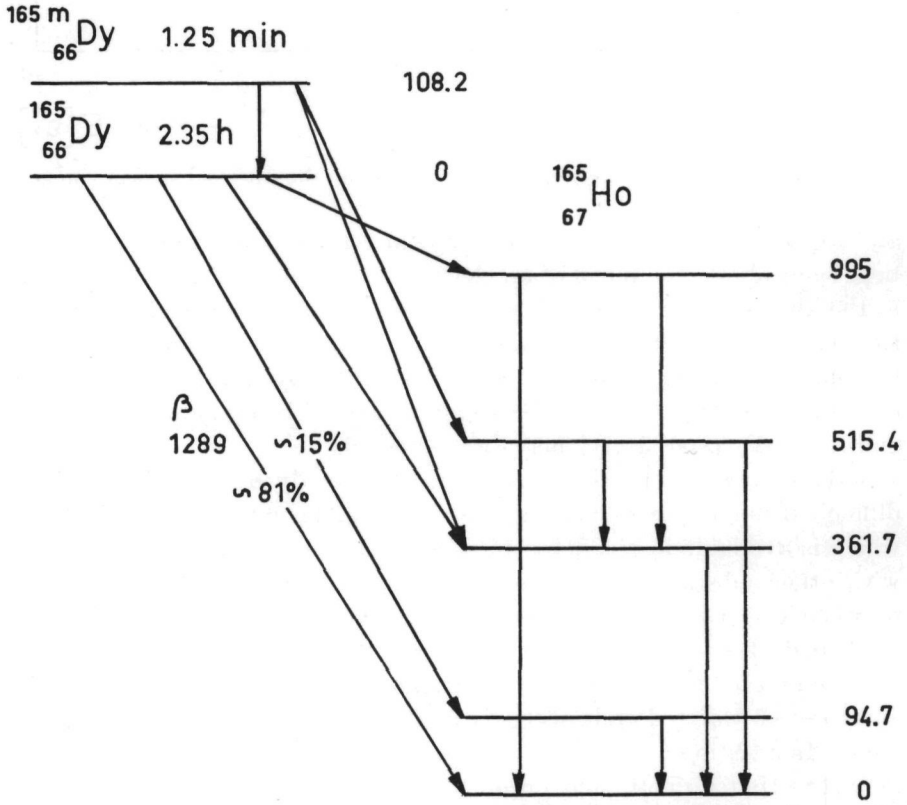


Fig. 5.3. Simplified decay scheme of $^{165}$Dy. (The energies are expressed in keV).

### 5.3.2 Wire scanning technique

From the decay scheme of $^{165}$Dy, which is given in a simplified form in Fig. 5.3, it can be seen that neutron capture in $^{164}$Dy is followed by the emission of a series of beta-particles, 81 % of which have the maximum decay energy of 1289 keV. In addition it yields gamma-rays varying in energy up to 995 keV.

The difference in penetration depth of gamma-rays and beta-particles having equal initial energy provides a method for determining the induced activity of a small part of a dysprosium wire. The range of 1.3 MeV beta-particles in brass is about 0.7 mm while the intensity attenuation of 1 MeV gamma-rays by one millimeter thick brass as a result of absorption is approximately 2 %. Consequently the beta-particles can be removed from the total radiation emitted by dysprosium by filtering through a 1 mm thick brass foil.

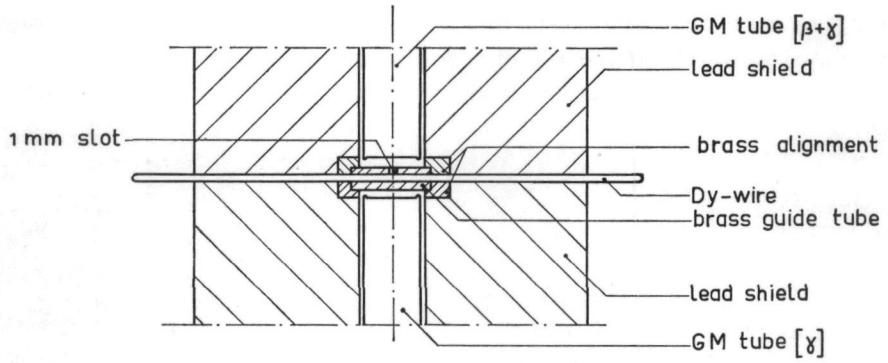


Fig. 5.4. Geometry of a dysprosium wire and two G.M.-tubes for scanning the induced beta-ray activity.

Applying this principle the activity of a small length of wire was determined as follows:

The activated dysprosium wire was shifted inside a brass guide tube having a wall thickness of 1 mm located in between two by lead surrounded G.M.-counters which faced each other. In front of one of the G.M.-counters this guide tube had a 1 mm slot (see Fig. 5.4). Thus one of the G.M.-tubes only counted the gross gamma-ray activity of the wire while the other detected the gross gamma-ray activity in addition to beta-particles emitted by 1 mm of dysprosium wire. The output signals of both counters were fed into an electronic subtraction unit. Since the G.M.-tube output-signal due to the gamma-rays only was measured to be a few percent of the output-signal resulting from beta-particles the inaccuracy introduced by the subtraction was negligible. It was experienced, that Compton electrons resulting from gamma-ray interactions with the brass guide tube, and bremsstrahlung as a result of electron capture in brass had a neglectable influence on the subtraction unit output-signal. Therefore the subtraction

unit output signal is proportional to the number of beta-particles emitted in the counting time by about 1 mm of wire. Because of the solid angle under which '$\beta+\gamma$' G.M.-tube 'sees' the wire the beta-activity counted results from a wire length which is only somewhat longer than 1 mm.

An extra feature was added to compensate for the decay of dysprosium while scanning the wire. An arbitrary part of another activated wire was counted by a third G.M.-counter in a fixed '*pre-set count*' time. By counting the successive parts of the detector wire, activated in a LEAD lattice cell, during this fixed '*pre-set count*' time (which varies of course in the sense of actual time units), the results were automatically corrected for radioactive decay. The pre-set number of counts was selected such that a 1 % statistical variation occurred in the 'gate-open' time. A block diagram of the instruments is given in Fig. 5.5. Further the scanning-device was constructed so that when the counting result of 1 mm wire had been printed, the G.M.-detectors moved 1 mm along the wire and the electronic counters were reset and restarted automatically. The two high voltage supplies connected to the set of G.M.-tubes were adjusted, so that both detectors would yield an equal count rate when exposed to the same source.

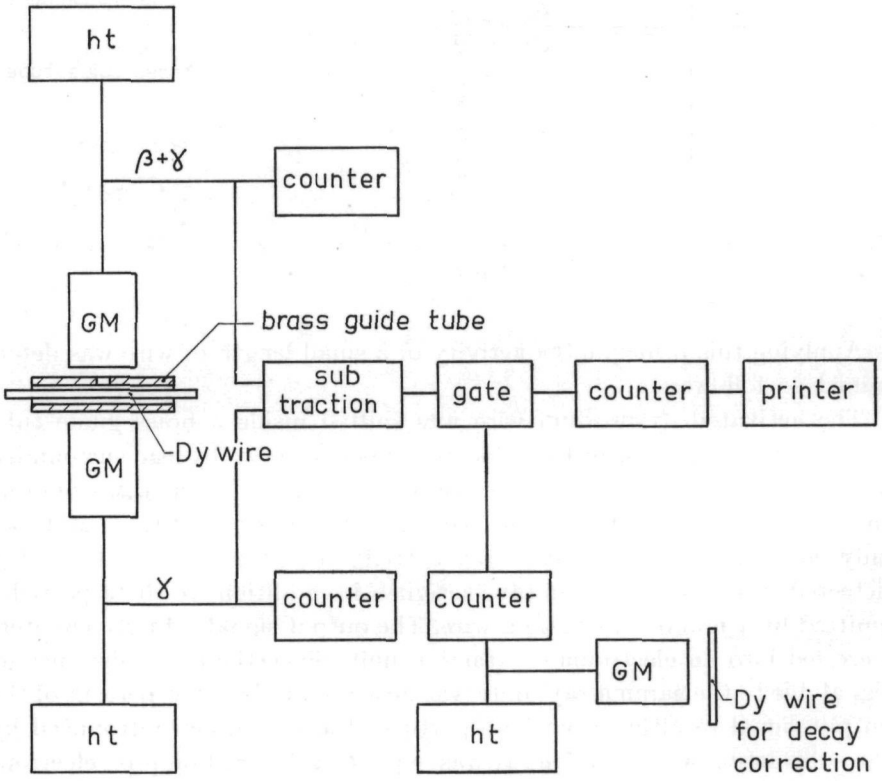


Fig. 5.5. Block diagram of the instruments used for the determination of the beta-ray activity over the length of a dysprosium wire, including automatic decay correction.

The monitor dead-time was measured to be about 360 $\mu$s. In order to avoid the necessity of dead-time corrections the count rates were kept under $10^4$ counts/min. The background activity was measured to be about 10 counts/min. Therefore a minimum count rate was allowed of the order of $5.10^2$ counts/min, in which case a correction of 2 % is to be made. The reproducibility of the monitor has been determined using a source with a relatively long half-life ($Co^{60}$, 5.2 a). The standard deviation was measured to be 1.6 %.

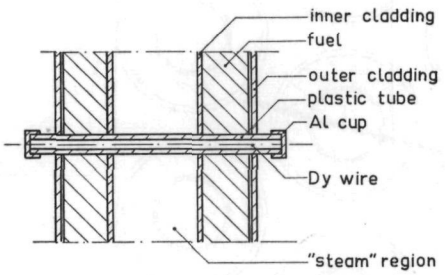


Fig. 5.6. Position of a dysprosium wire in a unit cell traversing a fuel element.

### 5.3.3 Fuel rod preparation

One of the LEAD fuel elements was prepared especially for measuring flux distributions throughout a unit cell. A hole 2.0 mm in diameter was drilled through the principle traverse axis of the element at about 45 cm from its lower end. Through this hole a tightly fitting stiff plastic tube was placed, having an internal diameter of 1.5 mm. This tube, which was glued to the fuel element outer cladding, served as a guide for the dysprosium wires while they were being activated. The length of this tube was selected so that it also supported the wire in the water region of the cell. Because of the exponential decay of the neutron flux in the assembly misalignment of the wire in the axial direction was considered undesired. To prevent water from leaking into the plastic tube, small aluminium cups were used at both ends. A cross-sectional drawing of the arrangement is presented in Fig. 5.6.

## 5.4 *Experimental procedures*

The experimental work directly related to the thermal utilization factor measurements in LEAD was very simple. A dysprosium wire of selected diameter was brought in position in the prepared fuel element as described in the preceding section. Thereafter the element was placed in the centre of one of the two regions in LEAD which could be voided. The orientation of the wire with respect to the unit cell was selected as indicated in Fig. 5.7. Thus the activation distribution over the wire represents a thermal energy averaged neutron distribution over the unit cell. Next the required void percentage in the particular seven-rod cluster was adjusted; then the HOR was brought to a power level of 200 kW with a period of 30 seconds. All

irradiations lasted two hours, after which the reactor was shutdown by a rapid insertion of the shim-safety rods.

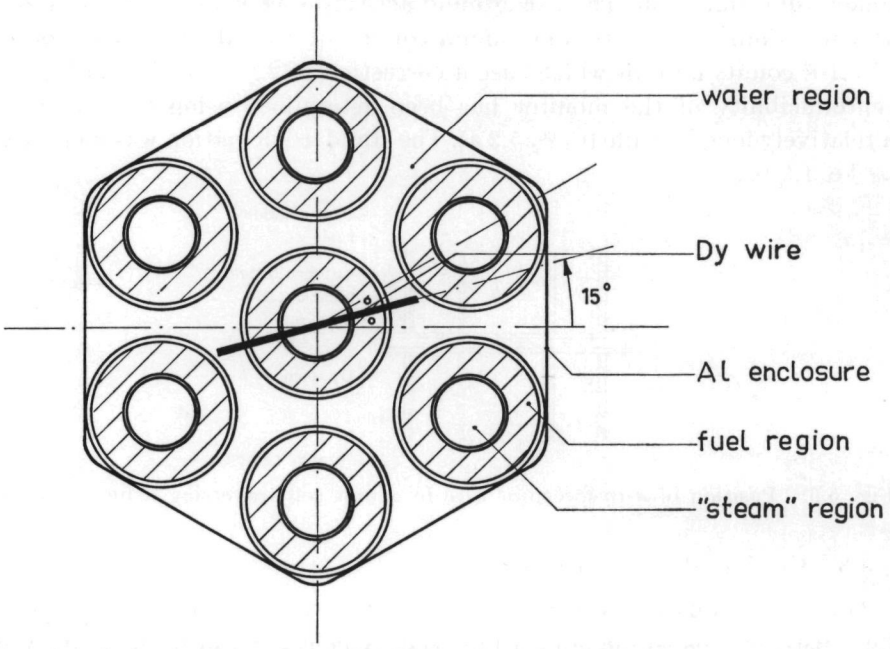


Fig. 5.7. Orientation of a dysprosium wire in a unit cell with respect to surrounding fuel elements while being activated.

Thereafter the wire-containing element was removed from the LEAD-facility and the wire was obtained for counting. Together with the detector wire, another dysprosium wire was activated for use in the automatic decay corrector. Counting of the wire started as soon as a beta-particle count rate was obtained of the order of $10^4$ counts/min.

Using these procedures wires of 1.2 mm, 0.9 mm, 0.6 mm, and 0.3 mm diameter were activated at 45 cm from the assembly bottom. In the central zone the irradiations were performed with 0 %, 10 %, 20 %, 30 % and 36 % moderator void, corresponding to water-to-fuel volume ratios of 1.14, 1.03, 0.91, 0.80 and 0.73 respectively. In the peripheral zone, the irradiations occurred with 0 %, 10 %, 20 % and 29 % void, equivalent to water-to-fuel volume ratios of 2.34, 2.10, 1.87 and 1.66.

## 5.5 *Data reduction and results*

### 5.5.1 Measurements

The results obtained from scanning the 1.2 mm diameter dysprosium wire have been plotted in Fig. 5.8a for the central zone and in Fig. 5.8b for the peripheral zone. For clearness the experimental points are given only for zero and maximum void fractions in each of the two zones. It should be noted that these points refer to the dysprosium activity measured.

In the two figures they have been normalized in regard to irradiation and decay times, so that the distributions may be compared with each other. Similar plots were obtained with the three other wires. Assuming for the moment that the energy dependence of the dysprosium capture cross-section is proportional to $1/v$ the experimental data also represent the neutron density distribution in the cell. In addition to the experimental results the thermal neutron density distribution as calculated by means of the K7-THERMOS code (see section 5.2) is presented in Fig. 5.8a and Fig. 5.8b with the drawn lines.

For processing the experimental results curves were drawn through the points obtained from each of the wires, which had been irradiated under conditions of various moderator void fractions. These curves were drawn so that a good average was obtained from the experimental data; the form was governed by that of the calculated distributions.

To calculate the thermal utilization factor the thermal neutron absorption in each of the regions of the unit cell must be obtained relative to the absorption in the fuel region. Frequently one first determines the neutron density disadvantage factors as defined in section 5.1.

For processing convenience a slightly different approach has been followed here:

The total thermal neutron absorption per unit time in an arbitrary region of an infinitely long unit cell of a reactor lattice may be generally expressed as:

$$\text{Abs.}_{\text{region}} = \int_0^{E_{th}} \int_{\substack{\text{region} \\ \text{vol.}}} \Sigma_{a_r}(E)\, \phi_r(E,\mathbf{r})\, dE\, dV \tag{5.5.1}$$

where the subscript r indicates the region and $V$ is the volume of the region. $E_{th}$ is the cut-off energy of the thermal spectrum based on considerations outlined in section 5.1. Changing the energy variable $E$ into the corresponding velocity $v$ and writing $\phi$ as $N.v.$, Eq. (5.5.1) can be written as:

$$\text{Abs.}_{\text{region}} = \int_0^{v_{th}} \int_{\substack{\text{region} \\ \text{vol.}}} \Sigma_a(v)\, N(v,\mathbf{r})\, mv^2\, dv\, dV \tag{5.5.2}$$

where the subscript r has been dropped to symplify the notation. Substitution of $\bar{\Sigma}_a\, \bar{v}/v$ for $\Sigma_a(v)$ in Eq. (5.5.2) results in:

$$\text{Abs.}_{\text{region}} = \bar{\Sigma}_a\, \bar{v} m \int_0^{v_{th}} \int_{\substack{\text{region} \\ \text{vol.}}} N(v,\mathbf{r})\, v\, dv\, dV \tag{5.5.3}$$

where $\bar{\Sigma}_a$ and $\bar{v}$ are the thermal spectrum averaged cross-section and velocity. Implicitly the assumption has been made that the absorption cross-section varies as $1/v$. However this approximation may be corrected for by using the appropriate cross-section in the final calculation.

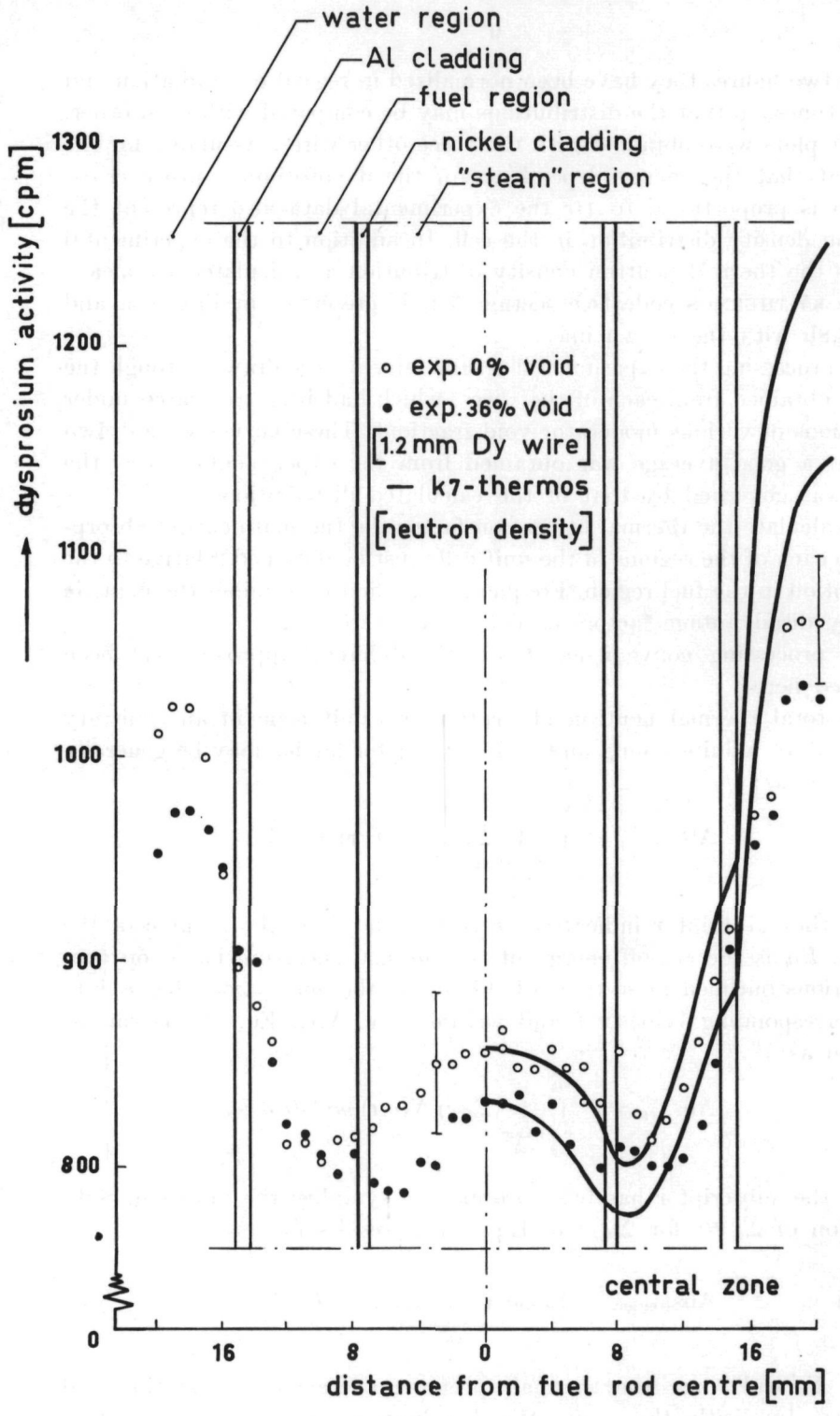


*a*) central zone

Fig. 5.8. Measured and calculated thermal neutron density distribution

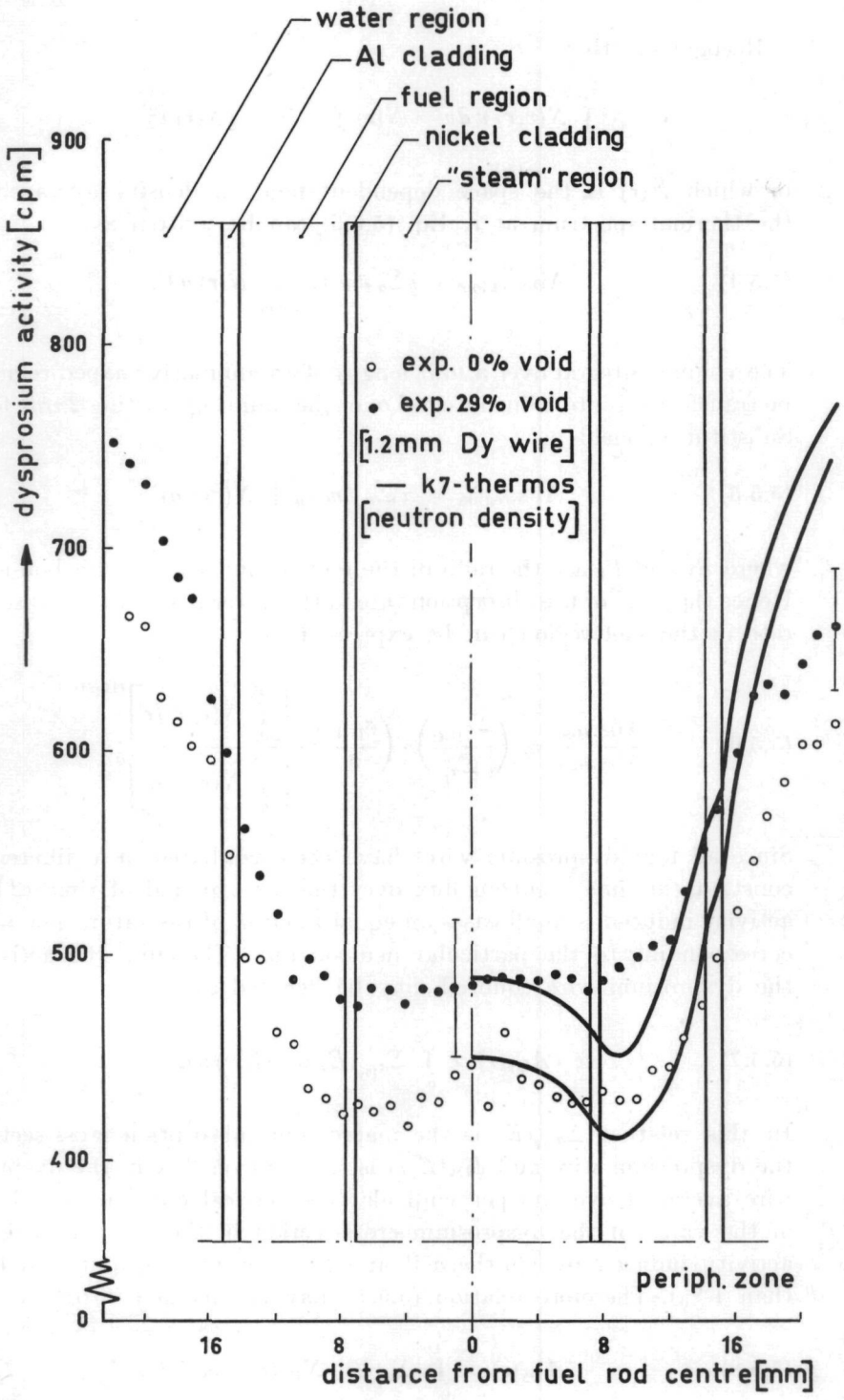


*b*) peripheral zone

in a unit cell for zero and maximum obtainable void percentages.

Recognizing that:

$$\int_0^{v_{th}} N(v,\mathbf{r})\, v\, dv = \bar{N}(\mathbf{r}) \int_0^{v_{th}} v\, dv = \tfrac{1}{2}\bar{N}(\mathbf{r})\, v_{th}^2$$

in which $\bar{N}(\mathbf{r})$ is the space dependent neutron density averaged over the thermal spectrum at $\mathbf{r}$, Eq. (5.5.3) can be written as:

$$\text{Abs.}_{\text{region}} = \tfrac{1}{2}\bar{\Sigma}_a\, \bar{v}m\, v_{th}^2 \int_{\substack{\text{region}\\ \text{vol.}}} \bar{N}(\mathbf{r})\, dV. \tag{5.5.4}$$

The volume integral over a unit length of an annularly shaped region can be transformed into a line integral over the radius by writing $2\pi r dr$ for $dV$. Substitution yields:

$$\text{Abs.}_{\text{region}} = \pi\, \bar{\Sigma}_a\, \bar{v}m\, v_{th}^2 \int_{R_1}^{R_2} \bar{N}(r)\, r\, dr \tag{5.5.5}$$

where $R_1$ and $R_2$ are the radii of the region's inner and outer boundaries. Hence the ratio of the absorption rate in the water region to the absorption rate in the fuel region can be expressed as:

$$\frac{\text{Abs.}_{\text{H}_2\text{O}}}{\text{Abs.}_{\text{fuel}}} = \left(\frac{\bar{\Sigma}_{a_{\text{H}_2\text{O}}}}{\bar{\Sigma}_{a_{\text{f}}}}\right) \cdot \left(\frac{\bar{v}_{\text{H}_2\text{O}}}{\bar{v}_{\text{f}}}\right) \cdot \frac{\left[\int_{R_1}^{R_2} \bar{N}(r)\, r\, dr\right]^{(\text{H}_2\text{O})}}{\left[\int_{R_0}^{R_1} \bar{N}(r)\, r\, dr\right]^{(\text{f})}} \tag{5.5.6}$$

Since all four dysprosium wires have been irradiated in a different but constant (in time) neutron flux over the same period of time (2 h) the activity induced is in all cases an equal fraction of the saturation activity corresponding to the particular neutron flux. Therefore the activity of the dysprosium wire counted may be denoted as:

$$A_{\text{Dy}}(r) \propto \int_0^{\infty} \Sigma_{a_{\text{Dy}}}(E)\, \phi_{\text{Dy}}(E,r)\, dE. \tag{5.5.7}$$

In this relation $\Sigma_{a_{\text{Dy}}}(E)$ is the macroscopic absorption cross-section of the dysprosium wire and $\phi_{\text{Dy}}(E,r)$ is the neutron flux in the dysprosium wire averaged over its perpendicular geometrical cross-section. In view of the value of the dysprosium cross-section in the thermal region the activity induced by epi-thermal and fast neutrons is quite small (less than 1 %). Therefore relation (5.5.7) may be changed into:

$$A_{\text{Dy}}(r) \propto \int_0^{v_{\text{Dy}}} \Sigma_{a_{\text{Dy}}}(v)\, N_{\text{Dy}}(v,r)\, mv^2\, dv. \tag{5.5.8}$$

Writing $\Sigma_{a_{\text{Dy}}}(v)$ as $\bar{\Sigma}_{a_{\text{Dy}}}\, \bar{v}_{\text{Dy}}/v$, where $\bar{\Sigma}_{a_{\text{Dy}}}$ is the dysprosium cross-section averaged over the neutron energy spectrum up to the dysprosium cut-off

energy and $\bar{v}_{Dy}$ is the 'dysprosium spectrum'-averaged neutron speed, relation (5.5.8) becomes:

$$A_{Dy}(r) \propto \bar{\Sigma}_{a_{Dy}} \bar{v}_{Dy}\, m \int_0^{v_{Dy}} v\, dv \cdot \bar{N}_{Dy}(r). \tag{5.5.9}$$

In this relation $\bar{N}_{Dy}(r)$ is the perturbed neutron density averaged over the energy spectrum up to the dysprosium cut-off energy. Assuming that $\bar{N}_{Dy}(r) = \gamma \bar{N}(r)$ where $\gamma$ is a correction factor for the neutron density depression caused by the presence of the wire in the region, relation (5.5.9) can be rearranged into:

$$\bar{N}(r) \propto \frac{2A_{Dy}(r)}{\gamma\, \bar{\Sigma}_{a_{Dy}}\, \bar{v}_{Dy}\, m\, v_{Dy}^2}. \tag{5.5.10}$$

Substitution of relation (5.5.10) into Eq. (5.5.6) then gives:

$$\frac{\text{Abs.}_{H_2O}}{\text{Abs.}_{fuel}} = \left(\frac{\bar{\Sigma}_{a_{H_2O}}}{\bar{\Sigma}_{a_f}}\right) \cdot \left(\frac{\bar{\Sigma}^{(f)}_{a_{Dy}}}{\bar{\Sigma}^{(H_2O)}_{a_{Dy}}}\right) \cdot \left(\frac{\gamma_f}{\gamma_{H_2O}}\right) \cdot \frac{\left[\int_{R_1}^{R_2} A_{Dy}(r)\, r\, dr\right]^{(H_2O)}}{\left[\int_{R_0}^{R_1} A_{Dy}(r)\, r\, dr\right]^{(f)}} \tag{5.5.11}$$

where the assumption has been made that the dysprosium cut-off energy is equal to the cut-off energy as described in Eq. (5.5.1). In that case the cross-sections $\bar{\Sigma}_{a_{H_2O}}$ and $\bar{\Sigma}_{a_f}$ should also be averaged over the spectrum up to the dysprosium cut-off energy. In the calculations the cross-sections are averaged up to 0.625 eV, which is somewhat lower than the dysprosium cut-off energy. The arguments for selecting the cut-off energy are discussed in section 5.1. Further it has been assumed that no spectrum changes occurred as a result of the insertion of the wire.

The influence of these assumptions on the value of the thermal utilization factor is discussed in section 5.7. From the K7-THERMOS calculations it was found that $(\bar{\Sigma}_{a_{Dy}})^{(f)}/(\bar{\Sigma}_{a_{Dy}})^{(H_2O)}$ was about 0.9 in a central zone cell and 0.89 in a peripheral zone cell for all void fractions. These values have been used while processing the experimental results.

Because

$$\int_{R_1}^{R_2} A_{Dy}(r)\, r\, dr \text{ may be approximated by } \sum_{i=1}^{n} A_i(r)\, r_i\, \Delta r$$

the line integral over the dysprosium activity distribution can be obtained by numerical integration of the experimental curves. By taking all intervals $\Delta r$ equal over all regions, the ratio of the absorption rate in the water to the absorption rate in the fuel then becomes:

$$\frac{\text{Abs.}_{H_2O}}{\text{Abs.}_{fuel}} = \left(\frac{\bar{\Sigma}_{a_{H_2O}}}{\bar{\Sigma}_{a_f}}\right) \cdot \left(\frac{\bar{\Sigma}^{(f)}_{a_{Dy}}}{\bar{\Sigma}^{(H_2O)}_{a_{Dy}}}\right) \cdot \left(\frac{\gamma_f}{\gamma_{H_2O}}\right) \cdot \frac{\left[\sum_{i=1}^{n} A_i(r)\, r_i\right]^{(H_2O)}}{\left[\sum_{j=1}^{m} A_j(r)\, r_j\right]^{(f)}}. \tag{5.5.12}$$

The expression for the density disadvantage factor $\delta_N$ may now be

written as:

$$(5.5.13) \qquad \delta_N = \left(\frac{V_f}{V_{H_2O}}\right) \cdot \left(\frac{\overline{\Sigma}^{(f)}_{a_{Dy}}}{\overline{\Sigma}^{(H_2O)}_{a_{Dy}}}\right) \cdot \left(\frac{\gamma_f}{\gamma_{H_2O}}\right) \cdot \frac{\left[\sum_{i=1}^{n} A_i(r)\, r_i\right]^{(H_2O)}}{\left[\sum_{j=1}^{m} A_j(r)\, r_j\right]^{(f)}}$$

where $V_{H_2O}$ is the moderator volume fraction and $V_f$ the fuel volume fraction in the cell.

In order to determine $\gamma_f$ and $\gamma_{H_2O}$ in a relatively simple way another series of assumptions is to be made. The flux depression is separable into a depression inside the wire and in a depression in the medium near the wire. Assuming that the ratio of the average flux in the wire to the flux at the wire surface is the same in all regions of the unit cell the quantity to determine is $\phi_s/\phi_0$ where $\phi_s$ is the flux at the wire surface and $\phi_0$ is the unperturbed neutron flux in the surrounding medium. Using the following model an expression can be derived for $\phi_s/\phi_0$:

*a*) The wire is infinitely long and introduced into an infinitely large medium, in which a constant source of thermal neutrons is homogeneously distributed.

*b*) The neutrons entering the wire make no scattering collisions in the wire, but continue along their original line of flight until they either are absorbed or escape from the wire.

*c*) The wire is exposed to an isotropic neutron flux.

*d*) Diffusion theory is valid everywhere in the surrounding medium.

Under these assumptions one finds that:

$$(5.5.14) \qquad \gamma = \frac{\phi_s}{\phi_0} = 1 - \frac{1}{\left[1 + 2D\varkappa \frac{K_1(\varkappa R)}{K_0(\varkappa R)} \left(\frac{1+\beta}{1-\beta}\right)\right]}$$

where $R$ is radius of the wire and the quantities $\varkappa$ and $D$ are the reciprocal diffusion length and the diffusion coefficient of the medium surrounding the wire. Further $K_1$ and $K_0$ are the first and zero order Bessel-functions of the second kind respectively. The factor $\beta$ is the transmission coefficient of the wire, defined as the fraction of all neutrons impinging upon the wire surface which pass through the wire without being absorbed. The transmission coefficient $\beta$ has been taken from MEGHREBLIAN and HOLMES [24].

The factor $\gamma$ has been calculated for the 1.2 mm wire, because in that case the influence of flux depression is most noticeable. Using the same cross-sections as applied in the K7-THERMOS calculations one finds that:

| | 0 % void | 36 % void |
|---|---|---|
| $\gamma_f$ | 0.803 | 0.816 |
| $\gamma_{H_2O}$ | 0.635 | 0.732 |
| $\gamma_f/\gamma_{H_2O}$ | 1.26 | 1.15 |

As can be seen the influence of the difference in flux depression in the region decreases with increasing moderator void fraction. Further $\gamma_f/\gamma_{H_2O}$ approaches unity as the diameter of the dysprosium wire reduces to zero. The values determined for $\gamma_f/\gamma_{H_2O}$ have been interpolated for other void fractions and other wire diameters. Using the procedure outlined above the density disadvantage factors have been calculated from the experimental data accounting only for the absorption in the water region. The results are tabulated in Table V.1.

A correction has been made for the change in the macroscopic flux distribution across the unit cell.

Using the K7-THERMOS cross-sections the thermal utilization factor has been determined from all the experimental data. The results are plotted in Fig. 5.9a for the central zone and in Fig. 5.9b for the peripheral zone. The influence of the neutron absorption in the nickel inner cladding of the fuel rod has been disregarded because of the small volume fraction of nickel present in the cell. Of course the influence of the presence of cladding

TABLE V.1

Experimental and theoretical values for the thermal utilization factor, and density disadvantage factors for LEAD lattice cells.

| void % | Central Zone | | | | | | | Peripheral Zone | | | | | |
|---|---|---|---|---|---|---|---|---|---|---|---|---|---|
| | Exp. | | | K7-Thermos | | Micro-flux | | Exp. | | K7-Thermos | | Micro-flux | |
| | wire diam. | $\delta$ | $f$ | $\delta$ | $f$ | $\delta$ | $f$ | $\delta$ | $f$ | $\delta$ | $f$ | $\delta$ | $f$ |
| 0 | 1.2 | 1.34 | 0.905 | | | | | 1.54 | 0.796 | | | | |
| | 0.9 | 1.31 | 0.907 | 1.422 | 0.878 | 1.525 | 0.869 | 1.46 | 0.808 | 1.593 | 0.788 | 1.752 | 0.771 |
| | 0.6 | 1.34 | 0.905 | | | | | 1.42 | 0.813 | | | | |
| | 0.3 | 1.34 | 0.905 | | | | | 1.40 | 0.815 | | | | |
| 10 | 1.2 | 1.43 | 0.908 | | | | | 1.54 | 0.813 | | | | |
| | 0.9 | 1.32 | 0.915 | 1.403 | 0.886 | | | 1.46 | 0.826 | 1.565 | 0.805 | | |
| | 0.6 | 1.31 | 0.915 | | | | | 1.46 | 0.826 | | | | |
| | 0.3 | 1.30 | 0.916 | | | | | 1.37 | 0.835 | | | | |
| 20 | 1.2 | 1.39 | 0.920 | | | | | 1.40 | 0.841 | | | | |
| | 0.9 | 1.30 | 0.926 | 1.384 | 0.895 | 1.474 | 0.888 | 1.36 | 0.850 | 1.534 | 0.822 | 1.662 | 0.809 |
| | 0.6 | 1.31 | 0.924 | | | | | 1.36 | 0.851 | | | | |
| | 0.3 | 1.23 | 0.928 | | | | | 1.33 | 0.853 | | | | |
| 30 | 1.2 | 1.40 | 0.927 | | | | | 1.36 | 0.859 | | | | |
| (29) | 0.9 | 1.30 | 0.932 | 1.367 | 0.903 | | | 1.30 | 0.870 | 1.508 | 0.838 | 1.620 | 0.826 |
| | 0.6 | 1.30 | 0.932 | | | | | 1.30 | 0.870 | | | | |
| | 0.3 | 1.22 | 0.936 | | | | | 1.28 | 0.871 | | | | |
| 36 | 1.2 | 1.29 | 0.939 | | | | | | | | | | |
| | 0.9 | 1.21 | 0.942 | 1.359 | 0.909 | 1.431 | 0.903 | | | | | | |
| | 0.6 | 1.18 | 0.944 | | | | | | | | | | |
| | 0.3 | 1.20 | 0.943 | | | | | | | | | | |

materials on the neutron flux distribution in the water and fuel region is inherently incorporated.

In addition the results of theoretical calculations described in the next section are presented in these figures.

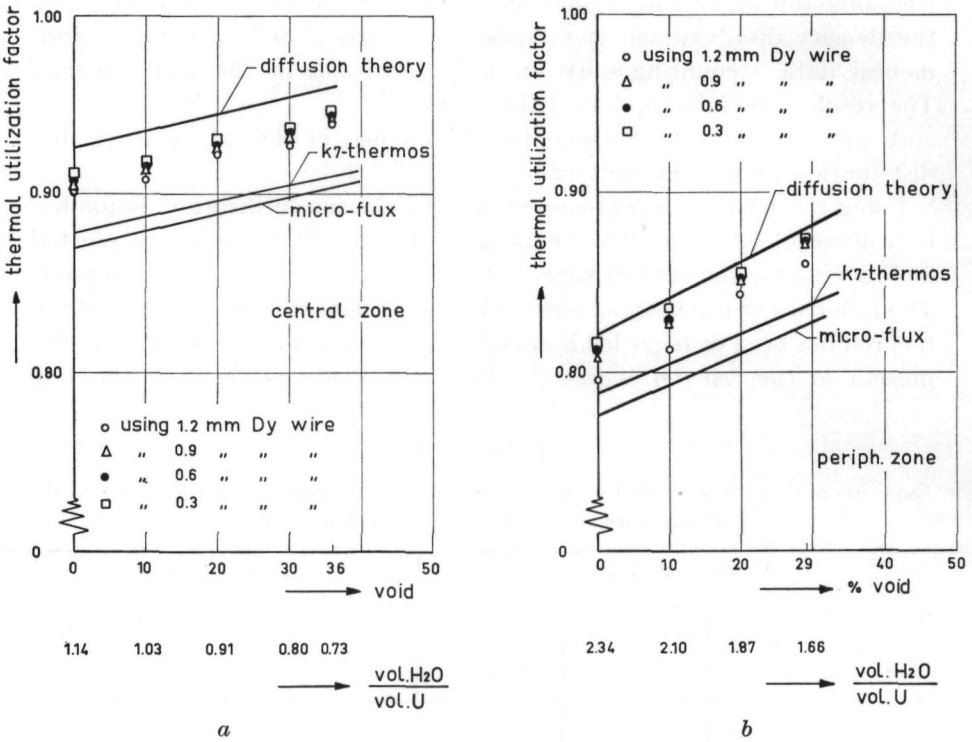


Fig. 5.9. Experimentally and theoretically obtained thermal utilization factors as a function of the moderator void fraction, *a*) for the central zone and *b*) for the peripheral zone.

### 5.5.2 Calculations

In order to make possible a comparison between the results of the experimental work described in this section and values obtained from present day calculation methods the thermal utilization factor was also computed using the K7-THERMOS code as well as with the MICRO-FLUX code. In addition the thermal utilization factor has been calculated by means of simple diffusion theory as described later in this section. In all these calculations it has been assumed that the influence of external source neutrons was negligible and that the unit cell under consideration was part of an infinitely large lattice.

K7-THERMOS is a multi-region multi-group computer code written in FORTRAN for the Control Data 3600 of the Kjeller Computer Installation – Norway by STAMM'LER [4], which gives as output the thermal neutron distribution in space and energy in an infinitely long heterogeneous reactor cell with cylindrical symmetry (WIGNER–SEITZ cell) and reflecting

boundary. In addition it calculates the thermal utilization factor. The code, which resembles HONECK's THERMOS program [25], solves the stationary integral equation describing neutron transport in the thermal energy region of a reactor cell, i.e.:

$$(5.5.15)\quad \begin{cases} vN(r,v) = \int_0^R 2\pi r'\, dr'\, T(r' \to r, v) \int_0^{v_{th}} dv'\, P(r', v' \to v)\, N(r', v') + \\ \qquad + \int_0^R 2\pi r'\, dr'\, T(r' \to r, v)\, S(r', v) \end{cases}$$

where:

$r$ is the radial coordinate in the cylindrical system

$R$ is the outer radius of the unit cell

$v$ is the dimensionless neutron speed in units of 2200 m/s

$v_{th}$ is the thermal cut-off speed above which no upward scattering is assumed to take place

$N(r,v)\, dv$ is the neutron density at $r$ for neutrons in the speed interval between $v$ and $v + dv$

$T(r' \to r, v)$ is the transport kernel for neutrons with speed $v$, which is defined as the contribution to the neutron flux $vN(r, v)$ at $r$, due to a unit isotropic source in an infinitesimal cylindrical shell at $r'$

$P(r', v' \to v)$ is the probability per unit time that a neutron at $r'$ with speed $v'$ will be scattered into the speed range $dv$ at $v$

$S(r',v)\, dv$ is the source of neutrons at $r'$ with speeds between $v$ and $v + dv$, due to slowing down of epi-thermal neutrons into the thermal range $(0 \to v_{th})$

The first term on the right hand side of Eq. (5.5.15) represents the contribution to the neutron flux $v \cdot N(r, v)$ from all scattering interactions inside the unit cell that change the neutron speed from any $v' \leqslant v_{th}$ to $v$. The second term accounts for the contribution of all sources of neutrons of speed $v$ inside the unit cell, resulting from slowing down. Scattering has been assumed to be isotropic in the laboratory system, but a transport correction has been applied. The boundary condition at the cell outer boundary is based on isotropic flux return (so called white boundary) which is obtained by adding an imaginary shell of 2.5 cm thickness to the unit cell. In this region absorption is assumed zero while a scattering cross-section $\Sigma_s$ of 1 $cm^{-1}$ is assumed for all energy groups. The energy transfer matrix used is an anisotropic version of NELKIN's – model which is due to KOPPEL and YOUNG [26]. This is an improvement over the NELKIN-model in that it accounts (by estimation) for the influence of the actual anisotropic motion of the proton on the neutron scattering kernel. In the runs made for the LEAD lattice cells, the thermal cut-off energy has been selected at 0.6249 eV.

MICRO-FLUX, written by A. TAS, *et al.* [5], is a program partly written in ALGOL and partly in X-1 machine language, that yields the space

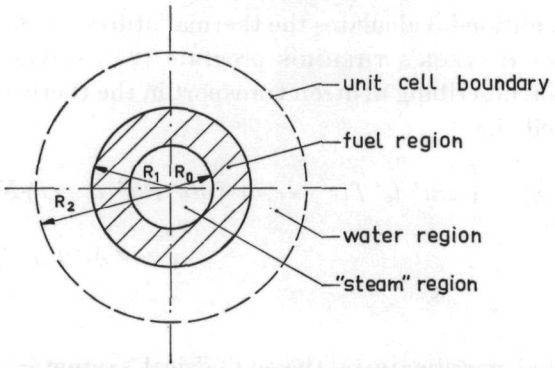


Fig. 5.10. Unit cell geometry used in a diffusion calculation of the thermal utilization factor.

and energy dependent thermal neutron density in infinitely long *hexagonal* and *rectangular* lattices. The basis of the program, just as the in K7-THERMOS code, is the integral transport equation. The scattering kernel used in this program has been calculated according to the atom model of BROWN and ST. JOHN [27]. No transport correction has been applied. The thermal cut-off energy was selected at 0.6324 eV.

The cross-sections used in both calculations were approximately equal. They have been obtained from reference [28] and from the Kjeller cross-section library. The results of the computer calculations with regard to the thermal utilization factor are presented in Fig. 5.9a and Fig. 5.9b together with the experimental results and are tabulated in Table V.1.

In addition to the calculation techniques described above, which require the use of a digital computor, an expression was derived for the thermal utilization factor in a unit cell of the LEAD-facility, using simple diffusion theory. The derivation of this expression is analogous to that described by GLASSTONE and EDLUND [29] for a solid fuel rod and therefore will not be presented in detail. A cylindrical cell model was used, the coordinate system of which is shown in Fig. 5.10. The inner radius of the fuel rod is $R_0$, the outer radius $R_1$ and $R_2$ is the unit cell outer radius. The slowing down density was assumed constant in the moderator and zero in the fuel region. By further taking the fuel rod to be infinitely long and assuming that no moderation occurs inside the fuel rod the following expression is found:

$$\frac{1}{f} = 1 + \frac{\Sigma_{a_{H_2O}}}{\Sigma_{a_f}} \cdot \frac{V_{H_2O}}{V_f} \cdot P + (Q-1) \tag{5.5.16}$$

where:

$$P \equiv \frac{(R_1^2 - R_0^2)}{2R_1} \cdot \varkappa_f \cdot \frac{I_0(\varkappa_f R_1) K_1(\varkappa_f R_0) + I_1(\varkappa_f R_0) K_0(\varkappa_f R_1)}{I_1(\varkappa_f R_1) K_1(\varkappa_f R_0) - I_1(\varkappa_f R_0) K_1(\varkappa_f R_1)}$$

$$Q \equiv \frac{(R_2^2 - R_1^2)}{2R_1} \cdot \varkappa_{H_2O} \cdot \frac{I_0(\varkappa_{H_2O} R_1) K_1(\varkappa_{H_2O} R_2) + I_1(\varkappa_{H_2O} R_2) K_0(\varkappa_{H_2O} R_1)}{I_1(\varkappa_{H_2O} R_2) K_1(\varkappa_{H_2O} R_1) - I_1(\varkappa_{H_2O} R_1) K_1(\varkappa_{H_2O} R_2)}.$$

The functions $I_0$ and $K_0$ are the zero-order, modified Bessel-functions of the first and second kind respectively; $I_1$ and $K_1$ are the first-order functions.

The parameters $\varkappa_f$ and $\varkappa_{H_2O}$ are the reciprocals of the thermal diffusion length in the fuel and water regions. Further $\Sigma_{a_f}$ and $\Sigma_{a_{H_2O}}$ are the thermal spectrum averaged absorption cross-sections in the fuel and water region, while $V_f$ and $V_{H_2O}$ are the respective fuel and water volume fractions in the unit cell.

Using Eq. (5.5.16) the thermal utilization factor was obtained for various void fractions in a unit cell of the central zone and a cell of the peripheral zone. The results are also given in Fig. 5.9a and Fig. 5.9b. The values used for $R_0$, $R_1$ and $R_2$, $\Sigma_{a_f}$, $\Sigma_{a_{H_2O}}$, $\varkappa_f$ and $\varkappa_{H_2O}$ are tabulated in Table V.2. The cross-sections used are equivalent to those applied in the K7-THERMOS calculation. Although the influence of the thermal neutron absorption in the cladding materials has not been accounted for in the diffusion expression for $f$, the final results have been corrected for this effect.

TABLE V.2

Values of parameters used in the diffusion calculation for the thermal utilization factor. The cross-sections equalize those applied in the K7-THERMOS computations.

| ZONE | Void % | $R_0$ (cm) | $R_1$ (cm) | $R_2$ (cm) | $V_{H_2O}/V_f$ | $\Sigma_{a_f}$ ($cm^{-1}$) | $\Sigma_{a_{H_2O}}$ ($cm^{-1}$) | $\varkappa_f$ ($cm^{-1}$) | $\varkappa_{H_2O}$ ($cm^{-1}$) |
|---|---|---|---|---|---|---|---|---|---|
| CENTRAL | 0 | 0.75 | 1.425 | 2.03 | 1.14 | 0.2263 | 0.0155 | 0.805 | 0.313 |
| | 10 | 0.75 | 1.425 | 2.03 | 1.14 | 0.2225 | 0.0137 | 0.793 | 0.278 |
| | 20 | 0.75 | 1.425 | 2.03 | 1.14 | 0.2180 | 0.0119 | 0.779 | 0.242 |
| | 30 | 0.75 | 1.425 | 2.03 | 1.14 | 0.2132 | 0.0103 | 0.764 | 0.210 |
| | 36 | 0.75 | 1.425 | 2.03 | 1.14 | 0.2089 | 0.0091 | 0.750 | 0.187 |
| PERIPHERAL | 0 | 0.75 | 1.425 | 2.41 | 2.34 | 0.2472 | 0.0170 | 0.871 | 0.340 |
| | 10 | 0.75 | 1.425 | 2.41 | 2.34 | 0.2449 | 0.0152 | 0.864 | 0.303 |
| | 20 | 0.75 | 1.425 | 2.41 | 2.34 | 0.2420 | 0.0133 | 0.855 | 0.266 |
| | 29 | 0.75 | 1.425 | 2.41 | 2.34 | 0.2388 | 0.0116 | 0.845 | 0.234 |

## 5.6 *The product p.f*

It is of interest to note the correlation that exists between $p.f$ and the moderator void fraction $\alpha$. In Fig. 5.11a and Fig. 5.11b this relationship, determined from experimentally obtained values for the resonance escape probability $p$ and the thermal utilization factor $f$, is shown for the central zone and the peripheral zone respectively. In addition a curve is presented in these figures, which is determined from the $p$-values obtained by a semi-empirical engineering calculation (see Chapter 4) and the $f$-results obtained with the K7-THERMOS code.

For the central zone a decrease in $p.f$ is observed, becoming more important at high void fractions. In addition to a small increase in the fast neutron leakage, the pronounced decrease in $p.f$ results from the

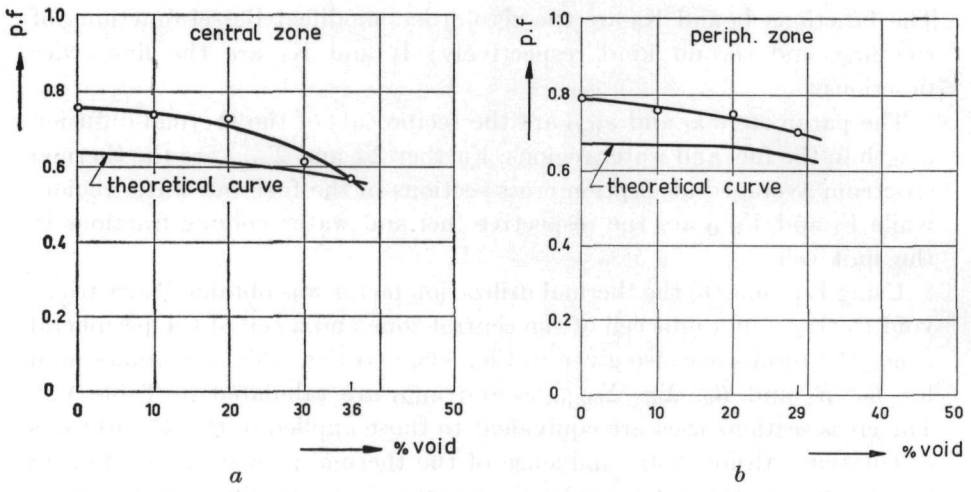


Fig. 5.11. The product $p.f$ as a function of the moderator void fraction *a*) for the central zone and *b*) for the peripheral zone.

observed strong decrease in the resonance escape probability, being larger than the increase in the thermal utilization factor.

In the peripheral zone – if one observes the 'theoretical' curve – the dependence on the void fraction is only noticeable at high void fractions where the condition of optimal moderation has been approached and the neutron spectrum tends to harden.

Because of hardening of the spectrum epi-thermal fission in $^{235}U$ will increase, while in addition, due to an increase of the neutron scattering mean free path in the moderator (as a result of the voids), the contribution of fast fission in $^{238}U$ becomes more important. Consequently the value of $k_\infty$ will not decrease proportional to $p.f$.

Comparing furthermore the results plotted in Fig. 5.11 with data shown in Fig. 1.5, it can be seen that for the central zone the decrease in $p.f$ according to diffusion theory is considerably less than experimentally determined.

An increase of $p.f$ was calculated (Chapter 1) for the peripheral zone, and based upon this result it was initially expected, that the macroscopic neutron flux level would rise in the peripheral zone with increasing void fraction. Whereas the fast fission factor in this zone will only be slightly affected by the voids, it can be concluded from the theoretical curve presented in Fig. 5.11b, but even more so from the experimental data, that an increase of the flux level occurs neither as a result of the introduction of voids (experiment) nor as a result of a reduction of the moderator density (theory) in an over-moderated lattice. In addition it can be seen, that a reduction of the moderator density cannot be interpreted as being equivalent to a change in the water-to-fuel volume ratio in under-moderated and slightly over-moderated lattices, as far as $p.f$ is concerned.

In view of conversion potential an under-moderated lattice is very attractive (high conversion-ratio). Furthermore it features a negative temperature coefficient of reactivity.

5.7 *Discussion of the results*

From the experimental results concerning the thermal utilization factor, which are summarized in Table V.1 and plotted in Fig. 5.9a and Fig. 5.9b it can be concluded that the increase of the thermal utilization factor, as a result of the introduction of voids in the moderator, is approximately 0.12 %/%-void in the central zone and 0.25 %/%-void in the peripheral zone. From the K7-THERMOS computations it can be derived that for the central zone the increase is 0.098 %/%-void, while a value of 0.22 %/%-void is found for the peripheral zone. As can be seen the rate of increase is about equal in experimental and theoretical results, while further the influence of spectral hardening is of minor importance.

The absolute values of the experimentally determined thermal utilization factors in both zones of the LEAD-facility are about 3 % to 4 % higher than the K7-THERMOS values. However, rather than speaking in terms of the thermal utililation factor it is more meaningful to compare the experimentally and theoretically obtained disadvantage factors. The experimental values of the density disadvantage factors for the central zone cell are 6 % to 10 % lower than the K7-THERMOS values, while in the peripheral zone where no proper correction could be made for thermal neutron leakage, the discrepancies range from 10 % to 16 %. The first of these percentages refers to the zero void condition and the latter to 36 % and 29 % void respectively. Thus, as the void fraction increases the agreement between experimental and theoretical results becomes even worse. It should be noted however that in the calculation of the experimental density disadvantage factors only the neutron absorption in the water region has been accounted for (next to the absorption in the fuel). The absorption in the nickel cladding and the expanded polystyrene have been disregarded. Consequently the discrepancies between theory and experiment are actually slightly less. Of course the influence of the cladding materials on the neutron flux distribution through the cell is inherently incorporated. BOYNTON [29] recently reported results of disadvantage factor measurements, performed in undermoderated water-$UO_2$ lattices. His experimentally obtained values for a water-to-fuel volume ratio of unity were also about 7 % lower than those obtained with a NELKIN-kernel THERMOS computation (upper limit 0.415 eV). Moreover this discrepancy increased when the lattices were further under-moderated. HONECK [3] has observed this trend for water-uranium metal lattices with water-to-fuel volume ratios greater than unity.

In the experiments described in this chapter a few errors have been introduced both random and systematic in nature. They will be discussed below. First the random errors are reviewed:

*a*) After a dysprosium wire is brought into its position in the plastic guide, which traverses the special fuel element, the latter is placed in the exponential assembly for irradiation. While positioning this fuel element in the assembly a small displacement of the wire-section in the water region may have occurred in axial direction. Assuming a misalignment of 1 mm in axial direction it was calculated by using the integral-axial neutron-flux plot shown in Fig. 1.8, that an error of about 1 % is introduced in the disadvantage factor.

*b*) Because of a possible variation in the distance between two neighbouring fuel rods (see Chapter 1) the water-to-fuel volume ratio was subject to random variations. As a consequence an error on the order of 0.5 % is likely to have been introduced in the disadvantage factor.

*c*) Because of the many experiments to be performed with the HOR only short time irradiations could be allowed. Together with the relatively low neutron flux in LEAD this led to relatively large statistical fluctuations in the counting results, especially in the fuel region. The counting time of each millimeter of wire is dictated by the decay corrector in combination with the activity of that particular section of the wire that has been irradiated in the water region. Consequently, the error in the counting results referring to the fuel region is larger. On the average an error of about 4 % occurred in the count rates. This error is of course reduced in the final results because of integration over the cell cross-sectional area.

The systematical errors, which have been introduced are:

*d*) No account has been made for the effect of neutron moderation inside the dysprosium wire, caused mainly by the 30 vol. % polyethylene which is used as a base material for the wire. The influence of moderation will be larger in the fuel than in the water region. It can be seen from Table V.1 that a tendency exists towards obtaining higher disadvantage factors with wires larger in diameter, which may be caused by this moderation effect in the wire. Although dependent on the thickness of the wire this effect will introduce an error of minor importance, the value of which is difficult to estimate because of the spreading in the results.

*e*) While processing the results, a simple correction has been made for the flux depression outside the wire. It has been assumed that the flux depression inside the wire is equal in both the water and the fuel region. However the flux depression inside the wire depends on the neutron spectrum near and in the wire. As a result the flux depression in the wire section located in the water region will be more pronounced than in the fuel region where the spectrum is harder. The net effect will be that the activity measured over the water-region is less than the actual activity resulting in a disadvantage factor, about 0.5 % too low.

*f*) The aluminium cups used to prevent water from leaking into the plastic guide also affect the experimental results. The absorption cross-section of aluminium is slightly less than the absorption cross-section of water, while the scattering cross-section of aluminium is considerably smaller than the water scattering cross-section. Also the logarithmic energy decrement is smaller for aluminium. Consequently, locally thermalization of neutrons will be less in particular in the zero void condition, resulting in a slight reduction of the wire activation. Therefore the flux peaking measured with the wire will be somewhat less than the actual flux peaking. The net effect is that the value of the experimentally obtained disadvantage factor has been reduced by about 1 %.

*g*) A systematical error is further introduced by the use of dysprosium as a detector. The activation of the dysprosium is caused by neutrons of all energies. Consequently part of the activation (about 1 %) results from epi-thermal activation. Although a correction has been included in the determination of the experimental disadvantage factors for the difference in the integral spectra in the various regions of the cell, see Eq. (5.5.13) an additional correction factor for epi-thermal activation would be required to make possible a comparison with the computer results, which are based on a thermal cut-off energy of about 0.625 eV. Whereas the spectrum in the fuel region is harder than in the water region epi-thermal activation of the dysprosium wire in the fuel region is higher. Application of a correction factor relevant to this effect would result in a small increase (about 0.5 %) in the experimental disadvantage factor.

*h*) While processing the experimental results no account has been made for the presence of the plastic guide while the wires were being activated. Whereas this guide is made of polyethylene which has approximately the same transport and absorption cross-section as water, the flux perturbation caused by this tube is in the water region of minor importance in the zero void condition. At higher void fractions a small local softening of the spectrum may occur which will lead to a slightly higher activation of the dysprosium wire. On the other hand the flux depression in the water region will increase somewhat, which has an adverse effect on the activation. The presence of the guide in the fuel region has also contradictional effects. It causes a local source of thermalization inside the fuel resulting in an increase of the fission density in the vicinity of the wire. On the other hand the neutron density distribution is disturbed since no fissions take place in the volume where the guide is located. The net effect of the guide is difficult to estimate. By using guides of different thicknesses and extrapolating the results to zero thickness it should be possible to obtain more exact information concerning their influence.

*i*) Another error is introduced by the method of scanning the wire, that is counting the induced activity millimeter after millimeter. In fact the integrated activity per millimeter length of wire is obtained. This includes, for instance, that maxima and minima occurring in the neutron density are not correctly determined. The flux peaking in the water region will be measured lower than the true value, while in the fuel region the measured flux depression will be less than the actual flux depression. Consequently the experimentally determined disadvantage factor will be too low. Assuming the computed neutron density distributions as indicated in Fig. 5.9 to be correct it was calculated that, as a result of the integration, the experimental value of the disadvantage factor is about 1.5 % too low.

This survey of errors indicates that most of the systematical errors cause the experimentally determined density disadvantage factors to be too low by about 3 % to 4 % while the random error is on the order of 2 %. The reason for using dysprosium wires of various diameters was the expectation that the final results could have been extrapolated to zero wire diameter. In that case half of the systematical errors could have been eliminated. Because of the spreading in the data obtained, it was felt that no interpretable results would be obtained in doing so.

Because of the small size of the unit cell it was not to be expected that diffusion theory would yield thermal utilization factors corresponding to the experimental values. The thermal utilization factors determined with diffusion theory are about 5 % too high for lattices equivalent to those used in LEAD.

The differences between the experimentally obtained disadvantage factors and those computed by means of the K7-THERMOS calculation that have remained unexplained, are primarily caused by the very pronounced flux peaking in the water region, obtained with the K7-THERMOS code, see Fig. 5.8. This is believed to be caused by possible errors in the value of the cross-sections used, as well as in the formulation of the scattering kernel and the transport matrix. This over-estimated flux peaking, observed due to differential measurements, may be interpreted in such a way that either the slowing down of neutrons or the thermal absorption in the water region is not properly accounted for in the calculation. To obtain a better agreement between theory and experiment it was found useful to multiply the disadvantage factors obtained from the K7-THERMOS computations with $\Sigma_s/\Sigma_t$, being the ratio of the scattering-to-total cross-section for an homogenized unit cell averaged over the thermal energy region. It is obvious that this factor decreases when the water-to-fuel ratio decreases so that also for very undermoderated lattices a good agreement may be obtained between experiment and theory. It is therefore recommended to use the empirical correction factor indicated above for further correction of density disadvantage factors obtained by THERMOS-type computer programs.

To obtain a more rigorous correction it is necessary to further improve the accuracy of the experimental techniques utilized as well as the computation methods applied.

In conclusion it may be stated that an exponential assembly such as LEAD has shown to be very useful for the experimental study of microscopic reactor parameters.

## REFERENCES


1. H. C. HONECK, The distribution of thermal neutrons in space and energy in reactor lattices, Part I: Theory, Nucl. Science and Eng. **8**, 193 (1960).
2. ————, The calculation of the thermal utilization and disadvantage factor in uranium water lattices, Technical Report Series No. 12, IAEA, Vienna, 233 (1962).
3. ————, The calculation of the thermal utilization and disadvantage factor in uranium water lattices, Nucl. Science and Eng. **18**, 49 (1964).
4. R. J. J. STAMM'LER, K–7 THERMOS (neutron thermalization in a heterogeneous cylindrically symmetric reactor cell), Kjeller report KR–47, (1963).
5. A. TAS, H. P. STRUCH and D. VAN LIGTEN, MICRO-FLUX, A program for the solution of the multigroup neutron transport equation in square and hexagonal lattices, RCN Internal Report No. 65–032 (1965).
6. M. J. POOLE, P. SCHOFIELD and R. N. SINCLAIR, Some measurements of thermal neutron spectra, Proc. Symposium on Exponential and Critical Experiments, IAEA, Vienna, Vol. III, 87 (1964).
7. DEUTSCH, R. W., Spatial dependence of thermal-neutron spectra and the interpretation of thermal utilization measurements, Nucl. Science and Eng. **10**, 400 (1961).
8. SHER, R., H. KOUTS, D. KLEIN, Spatial dependence of thermal neutron spectra and the interpretation of thermal utilization measurements, Nucl. Science and Eng. **12**, 432 (1962).
9. NICHOLS, P. F., J. R. WORDEN, F. C. ENGESSER and R. E. HEINEMAN, The measurement of lattice parameters of a gas cooled reactor lattice, Nucl. Science and Eng. **15**, 233 (1963).
10. GREEN, R. E., C. B. BIGHAM, I. H. GIBSON, R. G. JARVIS, M. J. HALSALL, F. E. DRIGGERS and C. H. MILLAR, Lattice studies at Chalk River and their interpretation, A/Conf. 28/P/25 (1964).
11. ANDERSON, E., D. BABALA, K. BRYHN–INGEBRIGTSEN, V. O. ERIKSEN, H. R. FRANZEN, C. H. MILLAR, H. MOEN, D. PERRICOS, J. SMIT, R. J. J. STAMM'LER, K. V. SUBBA RAO, J. A. THOMASSEN and Z. WEISS, Experimental and theoretical studies of uranium oxide lattices moderated by mixtures of light and heavy water, A/Conf. 28/P/669 (1964).
12. KRASIK, S. and A. RADKOWSKY, Pressurized water reactor (PWR) critical experiments, Proc. Intern. Conf. Peaceful Uses Atomic Energy, **5**, 203 (1956).
13. KLEIN, D., A. Z. KRANZ, G. G. SMITH, W. BAER and J. DE JUREN, Measurements of thermal utilization, resonance escape probability and fast effect in water moderated slightly enriched uranium and uranium oxide lattices, Nucl. Science and Eng. **3**, 403 (1958).
14. GROB, V. E., E. SANTANDREA and H. RITZ, Measurements of parameters leading to $p_{28}$, $f$ and $\varepsilon$ in light water moderated 4.48 % and 2.73 % enriched lattices, Nucl. Science and Eng. **7**, 514 (1960).

15. Hardy, J., J. J. Volpe, D. Klein, E. Schmidt and E. Gelbard, Thermal neutron spectral and spatial distribution in light-water-moderated lattices, Proc. Symposium on Exponential and Critical Experiments, IAEA, Vienna, Vol. II, 339 (1964).
16. Kouts, H., G. Price, K. Downes, R. Sher and V. Walsh, Exponential experiments with slightly enriched uranium rods in ordinary water, Proc. Intern. Conf. Peaceful Uses Atomic Energy, **5**, 183 (1956).
17. ———, R. Sher, H. R. Brown, D. Klein, S. Stein, R. L. Hellens, H. Arnold, R. M. Ball and P. W. Davison, Physics of slightly enriched normal water lattices (theory and experiment), Proc. Intern. Conf. Peaceful Uses Atomic Energy, **12**, 446 (1958).
18. Price, G. A., Experience at Brookhaven in the measurement of cell parameters, Proc. Symposium Exponential and Critical Experiments, IAEA, Vienna, Vol. II, 3 (1964).
19. ——— and R. L. Hellens, Lattice studies in light water moderated systems, A/Conf. 28/P/264 (1964).
20. Finn, H. F., and R. H. Vollmer, Pathfinder atomic plant detailed flux measurements in superheat cells, USAEC Report 62020, Allis-Chalmers Manufacturing Company, (1962).
21. General Electric Atomic Power Equipment Department, Nuclear superheat project, Ninth Quarterly Progress Report, July–September 1961, USAEC Report–GEAP–3877.
22. Sher, R., S. Tassan, E. V. Weinstock and A. Hellsten, Low energy neutron cross-sections of $^{164}$Dy, Nucl. Science and Eng. **11**, 369 (1961).
23. Beckurts, K. H. and K. Wirtz, Neutron physics, Chapter 11, Springer-Verlag Berlin (1964).
24. Meghreblian, R. V. and D. K. Holmes, Reactor analysis, Chapter V, 252, McGraw-Hill Book Company, Inc., New York (1960).
25. Honeck, H. C., 'THERMOS' — A thermalization transport theory code for reactor lattice calculations, BNL–5826 (1961).
26. Koppel, J. U. and J. A. Young, Neutron scattering by water taking into account the anisotropy of the molecular vibrations, Nucl. Science and Eng. **19**, 412 (1964).
27. Brown, H. and D. St. John, Neutron energy spectrum in $D_2O$, DP–33 (1954).
28. Hughes, D. J. and R. B. Schwartz, Neutron cross-sections, BNL–325, Second ed. (1958).
29. Glasstone, S. and M. C. Edlund, The elements of nuclear reactor theory, Chapter IX, D. Van Nostrand Company, Inc., New York (1952).
30. Boynton, A. R., Experimental disadvantage factors in some very undermoderated, 3 % enriched water-uranium oxide lattices, Transactions of the 1965 ANS Annual Meeting, Vol. 8, No. 1, 249 (1965).

## LIST OF SYMBOLS

| *Symbol* | *Quantity* | |
|---|---|---|
| $A$ | activity | Ci |
| $A$ | area | $m^2$ |
| $B^2$ | buckling of the neutron flux | $m^{-2}$ |
| $B_g^2$ | buckling of the neutron flux, geometrical | $m^{-2}$ |
| $B_m^2$ | buckling of the neutron flux, material | $m^{-2}$ |
| $CR$ | conversion-ratio | |
| $D$ | diffusion coefficient | m |
| $DG$ | Dancoff-Ginsburg factor | |
| $d$ | diameter | m |
| $E$ | energy of a neutron | eV |
| $f$ | thermal utilization factor | |
| $F$ | flow rate | $m^3/s$ |
| $g$ | correction factor for non $(1/v)$-dependence of absorption cross-section | |
| $k_\infty$ | multiplication factor for an infinite system | |
| $k_{eff}$ | multiplication factor for a finite system | |
| $L$ | diffusion length | m |
| $L$ | non leakage probability | |
| $L_s$ | slowing down length | m |
| $m$ | mass of a neutron | amu |
| $M$ | mass | kg |
| $MCR$ | modified-conversion-ratio | |
| $N$ | neutron density | neutronen/$m^3$ |
| $p$ | resonance escape probability | |
| $P$ | pressure | $N/m^2$, at |
| $q$ | slowing down density | neutronen/$m^3 \cdot s$ |
| $r$ | radius | m |
| $R$ | radius | m |
| $R$ | reaction rate | |
| $R_{Cd}$ | cadmium-ratio | |
| $RMCR$ | relative-modified-conversion-ratio | |
| $RI$ | resonance integral | $m^2$ |
| $S$ | neutron source intensity | neutronen/s |
| $S$ | surface | $m^2$ |
| $t$ | time | s |
| $T$ | reactor period | s |
| $T$ | temperature, absolute | °C, °K |

| *Symbol* | *Quantity* | |
|---|---|---|
| $T\frac{1}{2}$ | half-life of radioisotope | s |
| $u$ | lethargy | |
| $v$ | speed | m/s |
| $V$ | volume, fractional | $m^3$ |
| $Z$ | atomic number | |
| $\alpha$ | fractional voidage | |
| $\beta$ | transmission coefficient | |
| $\gamma$ | correction factor for flux depression | |
| $\delta$ | disadvantage factor | |
| $\varepsilon$ | fast fission factor | |
| $\eta$ | average number of fast neutrons emitted as a result of fission per thermal neutron absorbed in a fuel | |
| $\theta$ | angle | |
| $\varkappa$ | reciprocal diffusion length | $m^{-1}$ |
| $\lambda$ | decay constant of radioisotope | $s^{-1}$ |
| $\lambda$ | mean free path | m |
| $\mu$ | absorption coefficient | $m^{-1}$ |
| $\nu$ | average number of fast neutrons per fission | |
| $\xi$ | average logarithmic energy loss per neutron collision with a nucleus | |
| $\varrho$ | density | $kg/m^3$ |
| $\Sigma$ | macroscopic cross-section | $m^{-1}$ |
| $\sigma$ | microscopic cross-section | $m^2$ |
| $\tau$ | Fermi-age | $m^2$ |
| $\varphi$ | angle | |
| $\phi$ | neutron flux | neutronen/$m^2 \cdot s$ |

| *Indices* | *Refer to*: |
|---|---|
| $a$ | absorption |
| $c$ | capture |
| $f$ | fast neutron energy |
| $f$ | fission |
| $f$ | fuel |
| $m$ | moderator |
| $n$ | neutron |
| $o$ | 2200 m/s values |
| $r$ | resonance energy |
| $r$ | removal (from an energy interval) |
| $s$ | scatter |
| $s$ | source neutron energy |
| $th$ | thermal neutron energy |

## LIST OF ABBREVIATIONS

*Companies, Laboratories, Institutions*

| | |
|---|---|
| AC | Allis Chalmers Manufacturing Company |
| AEG | Allgemeine Elektrizitäts Gesellschaft |
| ANL | Argonne National Laboratory |
| BNL | Brookhaven National Laboratory |
| CEND | Combustion Engineering Nuclear Division |
| GE-APED | General Electric Atomic Power Equipment Department |
| GNEC | General Nuclear Engineering Corporation |
| MIT | Massachusetts Institute of Technology |
| RCN | Reactor Centrum Nederland |
| RID | Reactor Instituut Delft |
| USAEC | United States Atomic Energy Commission |

*Reactor facilities*

| | |
|---|---|
| BONUS | Boiling Nuclear Superheat Reactor |
| EBWR | Experimental Boiling Water Reactor |
| EGCR | Experimental Gas Cooled Reactor |
| HOR | Hoger Onderwijs Reactor |
| LEAD | Light water Exponential Assembly Delft |
| PCTR | Physical Constants Testing Reactor |

*Reactor types*

| | |
|---|---|
| BWR | Boiling Water Reactor |
| PWR | Pressurized Water Reactor |

## ACKNOWLEDGEMENTS

A. W. van der Heijden, A. L. Dekker, H. van Dam, B. Th. Eendebak, W. E. During and W. L. Korfker participated as students in various experimental projects of this study while fulfilling their requirements for the degree of Natuurkundig Ingenieur. Their assistance is gratefully acknowledged. Further I am indebted to R. J. J. Stamm'ler and A. Tas for the computer calculations performed in regard to the thermal utilization factor. Finally I would like to thank the Central Laboratory of the Netherlands State Mines for fabricating the dysprosium wires.

## SUMMARY

Although the integral neutron multiplying properties of an infinitely sized fuel-moderator mixture are already largely characterized by the infinite multiplication factor $k_\infty$, it is for a number of reasons desirable to have more detailed knowledge of the microscopic reactor parameters $\eta$, $\varepsilon$, $p$ and $f$ which, formally but very practically, account for all effects affecting the multiplication.

This knowledge is in the first place required to obtain $k_\infty$ itself. Generally $k_\infty$ is calculated by determining each of the microscopic reactor parameters from semi-empirical calculation models. On the contrary, experimentally $k_\infty$ is often obtained from integral measurements that do not yield any information concerning the physical structure of this factor. Consequently an analysis of possible discrepancies between calculated and experimental results is impossible. Further it is essential, when determining reactor operational policy to have more knowledge about the composition of $k_\infty$ especially for the estimation of the fuel cycle costs. In addition it is of importance to know the dependence of the microscopic parameters on the operational conditions that exist in a reactor. A change in temperature, in general, and the formation of bubbles in a water-reactor in particular, result among other things in a change of the resonance escape probability $p$ and the thermal utilization factor $f$. In how far the product of these two parameters is affected by a variation in the operational conditions depends, as is also demonstrated by the experiments, on the water-to-fuel volume ratio. Moreover optimization of a reactor design also requires knowledge concerning the detailed composition of $k_\infty$.

Therefore it is important to have available experimentally proven calculation schemes for the determination of the previously mentioned microscopic reactor parameters, giving accurate results.

In this thesis it is demonstrated that it is indeed possible to measure these parameters together with their dependence upon some operational conditions with exponential assemblies rather than with more expensive critical facilities.

Using normal water and annularly shaped natural uranium metal fuel slugs (external diameter 28.5 mm – internal diameter 15.0 mm) an exponential assembly was constructed, designated LEAD (Light water Exponential Assembly Delft). In this facility a few operational conditions were simulated in a simple way, at room-temperature, that exist in a water-moderated reactor in which this water is heated to boiling on the outside of the fuel elements and the saturated steam is superheated inside these elements. Boiling of water (bubble-formation) was simulated by injecting

air near the bottom of the assembly, while by using expanded polystyrene, inserted in the central gap of a limited number of elements, moderation effects were introduced almost analogous to those caused by superheated steam. To obtain a more flat radial neutron flux distribution the LEAD core was composed of two concentric zones each with a uniform but different water-to-fuel volume ratio. In the central zone which is undermoderated the water-to-fuel volume ratio was 1.14 while in the overmoderated peripheral zone this ratio was selected as 2.34. The assembly was positioned in the vertical access of the thermal column of the pool reactor HOR, one of the irradiation facilities of the Reactor Institute in Delft. This reactor functioned as the neutron source. At a power level of 200 kW a neutron flux of about $5 \times 10^6$ n/cm$^2$·s was obtained at measuring positions in LEAD.

The resonance escape probability and the thermal utilization factor are the most sensitive for changes in the above-mentioned operational conditions. These two factors have been measured as a function of the void fraction in the water up to a void volume of about 40 %.

Because this research program was more directed to the study of fundamental reactor physics aspects rather than to the determination of absolute values, the fact that natural uranium metal has been used instead of slightly enriched $UO_2$, which is common for water-reactors, is of minor importance for the interpretation of the results. Moreover the parameters measured are more closely related to the neutron energy spectrum and the moderator-to-fuel ratio than to the enrichment as long as it is small.

In Chapter 1 of this thesis the advantages and disadvantages of exponential assemblies are discussed in regard to their usefulness for experimental reactor physics research. It is emphasized that these assemblies, which initially were only used to determine macroscopic parameters such as the material buckling, are more appropriate for analysing microscopic effects. In addition the construction as well as the integral reactor physical properties of LEAD are discussed.

Chapter 2 is introduced with a consideration of the advantages and disadvantages of different methods that can be applied for the simulation of voids from a nuclear point of view, that occur as a result of water boiling. Injection of air over a sufficiently large region in each of the two zones of the assembly was selected. In this region in the central zone of LEAD a void fraction of 36 % can be obtained, while in the peripheral-zone region a void fraction of 29 % can be reached. The maximum allowable void fraction is limited by instabilities in the bubble distribution in the water at higher void fractions (channeling effect). In addition, at higher void fractions the neutron energy spectrum in the assembly affects the spectrum in the voided area.

The relationship between the void fraction and the air flow rate was determined from cadmium-ratio measurements. Especially at high void fractions rather accurate results can be obtained by this method. In the same way the

height in the assembly was determined where the axial neutron energy distribution would reach an equilibrium corresponding to the particular void fraction. From the results it could be concluded that the microscopic parameters could be measured at approximately 45 cm above the bottom of the assembly.

Since the experiments are closely related to boiling water reactors in which the produced steam is also superheated some of the most important reactor physics aspects of these reactors are discussed in Chapter 3. For power reactors in the medium energy range a number of technological arguments can be given claiming that a system where superheating of steam takes place throughout the core is more attractive than the application of separate boiling and superheater zones, as is the case in some reactors in the United States.

Chapter 4 describes the experiments in relation to the resonance escape probability. This parameter is obtained from a measured relative-conversion-ratio determined by a so-called differential technique. Therefore the spatial distribution of the fission density in the fuel and the neutron absorption in $^{238}U$ were measured over a cross-sectional area of a uranium rod at various void fractions in the water and in both zones of LEAD. The experimental results have been compared with those obtained from a simple semi-empirical calculation method using different resonance integrals. In the case that no air is injected the experimental results are about 14 % higher than the predicted values. The difference decreases as more air is injected. The gradient in the experimentally obtained relations differs noticeably from that calculated. In the latter case the gradient is also influenced by the value of the resonance escape probability when no air is being injected. The increase measured in the neutron absorption in $^{238}U$ throughout the entire volume of the fuel rods at increasing void fractions can only result from epi-thermal neutron absorption. Therefore the discrepancy between the calculated and experimental values of the resonance escape probability is probably due to the resonance integrals that have been used. Obviously they do not sufficiently account for the volume absorption effect. When $\sqrt{S/M}$ is replaced by a factor $\sqrt{S/4M}$ in the resonance integral, better agreement can be obtained between experiment and theory. Therefore it is recommended that these experiments should be repeated with fuel rods having $(S/M)$-values smaller than 0.1 (the $(S/M)$-value of the LEAD fuel rods). It should be noted that fuel rods of this type are not attractive for light water-reactors.

Chapter 5 deals with the thermal utilization factor which is determined from a measured microscopic neutron flux distribution throughout a unit cell at various void fractions and in both zones of the assembly. Wires composed of a mixture of dysprosium oxide and polyethylene, traversing the unit cell, while being activated, were employed to determine the flux profiles.

In addition the thermal utilization factor was calculated using two

existing nuclear digital codes, K7-THERMOS and MICRO-FLUX, both based upon integral transport theory and by using simple diffusion theory. The experimental results lie between those of the transport and diffusion calculations. The gradients in all results are almost equal. The experimentally obtained disadvantage factors are 6 % to 10 % lower than the theoretically obtained values for the central zone; in the peripheral zone the discrepancies are even larger. However, due to systematical errors in the experiments the measured values are about 4 % too low. The remaining differences between the calculated and experimental values result from an overestimation of the calculated flux peaking in the water. Disadvantage factors calculated by codes such as THERMOS, for undermoderated lattices can be multiplied by an empirical factor $\Sigma_s/\Sigma_t$, this being the ratio of the scattering to the total cross-section of the homogenized unit cell, to obtain reasonable agreement between calculated and experimental results.

# SAMENVATTING

Hoewel de integrale neutronen-multiplicerende eigenschappen van een splijtstof-moderator mengsel van oneindige afmetingen reeds in belangrijke mate worden gekarakteriseerd door de vermeningvuldigingsfactor $k_\infty$, is het om een aantal redenen gewenst de microscopische reactorparameters $\eta$, $\varepsilon$, $p$ en $f$, waarin alle de multiplicatie beinvloedende effecten, formeel doch uiterst practisch zijn verdisconteerd, nader te kennen.

In de eerste plaats is dit noodzakelijk voor het verkrijgen van de factor $k_\infty$ zelf. In het algemeen wordt $k_\infty$ namelijk berekend door elk van de microscopische reactorparameters te bepalen aan de hand van daartoe opgestelde (semi-empirische) rekenmodellen. Daarentegen wordt een via experimenten verkregen waarde van $k_\infty$ meestal afgeleid uit integrale metingen, die geen informatie geven over de fysische structuur van deze factor. Hierdoor ontbreekt de mogelijkheid eventuele afwijkingen tussen berekende en experimentele resultaten nader te analyseren. Voorts is het ten behoeve van de bedrijfsvoering van een reactor en wel met name voor de bepaling van de splijtstofkosten essentieel de opbouw van $k_\infty$ meer precies te kennen. Daarbij is het tevens van belang te weten hoe elk van de microscopische reactorparameters afhankelijk is van de bedrijfscondities, die zich in een reactor voordoen. Een wijziging van de temperatuur in het algemeen, en de formatie van stoombellen in een water-reactor in het bijzonder, resulteren onder meer in een verandering van de resonantie-ontsnappingskans $p$ en de factor voor het thermisch rendement $f$. In hoeverre het product van deze twee parameters door een variatie in de vermelde bedrijfscondities wordt beinvloed hangt, zoals ook uit de experimenten is gebleken, samen met de volumeverhouding van moderator en splijtstof. Behalve voor de hiervoor genoemde punten is eveneens een inzicht in de gedetailleerde opbouw van $k_\infty$ nodig voor het optimaliseren van een reactorontwerp.

Het is derhalve van belang te kunnen beschikken over experimenteel beproefde, nauwkeurige resultaten leverende rekenschema's voor de bepaling van de genoemde microscopische reactorparameters.

In dit proefschrift wordt aangetoond, dat het zeer wel mogelijk is deze parameters, alsmede hun afhankelijkheid van een aantal bedrijfscondities te meten met behulp van exponentiële ensembles, in plaats van met zoveel duurder zijnde kritische opstellingen.

Gebruik makende van normaal water en holle, cylindervormige natuurlijk-uranium metaal staven (uitwendige diameter 28,5 mm – inwendige diameter 15,0 mm) werd een exponentieel ensemble geconstrueerd, dat de naam LEAD (Light water Exponential Assembly Delft) kreeg. In deze

faciliteit werden op eenvoudige wijze, bij kamertemperatuur, enkele bedrijfscondities gesimuleerd, die optreden in een water-gemodereerde reactor, waarbij dit water aan de buitenzijde van de splijtstofelementen tot koken wordt gebracht en de gevormde stoom wordt oververhit binnenin deze elementen. Het koken van water (bel-vorming) werd gesimuleerd door het injecteren van lucht aan de onderzijde van het ensemble, terwijl met polystyreen-schuim aangebracht in de centrale holte van een beperkt aantal elementen moderatie-effecten werden geintroduceerd, die vrijwel analoog zijn aan die, teweeg gebracht door oververhitte stoom. Teneinde een meer vlak radiaal neutronen-fluxprofiel te verkrijgen, werd de kern van LEAD uitgevoerd in twee concentrische zones, elk met een uniforme doch van elkaar verschillende volumeverhouding van water en uranium. In de binnen-zone, die is onder-gemodereerd bedroeg de water-uranium verhouding 1,14 terwijl in de over-gemodereerde buiten-zone voor deze verhouding 2,34 werd gekozen. Het ensemble werd geplaatst in de verticale toegang van de thermische kolom van de bassin-reactor HOR, één van de bestralingsfaciliteiten van het Reactor Instituut te Delft. Deze reactor functioneerde als neutronenbron. Bij een vermogen van 200 kW werd daarmee op de meetposities in LEAD een neutronenflux van circa $5 \times 10^6$ n/cm$^2$·s bereikt.

Het meest gevoelig voor variaties in de genoemde bedrijfscondities zijn de resonantie-ontsnappingskans en de factor voor het thermisch rendement. Deze twee factoren zijn gemeten als functie van de bellen-fractie in het water tot een belvolume van ongeveer 40 %.

Omdat het onderzoek meer gericht was op een bestudering van de fundamenteel reactorfysische aspecten dan op het bepalen van absolute waarden, is het feit dat natuurlijk-uranium metaal werd toegepast in plaats van licht-verrijkt $UO_2$, dat gebruikelijk is bij waterreactoren, van ondergeschikt belang voor de interpretatie van de resultaten. Bovendien zijn de gemeten parameters sterker gelieerd met het energie-spectrum van de neutronen en de moderator-splijtstof verhouding dan met de verrijking, zolang als deze tenminste gering is.

In hoofdstuk 1 van deze dissertatie worden de voor- en nadelen besproken van exponentiële ensembles met betrekking tot hun bruikbaarheid voor experimenteel reactorfysisch onderzoek. De nadruk wordt daarbij gelegd op het feit, dat deze ensembles, die aanvankelijk slechts werden gebruikt voor het bepalen van macroscopische parameters, zoals de materiële bolling, zich veeleer lenen voor het analyseren van microscopische effecten. Voorts worden in dit hoofdstuk de constructie alsmede de integrale reactorfysische eigenschappen van LEAD behandeld.

Hoofdstuk 2 wordt ingeleid met een beschouwing over de voor- en nadelen van verschillende methoden die toegepast kunnen worden voor de nucleaire simulatie van bellen, die optreden als gevolg van het koken van water. Gekozen is een methode waarbij lucht wordt geinjecteerd in een gebied van voldoende omvang in elk der twee zones van het ensemble.

In het gebied in de binnen-zone van LEAD is daarmee een bellenfractie van 36 % bereikbaar. In de buiten-zone blijkt een bellenfractie van 29 % haalbaar. De maximaal toelaatbare bellenfractie wordt gelimiteerd door het optreden van instabiliteiten in de bellendistributie in het water, alsmede door de bij hogere bellenfracties sterker wordende beinvloeding door de neutronen-energieverdeling van het spectrum in de het bellen-gebied omringende sectie van het ensemble. De bellenfractie als functie van de hoeveelheid geinjecteerde lucht werd bepaald met behulp van cadmium-verhouding metingen. Vooral bij een hoge bellenfractie zijn met deze methode nauwkeurige resultaten te verkrijgen. Tevens is op deze wijze de hoogte in het ensemble bepaald waar de axiale energieverdeling van de neutronen een met de bellenfractie corresponderende evenwichtswaarde bereikt. Aan de hand van meetresultaten kon worden vastgesteld, dat de microscopische parameters op circa 45 cm van de bodem gemeten konden worden.

Aangezien de onderzoekingen een nauwe relatie hebben met kokend water-reactoren, waarin de gevormde stoom tevens wordt oververhit, worden in hoofdstuk 3 de belangrijkste reactorfysische aspecten van dergelijke reactoren besproken. Voor reactoren, die een middelgroot vermogen moeten leveren, zijn een aantal argumenten van voornamelijk technologische aard aan te voeren, die stellen, dat een systeem waarin oververhitten van stoom plaats heeft door de gehele kern, meer aantrekkelijk is dan de toepassing van aparte kook- en oververhitter-zones, zoals dat het geval is bij enkele in Verenigde Staten gerealiseerde projecten.

Hoofdstuk 4 beschrijft de experimenten uitgevoerd ter bepaling van de resonantie-ontsnappingskans. Deze parameter is afgeleid uit een gemeten relatieve conversie-verhouding, die bepaald werd via een zo genaamde differentiële methode. Daartoe werd de ruimtelijke verdeling van de splijtingsdichtheid in de splijtstof en de neutronen-absorptie in $^{238}U$ over de doorsnede van een uranium staaf gemeten bij verschillende bellenfracties in het water en in beide zones van LEAD. De experimenteel gevonden resultaten werden vergeleken met die volgende uit een eenvoudige semi-empirische berekeningsmethode waarbij verschillende resonantie-integralen werden gebruik. In het geval dat geen lucht wordt geinjecteerd zijn de experimentele waarden ongeveer 14 % hoger dan de berekende. Het verschil wordt kleiner naarmate meer lucht wordt geinjecteerd. De gradient in de experimenteel gevonden ($p$–$\alpha$)-relaties wijkt in belangrijke mate af van die in de berekende. In het laatste geval wordt de helling mede bepaald door de waarde van de resonantie-ontsnappingskans, indien geen lucht wordt geinjecteerd. De gemeten toename van de neutronenabsorptie in het $^{238}U$ over het gehele volume van de staaf bij stijgende bellenfracties kan slechts het gevolg zijn van epithermische neutronen-absorptie. In verband hiermee moet de oorzaak van de afwijking tussen de berekende en de experimenteel gevonden waarden voor de resonantie-ontsnappingskans gezocht worden in de gebruikte resonantie-integralen. Blijkbaar wordt

daarmee het volume-absorptie effect onvoldoende in rekening gebracht. Indien in de resonantie-integraal in plaats van $\sqrt{S/M}$ een factor $\sqrt{S/4M}$ wordt gebruikt blijkt een betere overeenstemming tussen experiment en theorie verkrijgbaar te zijn. In verband daarmee wordt aanbevolen deze experimenten te herhalen met splijtstofstaven met $(S/M)$-waarden kleiner dan 0,1, zijnde de $(S/M)$-waarde van de LEAD splijtstofstaven. Hierbij moet worden aangetekend, dat dergelijke staven voor licht water-reactoren niet aantrekkelijk zijn.

Hoofdstuk 5 handelt over de factor voor het thermisch rendement, die bepaald is aan de hand van gemeten microscopische neutronenflux verdelingen door een eenheidscel bij verschillende bellenfracties en in beide zones van het ensemble. Dit fluxprofiel werd bepaald door draden bestaande uit een mengsel van dysprosiumoxyde en polytheen, geplaatst dwars door een eenheidscel, te activeren. Voorts werd de factor voor thermisch rendement bij verschillende bellenfracties berekend met behulp van twee bestaande nucleaire digitale rekencodes namelijk K7-THERMOS en MICRO-FLUX, beide gebaseerd op integrale transporttheorie en met behulp van eenvoudige diffusie-theorie. De experimentele resultaten liggen tussen die van de transport en diffusie berekeningen, waarbij de gradient in alle resultaten vrijwel analoog is. De experimenteel verkregen nadeelsfactoren zijn voor de binnenzone 6 % tot 10 % lager dan de theoretisch verkregen waarden; in de buitenzone zijn de afwijkingen nog groter Door systematische fouten in het experiment zijn echter de gemeten waarden ongeveer 4 % te laag. De resterende discrepantie tussen de berekende en de experimentele waarden is het gevolg van een uit de berekening resulterende te hoge fluxpiek in het water. Door de voor ondergemodereerde roosters, met codes zoals THERMOS, berekende nadeelsfactoren te vermenigvuldigen met een empirische factor $(\Sigma_s/\Sigma_t)$ waarbij $\Sigma_s$ en $\Sigma_t$ de verstrooiings- en totale doorsneden zijn van een gehomogeniseerde eenheidscel blijken de berekende resultaten redelijk in overeenstemming te brengen met de experimenteel gevonden waarden.

# STELLINGEN

## I

Een exponentieel ensemble is bij uitstek geschikt om gebruikt te worden voor het verkrijgen van microscopische reactorparameters als functie van bepaalde bedrijfscondities. Indien deze parameters voorts via differentiële metingen worden bepaald, wordt daarmee bruikbare informatie verkregen ter verifiëring van berekeningsmethodieken, hetgeen onmogelijk is indien z.g. integrale meetmethoden worden toegepast.

Dit proefschrift.

## II

De wijze waarop door Thie, Beidelman en Hoglund de resultaten van cadmium-verhouding metingen worden verwerkt ter bepaling van bellenfracties in een in bedrijf zijnde kokend waterreactor is niet algemeen aanvaardbaar.

J. A. Thie, J. Beidelman, and B. Hoglund, Nucl. Science and Eng., **11**, 1 (1961)

## III

Voor energiereactoren van het kokend water type waarin tevens stoom wordt oververhit en die naar huidige begrippen een middelgroot vermogen moeten leveren, verdient een uitvoering waarbij het oververhitten van stoom door de gehele kern plaats heeft voorkeur boven een systeem waarin de stoom wordt oververhit in een in de kern aangebrachte separate oververhittersectie.

Dit proefschrift.
H. R. Kleijn, Atoomenergie en haar toepassingen, **5**, 110 (1965).

## IV

In de „technische" literatuur dient duidelijker gewezen te worden op het feit, dat voor de toepasbaarheid van de methode van separatie van variabelen bij het oplossen van partiële differentiaal vergelijkingen niet alleen de representatie van de differentiaal vergelijking maar ook de gedaante van de bijbehorende randvoorwaarden van betekenis is.

Vele leerboeken op het gebied van de reactorfysica.

## V

De bij Algemene Maatregel van Bestuur met betrekking tot Artikel 6 van de Veiligheidswet 1934 vastgelegde voorwaarden ten aanzien van de grootte van raamoppervlakken in fabrieken of werkplaatsen ter verkrijging van verlichting door daglicht zijn niet wel overdacht. Bovendien moeten deze in verband met de bereikte resultaten op het gebied van verlichting door kunstlicht als verouderd en derhalve als niet meer toepasbaar worden aangemerkt.

Veiligheidswet 1934; AMvB, Hoofdstuk II, par. 2, artikel 9.

## VI

De z.g. moderatieverhouding $\xi\Sigma_s/\Sigma_a$ geeft slechts een bepaald aspect aan van de kwaliteit van een moderator. In tegenstelling tot hetgeen nog veelal wordt beweerd, brengt deze verhouding geenszins de effectiviteit van de moderator tot uitdrukking.

S. Glasstone and M. C. Edlund, The Elements of Nuclear Reactor Theory, Chapter VI, section 6.26, New York (1957).

## VII

Het verdient aanbeveling om in het studieprogramma van alle studierichtingen aan de Technische Hogescholen in Nederland een verplicht college „rapporteringstechniek" op te nemen in het laatste deel van dit programma. In dit college zouden zowel problemen met betrekking tot de schriftelijke- als de mondelinge rapportering behandeld dienen te worden.

## VIII

Een kernreactor, die toegepast wordt als stralingsbron voor wetenschappelijk onderzoek in uiteenlopende disciplines geeft een zekere tijd na inbedrijfstelling aanleiding tot een ongewenste begrenzing van het experimentele programma. In verband daarmee verdient het aanbeveling bij nieuw te bouwen reactoren met gelijk gericht doel een zekere selectiviteit te betrachten bij de bestemming.

## IX

Het verdient, op grond van experimentele overwegingen, aanbeveling om in grafische voorstellingen van de relatie tussen een grootheid evenredig met de kans op een bepaalde neutron-kern interactie en de neutronenenergie, voor deze grootheid het product te kiezen van de doorsnede en de neutronensnelheid, in plaats van alleen de doorsnede zoals thans gebruikelijk is.

## X

Aangezien Wilson en Grenda geen melding maken van de luchtfractie in het water bij hun vloeistofstroom-afbuigingsexperimenten aan vlakke oppervlakken kunnen hun resultaten niet vergeleken worden met andere experimenten van deze aard.

J. F. Wilson and R. J. Grenda, Allis Chalmers report No. ACNP–6105.

*Proefschrift:* H. R. KLEIJN
Delft, 12 januari 1966.